SOURCES AND CHARACTERISTICS OF OIL CONSUMPTION IN A SPARK-IGNITION ENGINE

by

Ertan Yilmaz

Diplom - Ingenieur
Rheinisch-Westfälische Technische Hochschule Aachen, Germany
(1997)

Submitted to the Department of Mechanical Engineering
in Partial Fulfillment of the Requirements for
the Degree of Doctor of Philosophy

at the

MASSACHUSETTS INSTITUTE OF TECHNOLOGY

September 2003

Signature of Author_____
Department of Mechanical Engineering
September, 2003

Certified by_____
John B. Heywood
Sun Jae Professor of Mechanical Engineering
Thesis Supervisor

Certified by_____
Victor W Wong
Lecturer, Department of Mechanical Engineering
Thesis Supervisor

Accepted by_____
Ain A Sonin
Chairman, Department of Graduate Committee

(This page was intentionally left blank)

SOURCES AND CHARACTERISTICS OF OIL CONSUMPTION IN A SPARK-IGNITION ENGINE

by

Ertan Yilmaz

Submitted to the Department of Mechanical Engineering
on August 14, 2003 in Partial Fulfillment of the Requirements for
the Degree of Doctor of Philosophy

ABSTRACT

Engine oil consumption is an important source of hydrocarbon and particulate emissions in automotive engines. In addition, chemical compounds present in oil additives poison catalytic converters and reduce their conversion efficiency. As a part of the effort to comply with increasingly stringent emission standards, engine manufacturers strive to minimize engine oil consumption. This requires the advancement of the understanding of the characteristics, sources, and driving mechanisms of oil consumption. There is a general lack of oil consumption studies that connect comprehensive experiments and theoretical analysis.

In this work, a combined theoretical and experimental approach was used to separate and quantify different oil consumption sources in a production spark ignition engine at different engine operating conditions. An extensive diagnostic system was successfully implemented on the test engine to measure real time oil consumption and in-cylinder parameters that affect major consumption sources such as inter-ring pressures, oil film thickness in the piston-ring-pack, and liner temperatures.

A multi-species liner evaporation model was developed and verified by testing two oils with different volatility at varying cylinder liner temperatures and engine speed and load conditions. The experimental and modeling results were used to separate and quantify the contributions of oil evaporation, oil entrained in the blowby gas flow, and oil flow into the combustion chamber passing by the piston system to total engine oil consumption. The results show that the contribution of each consumption source varies with engine operating conditions. At low load, oil flowing past by the piston was found to be the major consumption source, while the contributions of oil evaporation and of blowby entrainment became more significant with increasing engine load.

Furthermore, an extensive study was conducted to measure and analyze the oil consumption behavior during engine load transients to simulate real driving conditions.

This work is an important step in advancing the understanding of oil consumption sources in spark ignition engines.

Thesis Supervisors:

John B. Heywood
Professor, Department of Mechanical Engineering

Victor W. Wong
Lecturer, Department of Mechanical Engineering

(This page was intentionally left blank)

ACKNOWLEDGEMENTS

I would like to thank the members of my doctoral thesis committee who have given me their guidance, and through feedback and suggestions have improved my research. In particular, I would like to thank my thesis supervisors Professor John B. Heywood and Dr. Victor W. Wong for their support and insightful advice throughout the project, and for their focus on the important that kept me in the right track. I would like to express my gratitude to Dr. Tian Tian for the continuous help and the numerous helpful discussions over the years. Tian took part in my thesis committee and has been a constant source of advice for my work. His broad scientific knowledge, insight, and expertise in the field of engine lubrication have contributed significantly to this thesis. My sincere thanks to Professor Mikić for accepting being part of the committee and for his careful criticism and suggestions. I would also like to thank Professor Wai Cheng for his support and advice. Furthermore, I would like to thank Professors John B. Heywood and Simone Hochgreb for giving me the opportunity to conduct my doctoral research at MIT.

I would like to thank PSA Peugeot Citroën and the members of the Consortium on Lubrication in Internal Combustion Engines at MIT (current members include Dana Corporation, Mahle GmBh, Renault SA, PSA Peugeot Citroën, and Volvo AB) for sponsoring this research. I would like to thank Dr. Bernard Cousyn, Nicholas Lee, and Dr. Sébastien Messé at PSA Peugeot Citroën for their support and help in this project. I would like to thank Rémi Rabuté at Dana for his support and valuable technical inputs over the years. I would also like to thank Fredrik Stromstedt, Bengt Olson, Dr. Adam Blomburg, and Jonas Rick at Volvo, Dr. Rolf-Gerhard Fiedler and Dr. Eberhard Kopf at Mahle, Randy Lunsford and Kim Karrip at Dana, and Dr. Mokhtar Maamouri at Renault for their interest and support. I would like to express special thanks to Lubrizol Corporation for formulating and providing the special lubricants for this project.

I gratefully acknowledge the support of the Sloan Automotive Laboratory staff. Brian Corkum, Peter Menard, and Thane Dewitt deserve special credit for their technical assistance. I would also like to thank Alexis Rozantes, Nancy Cook, Susan Lutin, and Karla Stryker for their help and pleasant attitude. Special thanks also to Leslie Reagan for her support and help.

Bertrand Lecointe, Gerald Chamarre, Yonggy Shin, Daisuke Suzuki, and Oscar Lopez deserve special credit for their contributions to the test facility set-up and measurements.

I would like to thank Benoist Thirouard, Conor McNally and Liang Liu for the helpful discussions and most importantly for having made my stay at MIT both rich and enjoyable experience. Particularly, I would like to thank Benoist for providing valuable 2D-LIF images. I would also like to thank the following list of graduate students and visiting engineers in the Sloan Automotive Laboratory for their help and for making my research in the laboratory enjoyable: Morgan Andreae, Jinchul Hong, Grant Smedley, Jeff Matthews, Yong Li, Jim Cowart, Robert Meyer, Matt Rublewski, Adam Vokac, Fiona McClure, Mohammad Rassuli, Franck Gambin, Michael Bourgeois, Brian Hallgren, Ioannis Kitsopanidis, Joseph Acar, Jeremy Llaniguez, Yuetao Zhang, Kevin Lang, Gerardo Jose Cordova Lao, Halim Santoso, and Yeunwoo Cho.

Outside the Sloan Automotive Laboratory, I would like to thank Cornelius O'Sullivan, Dimitrios Rovas, Michaela Wiegel, A. Burak Guner, Cagri Savran, Dr. Wolf-Dietrich Bauer, and Efstratios Mylidakis for their friendship, help, and support. I would especially like to thank Cynthia Galvan for her support, care, and understanding. She has been a constant source of encouragement to me.

I would like to express my special thanks to all members of my family. This thesis would not have been completed without their unconditional support. In particular, I am very grateful to my mother, father, and sister Eda for their continuous encouragement and support.

Cambridge, October 2003

(This page was intentionally left blank)

Table of Content

Abstract 3

Acknowledgements 5

Table of Content 7

Chapter 1 Introduction 16

1.1 Engine Lubrication and Oil Consumption 16

1.2 Research on Oil Consumption 17

1.3 Oil Consumption Sources and Transport Mechanisms in SI Engines 18

1.4 Project Scope 22

Chapter 2 Experimental Setup 25

2.1 Experimental Objectives 25

2.2 Test engine: Production Spark Ignition Engine 26

2.3 Measurement Techniques 27

2.3.1 Total Output Measurements 27

2.3.1.1 Oil Consumption 27

2.3.1.1.1 High Sulfur Oil 28

2.3.1.1.2 Low Sulfur Fuel 30

2.3.1.1.3 Oil Consumption Measurement Setup 30

2.3.1.1.4 Oil Consumption Formula 32

2.3.1.2 Blowby 34

2.3.1.3 SMPS 36

2.3.2 In-cylinder Measurements 37

2.3.2.1 Laser-Induced-Fluorescence (LIF) System 39

2.3.2.2 Cylinder and Land Pressures 47

2.3.2.3 Liner Temperatures 50

2.4 Experimental Conditions 50

2.4.1 Engine Operating Conditions 50

2.4.1.1 Steady State Engine Operation 50
2.4.1.2 Engine Transients 52
2.4.2 Ring-pack Design 53

Chapter 3 Oil Consumption Characteristics during Steady State and Transient Operation 55

3.1 Factors Influencing Oil Consumption at Different Speed and Load 55
3.2 Simulation of Piston-Ring-Pack Performance 56
3.3 Speed and Load Effects on Oil Consumption and In-Cylinder Parameters 58
3.3.1 Oil Consumption Measurements 59
3.3.2 Blowby 60
3.3.2.1 Blowby Flow Structure 60
3.3.2.2 Blowby Gas Flow Oil Dragging 62
3.3.2.3 Blowby Measurements 64
3.3.3 Oil Distribution along Piston 66
3.4 Analysis of Oil Consumption Behavior during Transients in Load 72
3.4.1 Introduction 72
3.4.2 Oil Consumption Measurements 74
3.4.3 Blowby, Land Pressures and Oil Film Thickness 78
3.4.4 Gas Flow and Ring Dynamics 83
3.4.5 2-D LIF Observations 90
3.4.6 Summary for Analysis of Oil Consumption during Transients in Load 91

Chapter 4 Oil Consumption Sources 93

4.1 Blowby 93
4.1.1 Blowby Contribution to Oil Consumption at Different Speed and Load 94
4.1.2 Particle Size Distribution in the Blowby 101
4.1.3 Summary of the Oil Consumption due to Blowby 105
4.2 Oil Evaporation 106
4.2.1 Introduction 106
4.2.2 Experimental Methodology and Conditions 107

4.2.2.1 Oil Specifications 107
4.2.2.2 Experimental Conditions 112
4.2.3 Effect of Cylinder Liner Temperature on Oil Consumption 115
4.2.4 Effect of Oil Volatility on Oil Consumption 118
4.2.5 Estimation of Liner Evaporation 120
4.2.5.1 Analytical Liner Evaporation Model 123
4.2.6 Analysis of Model Results and Comparison with Experiments 131
4.2.7 Summary of the Oil Evaporation Study 139
4.3 Contribution of Different Sources to Total Oil Consumption 140
4.3.1 Separation of Three Different Oil Consumption Sources 141
4.3.2 Variation of the Oil Consumption Sources with Engine Load 144
4.3.3 Variation of the Oil Consumption Sources with Engine Speed 150
4.3.4 Summary of the Contribution of Different Sources to Oil Consumption 153
Chapter 5 Conclusions **155**
Appendices **165**

List of Figures

Figure 1-1 Oil consumption sources 19
Figure 1-2 Schematic of oil transport through the piston-ring-liner system clearances ... 21
Figure 2-1 Baseline oil sulfur content with distillation 29
Figure 2-2 Schematic of oil consumption measurement setup 30
Figure 2-3 Antek® sulfur detector 32
Figure 2-4 Variation of the crankcase volume during one engine cycle 36
Figure 2-5 Schematic of the classification of particles in the SMPS 37
Figure 2-6 Measurement locations of in-cylinder variables 38
Figure 2-7 Schematic of LIF system setup 40
Figure 2-8 Axial position of LIF probes and of different piston regions with crank angle 41
Figure 2-9 Modified engine block for optical access 42
Figure 2-10 LIF window dimensions 42
Figure 2-11 Surface profile along liner and bottom window at the anti-thrust side 43
Figure 2-12 Arrangement of LIF housing sleeve and probe assembly 44
Figure 2-13 Piston scratch mark dimensions 46
Figure 2-14 Surface profile of piston skirt and scratch marks at anti-thrust side 46
Figure 2-15 Sample LIF traces 47
Figure 2-16 Axial positions along liner of different piston region as a function of CA ... 48
Figure 2-17 Side view schematic of engine with mounted pressure transducer adapter .. 49
Figure 2-18 Sample second and third land pressure measurements with the liner pressure transducers at 75% load, 2500 rpm 49
Figure 2-19 Torque at full load (100%) as a function of speed 51
Figure 2-20 Investigated steady state engine operating conditions 51
Figure 2-21 Investigated operating conditions of blowby contribution to total oil consumption 52
Figure 2-22 Description of the ramp transient experiments in load 53
Figure 2-23 Piston and baseline ring-pack geometry 54
Figure 2-24 Details of the ring-pack geometry used for ramp transient experiments 54

Figure 3-1 Schematic of the believed U-flex OCR flank shape after installation..... 57
Figure 3-2 Predicted and measured land pressures and blowby at 75% load, 2500 rpm.. 58
Figure 3-3 Oil consumption at different engine speed and load 60
Figure 3-4 Pressures in different regions and gas flows through ring gap at 25% load, 3500 rpm 61
Figure 3-5 Schematic of the main blowby flow path through the piston-ring-pack with a U-flex oil control ring..... 62
Figure 3-6 Schematic of the transport mechanism of gas flow oil dragging on surfaces . 62
Figure 3-7 Blowby flow rate (liter/minute) at different engine speed and load..... 65
Figure 3-8 Blowby (cm^3/cycle) dependency on engine speed and load 65
Figure 3-9 Sample LIF trace with control volumes of piston land for averaging..... 67
Figure 3-10 Effect of engine speed and load on the oil accumulation on top and 2^{nd} land..... 68
Figure 3-11 Circumferential volumetric gas flow on the second land..... 69
Figure 3-12 Sample 2-D LIF image 74
Figure 3-13 Oil consumption and blowby during transient in load (0% to 100%) at different speeds 75
Figure 3-14 Oil consumption during transient in load and the importance of the initial load at 4000 rpm 76
Figure 3-15 Effect of blowby on oil consumption during ramp transient in load..... 77
Figure 3-16 Predicted and measured land pressures and blowby at no load (0%), 3500 rpm 79
Figure 3-17 Blowby dependency on speed and load with ring-pack used for transient experiments 79
Figure 3-18 Oil accumulation on top land with varying load and speed 80
Figure 3-19 Oil film thickness evolution during ramp transient in load from no load (0%) to full load (100%) at 3500 rpm..... 81
Figure 3-20 Change in oil film thickness after transient in load from no load (0%) to full load (100%) at different speed..... 82
Figure 3-21 Comparison of measured and predicted land pressures at 4200rpm 84
Figure 3-22 Top ring dynamics at 4200 rpm 85

Figure 3-23 Schematic of top ring reverse flutter 86
Figure 3-24 Illustration of the sequence of events during top ring reverse flutter 87
Figure 3-25 Gas flows through top ring groove and gap during reverse flutter at full load (100%), 4200 rpm 88
Figure 3-26 Oil flow during transient at 2500 rpm 91
Figure 4-1 Illustration of the inertial separator 96
Figure 4-2 Typical efficiency curve of an inertial separator 97
Figure 4-3 Oil consumption due to oil entrainment in the blowby gas flow at different speed and load 98
Figure 4-4 Contribution of the oil in the recycled blowby gases to total oil consumption at different speed and load 99
Figure 4-5 Oil loading in the blowby gas flow into the intake manifold system 100
Figure 4-6 Particle mass distribution in the blowby flow of different engines 101
Figure 4-7 Load effect on particle size distribution in the blowby flow at 2500 rpm 102
Figure 4-8 Particle size distribution in the exhaust of a spark ignition engine 103
Figure 4-9 Load effect on droplet volume concentration at 2500 rpm 104
Figure 4-10 Liquid oil particle proportion of total oil in the blowby gases 105
Figure 4-11 Typical operating temperatures on the piston surface at full load 110
Figure 4-12 Comparison of the viscosity of both test oils 111
Figure 4-13 Synthetic oil sulfur content with distillation 112
Figure 4-14 Relation between coolant and liner temperatures at 75% load, 3500 rpm .. 113
Figure 4-15 Effect of coolant outlet temperature on liner temperature at the TDC location of the scraper ring at different load, 3500 rpm 114
Figure 4-16 Investigated operating conditions (evaporation study) 115
Figure 4-17 Oil consumption dependence on liner temperature at different load, 3500 rpm 116
Figure 4-18 Oil consumption dependence on liner temperature at different speed, full load (100%) 117
Figure 4-19 Difference in oil consumption due to oil volatility at different speed and load 119

Figure 4-20 Decrease of oil consumption (as percent of the baseline oil consumption) due to reduction of volatility at different speed and load 120
Figure 4-21 Schematic of the oil consumption mechanisms from the top land 121
Figure 4-22 Oil film thickness distribution at different coolant outlet temperature at 75% load, 3500 rpm 122
Figure 4-23 Schematic of the liner oil evaporation process 123
Figure 4-24 Mass transfer Biot number distribution on the liner for the first two species of the baseline oil at 100% load, 3500 rpm, and 93°C coolant outlet temperature 126
Figure 4-25 Typical cylinder pressure measurement with computed bulk gas temperature 128
Figure 4-26 Variation of the liner temperature distribution for different load conditions at 3500 rpm, standard coolant outlet temperature (a); and for different coolant outlet temperatures at 100% load, 3500 rpm (b) 129
Figure 4-27 Distillation curves of baseline and synthetic oil 130
Figure 4-28 Typical trace of the oil film thickness left on the liner after the intake and expansion stroke 131
Figure 4-29 Oil evaporation dependence on liner temperatures at 75% load, 3500 rpm 131
Figure 4-30 Total oil consumption and predicted liner evaporation dependence on liner temperature at different load, 3500 rpm 133
Figure 4-31 Oil volume held by the top ring and liner oil film thickness after downstrokes at the minor thrust side for 100% load, 3500rpm 134
Figure 4-32 Cumulative total oil evaporation and proportions of the lightest four species during one engine cycle at 100% load, 3500 rpm, and 93°C coolant outlet temperature 135
Figure 4-33 Effect of the liner oil composition variation (baseline oil) on the evaporation at 100% load, 3500 rpm 137
Figure 4-34 Measured total oil consumption and predicted liner evaporation dependence on liner temperature at different load (50%, 75%, and 100%), 3500 rpm. Exponential curve fit to each data set and corresponding R^2 correlation coefficient shown. 138

Figure 4-35 Measured total oil consumption and predicted liner evaporation dependence on liner temperature for synthetic oil at different load (50, 75, and 100%), 2500 rpm. Exponential curve fit to each data set and corresponding R^2 correlation coefficient shown. 139
Figure 4-36 Illustration of the separated oil consumption sources 142
Figure 4-37 Schematic illustrating the separation of the three oil consumption sources 144
Figure 4-38 Effect of engine load on different oil consumption sources and on total oil consumption at 3500 rpm for the baseline oil 144
Figure 4-39 Reverse gas flow through top ring gap at different engine load 146
Figure 4-40 Computed oil flow with reverse gas flow through top ring gap and separated oil transport rate at different engine load 147
Figure 4-41 Effect of engine load on the relative importance of different oil consumption sources to total oil consumption at 3500 rpm for the baseline oil 149
Figure 4-42 Effect of engine speed on different oil consumption sources and on total oil consumption at 100% load for the baseline oil. 150
Figure 4-43 Effect of engine speed on the relative importance of different oil consumption sources to total oil consumption at 100% load for the baseline oil 152

List of Tables

Table 2-1 Test engine characteristics 26
Table 2-2 Relevant baseline oil specifications 29
Table 2-3 Relevant fuel specifications 30
Table 2-4 Blowby meter specifications 35
Table 2-5 LIF specifications 40
Table 2-6 Investigated load transients at constant speed 53
Table 3-1 Average reverse gas flows and oil transport (assuming 1 percent oil loading in the gas) into the combustion chamber at 4200 rpm. 89
Table 4-1 Relevant oil specifications of the test oils 109

Chapter 1 Introduction

1.1 Engine Lubrication and Oil Consumption

The piston assembly creates the boundary between the combustion chamber and the crankcase, therefore it is essential as it provides and maintains the only seal for the high pressure combustion gases. Sealing is accomplished by the piston rings, moving in the ring grooves within the piston and sliding along the liner. The interaction among liner, piston, and rings during engine operation requires sufficient lubrication of the surfaces in relative motion to minimize friction and wear, thereby enhancing the lifetime of the engine. Another task performed by the piston-ring-pack is the supply of oil to all surfaces of relative motion, i.e. to all ring grooves and the liner. This supply of oil, however, must be controlled, because excess oil in regions adjacent to the combustion chamber results in unfavorable oil consumption.

Oil consumption from the piston-ring-liner system significantly contributes to total engine oil consumption [1]. Engine oil consumption is recognized to be a significant source of pollutant emissions in automotive engines. Unburned or partially burned oil in the exhaust gases contributes directly to hydrocarbon and particulate emissions [2][3][4]. Moreover, chemical compounds in oil additives can poison exhaust gas treatment devices and can severely reduce their conversion efficiency [5][6]. Oil consumption is also an important indicator for engine performance and, consequently, customer satisfaction.

The trade-off between the objectives of adequate oil supply for lubrication and minimizing oil consumption has always been a difficult task due to the lack of physical understanding of the oil flow in the piston ring assembly. This inadequate physical understanding of oil transport and consumption has resulted in the empirical development of most piston and piston ring designs. As a part of the effort to comply with increasingly stringent emission standards, engine manufacturers strive to optimize the piston-ring-pack performance in terms of oil consumption and friction. Moreover, to reduce development lead-time and costs, there exists increasing demand for analytical

tools to predict oil consumption and friction. However, the prediction of oil consumption requires an understanding of oil transport and of the contributing oil consumption sources.

1.2 Research on Oil Consumption

Oil consumption from the piston-ring-liner system and from the crankcase ventilation systems are considered to be the major contributors to total engine oil consumption in modern automotive engines.

Studies on crankcase ventilation systems focused on the contribution of the crankcase blowby gases to oil consumption and the performance of oil separators [7][8][9][10][11].

Numerous studies have been carried out to analyze the impact of different parameters of the piston-ring-liner system on oil consumption. Oil consumption was found to be affected by the geometrical details of the piston and the rings [12][13][14][15][16], liner surface finish[17][18][19], cylinder bore distortion[20][21], component temperatures[22], oil properties[23][24], and engine operation conditions such as speed, load, and whether the engine operates in a steady state.

To gain more insight regarding oil consumption sources from the piston-ring-pack, measurements were conducted on the inter-ring pressures and the relative ring positions in the groove [25][26]. In addition, studies of the oil film thickness on the piston and between the rings and liner using the Laser Induced Fluorescence (LIF) technique, determined the oil accumulation characteristics in various engines at different engine operating conditions, showing consistently partial flooding of the piston top, second, and third lands [28][29][30][31][32][33][34][35]. In most of these studies oil consumption mechanism hypothesis were formulated and oil consumption sources were postulated. However, a complete oil consumption model is still out of reach. Among other invariably non-quantitative mechanisms, gas flows have been found to transport oil into the combustion chamber via two paths. First, oil may be dragged or entrained by the reverse gas flow from the second land through the top ring gap and groove, as the second land pressures become greater than the cylinder pressure at the end of expansion and early exhaust stroke. Oil flow through the top ring gap was observed on a one-cylinder research engine at low load conditions when the top ring was pinned [36][37]. Second,

oil mist present in the blowby gases is recycled into the intake manifold. Other hypotheses supported by experimental data relate oil consumption to the mechanical transport of liquid oil into the combustion chamber due to inertia forces caused by acceleration and deceleration of the piston. Oil throw off from the top land was also visualized in one-cylinder research engines at low load conditions [38][39]. Other, experimental studies show that evaporation from the liner and piston may be a substantial contributor to oil consumption [22][23][24]. A number of theoretical approaches studied the oil evaporation from the liner and found the evaporation process sensitive to oil composition and liner temperatures [40][42].

However, oil from the crankcase has to traverse many paths before being transported into the combustion chamber via these routes. Recently, extensive and reliable ring-pack models have been developed at the MIT (Sloan Automotive Laboratory) that predict ring dynamics, gas flows, and ring-liner lubrication to estimate oil transport along the piston, along the liner, and from liner to piston [43][44][45]. Moreover, physical models for the oil transport mechanisms along the piston have been suggested utilizing 2-D LIF observations on a one-cylinder research engine derived from the production engine used for this study [46]. Despite these efforts, further experimental and modeling work are still needed in order to connect these predicted driving forces and oil transport with oil consumption. In summary, so far little work has been done combining oil consumption measurements, in-cylinder measurements and advanced modeling. Consequently, due to the complex character of oil consumption and lack of comprehensive experimental data, a complete picture that describes the contribution of different sources to total oil consumption has not been obtained for any engines.

1.3 Oil Consumption Sources and Transport Mechanisms in SI Engines

Five possible oil consumption sources have been suggested to contribute to total oil consumption of spark ignition engines during engine operation. These sources are illustrated in Figure 1-1.

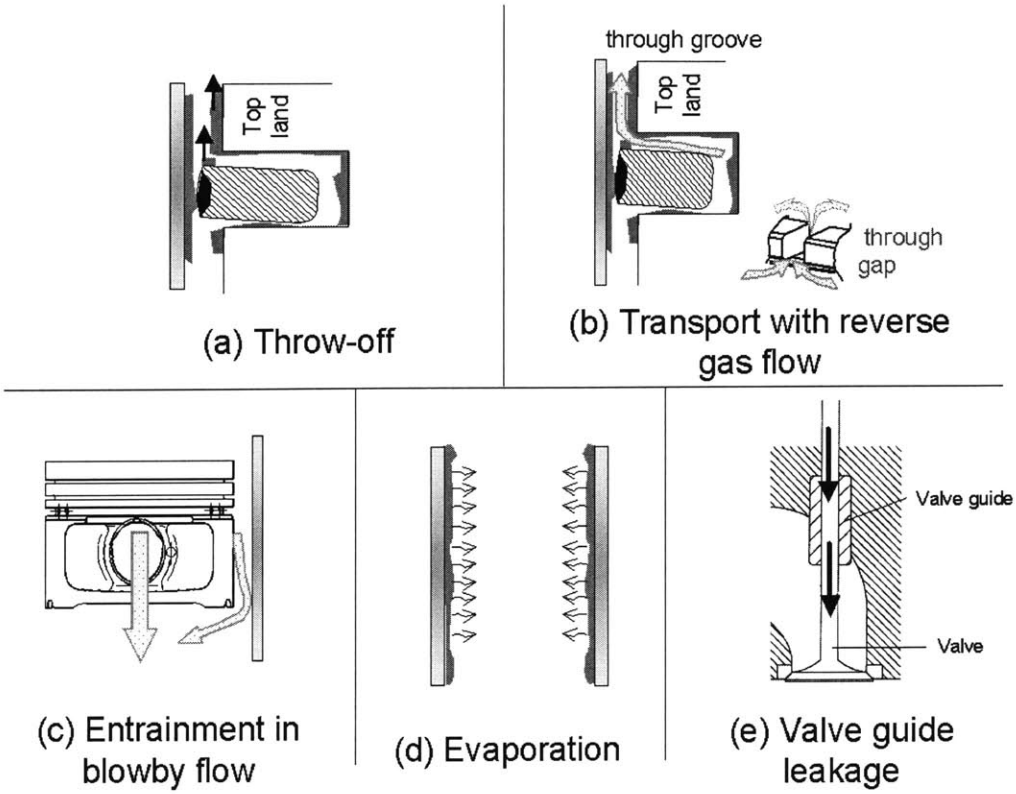

Figure 1-1 Oil consumption sources

As indicated earlier, the oil accumulation on the piston's top land may become high during low load conditions [38][39]. This oil may be thrown off the top land (Figure 1-1a) directly to the combustion chamber due to inertia forces resulting from the acceleration and deceleration of the piston assembly. The importance of this driving mechanism is dependent on the accumulated oil film on the top land and ring.

In other studies direct oil transport to the combustion chamber was found to depend on gas flow in the piston-ring-liner system. Gas pressures in the second land clearance, i.e. the volume between the top ring and second ring, can become greater than the combustion chamber pressure during some periods of the engine cycle. This pressure gradient will cause a reverse gas flow into the combustion chamber through the top ring gap and around the top ring groove if the top ring looses its stability in the groove. The reverse gas flow may transport oil in both liquid and mist form (Figure 1-1b) into the combustion chamber. This transport mechanism is supported by visualization studies of

the oil distribution in the piston-ring-pack, when the top ring was pinned. In these studies, oil flow through the top ring gap towards the combustion chamber was observed during low load conditions [36][37].

Oil mist, also present in the recycled blowby gas flow (Figure 1-1c), has been found to enter the combustion chamber via the intake manifold system. Experimental studies on different engines quantified the contribution of oil in the crankcase ventilation gases to total oil consumption [1][7]. It was found that this oil consumption source could contribute significantly, depending on the specific engine, to total oil consumption.

Oil evaporation (Figure 1-1d) from the piston-ring-liner system is also believed to contribute significantly to total oil consumption, especially during severe operation conditions when the thermal loading of engine components is high. Several experimental results indicated that oil evaporation from the liner and piston might contribute substantially to oil consumption [23][24][22]. In addition, a number of purely theoretical approaches studied oil evaporation from the liner and found sensitivities in the evaporation process to oil composition and to component temperatures [40][41][42]. However, uncertainties in predictions of the oil evaporation rate remain in the order of oil consumption.

In earlier spark ignition engine designs, oil transport from the cylinder head through the valve guide into the intake port (Figure 1-1e) contributed to oil consumption during part load conditions, when the intake manifold pressure is significantly below atmospheric. However, this oil leak path is effectively sealed in modern engines by employing positive valve stem seals [1]. Therefore, this oil consumption source is considered to contribute little to the total oil consumption in today's spark ignition engines.

All of these consumption sources contribute to total oil consumption during engine operation. All mechanisms, except oil transport through the valve guide, are related to the performance of the piston assembly. Whether one or the other mechanism dominates depends mostly on the engine design specific oil transport rates, engine operating parameters, and lubricant properties. The oil must traverse a complex course before being transported into the combustion chamber, as indicated in Figure 1-2.

The difficulty in modeling oil consumption lies in predicting oil transport, and the amount of oil present in the clearances of the partially flooded piston-ring-liner system. Therefore, the key to understand oil consumption and its sources is oil transport in the piston-ring-liner system to the consumption regions. The oil transport rate to the upper piston regions is governed by different mechanisms in different regions, such as gas flow, inertia forces due to piston movement, and interactions between the rings and grooves as well as between rings and liner. When oil is on the piston lands it is moved by both inertia force and the interfacial shear force created by gas flow. When oil is inside the ring grooves, its flow is controlled by the gas flow and the pumping effects caused by ring motion. Oil mist present in the gas is transported to different regions with the gas flow. Oil transport along the liner and from liner to piston is governed by ring-liner lubrication.

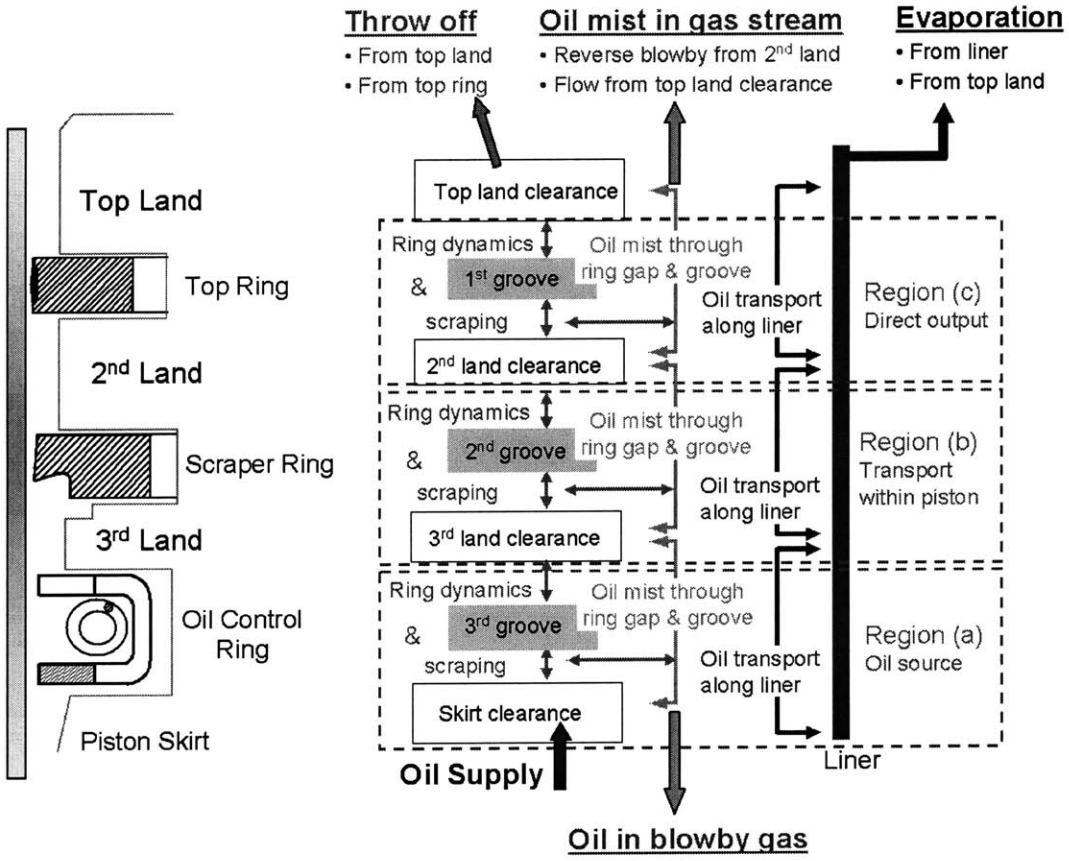

Figure 1-2 Schematic of oil transport through the piston-ring-liner system clearances

All these driving forces for oil transport are sensitive to engine speed and load. Therefore, to understand and model oil consumption sources it is critical to isolate different driving forces for oil transport by changing engine operating conditions, and then to connect them with oil consumption. To investigate the effects of engine operating conditions on the flow and accumulation of oil, the piston-ring-pack region is subdivided into three regions (see Figure 1-2):

Region (a): This region includes the clearances in the upper piston skirt and the oil control ring groove. The oil supplied from the piston skirt must pass region (a) to reach the upper piston ring-pack. Therefore, region (a) controls the gross oil on the liner and determines the supply of oil to the upper piston regions.

Region (b): This region includes the clearances in the third land and the second ring groove. This region also controls the oil on the liner and determines the oil supply to the second land and top ring groove.

Region (c): This region includes the clearances on the second land and top ring groove. The contribution of the direct oil consumption sources is mainly determined in this region. Oil removal from region (c) to the crown land both with the reverse gas flow or from the groove is theorized to be irreversible, and thus considered as oil consumption. This region determines the oil left on the liner during down strokes and therefore affects oil evaporation and ring scraping. High gas flows through the rings gaps affect the oil entrainment in the blowby gases.

1.4 Project Scope

A major difficulty in the development of analytical tools to predict oil consumption is the lack of understanding of the contribution of major oil consumption sources to total engine oil consumption. This thesis work is intended to quantify important oil consumption sources and to advance the overall understanding of the contribution of different oil transport mechanisms to oil consumption in a spark ignition engine. It

characterizes oil transport, oil consumption, and the contribution of different oil consumption sources at different engine operating conditions, by combining comprehensive measurements and physics-based modeling work. Emphasis was placed on the investigation and quantification of major oil consumption sources during different steady state operating conditions and on the analysis of the oil consumption behavior during ramp transients in load.

On a modern, four-cylinder production spark ignition engine an extensive diagnostic system was developed and implemented to measure and identify key oil consumption sources and their contribution to total engine oil consumption. This diagnostic system has the capability to simultaneously measure oil consumption, blowby, and in-cylinder variables such as oil film distribution in the piston-ring-pack, inter ring pressures, cylinder pressure, and liner temperatures. The experimental setup is presented in Chapter 2.

In Chapter 3 the influence of different steady state engine speed and load conditions on oil consumption, blowby, and in-cylinder parameters is analyzed. The simulation codes developed at MIT were applied in order to evaluate driving forces for oil transport and oil consumption such as gas flow in different regions, ring dynamics, and ring liner lubrication. Furthermore, an extensive study was conducted to measure and analyze the oil consumption behavior during engine load transients at constant speed. Emphasis was placed on the analysis of the oil consumption behavior during transients from low load to full load by combining oil consumption measurements, in-cylinder measurements, and theoretical modeling.

In Chapter 4 the contribution of different oil consumption sources to total engine oil consumption is characterized and quantified at different steady state speed and load conditions. First, the contribution of oil entrained in the blowby gas to total oil consumption is analyzed. Then the impact of oil evaporation to oil consumption is characterized. A physics-based liner evaporation model is proposed and verified experimentally by varying oil volatility, liner temperature, and engine operating conditions. Finally, the contributions of oil evaporation, oil entrained in the blowby gas flow, and oil flow through various pathways into the combustion chamber to total oil consumption are assessed by combining the experimental and modeling results.

(This page was intentionally left blank)

Chapter 2 Experimental Setup

2.1 Experimental Objectives

A critical issue in experimental investigations is the choice, development, and implementation of suitable experimental techniques. In this section, the experimental objectives and the technical approach to meet these objectives are discussed.

As described in Section 1.3, oil transport in the piston-ring-liner system is governed by ring-liner lubrication, piston and ring dynamics, and gas flow. All these driving forces vary with engine operating conditions, but can be predicted using computer models that were developed at MIT (see Section 3.2). However, these models require in-cylinder parameters such as cylinder pressure traces, component geometries during engine operation, oil volumes accumulated on different regions of the piston, and component thermal conditions. All parameters, but in particular the thermal expansion of component geometries, change with operating conditions and need to be estimated for each condition. These unknown parameters can, however, be adjusted within a reasonable range, until the model predictions match with measurements of land pressures and blowby. In addition, thermal conditions on the cylinder liner are believed to directly affect the oil evaporation process. Moreover, oil consumption has been found to vary for identical engine designs at same operating conditions. This is most likely caused by the variations in oil transport inside the piston-ring-pack, and thus in oil consumption sources. Therefore, to thoroughly study oil consumption and its sources it is essential to obtain simultaneous measurements of oil consumption and in-cylinder variables affecting oil transport to the main consumption sources.

Consequently, for this study a comprehensive experimental setup was needed with the capability to measure not only oil consumption, but also blowby and in-cylinder variables that govern the oil transport and consumption mechanisms. The experimental objectives can be summarized as follows:

1 - Provide relatively fast and accurate measurements of total engine oil consumption and oil consumption sources.
2 - Provide blowby measurements.
3 - Provide measurements of in-cylinder parameters that affect oil transport in the piston-ring-liner system and thus oil consumption.
    - Measurements of the oil film behavior in the piston-ring-pack
    - Measurements of inter-ring and cylinder pressures
    - Measurements of thermal conditions on the cylinder liner

2.2 Test engine: Production Spark Ignition Engine

A typical, modern, four-cylinder production spark ignition engine was used as the test engine. The engine characteristics are shown in Table 2-1.

Engine Type	Port injected spark ignition engine
Number of cylinders	4
Displacement	2.01 liter
Bore	86.25 mm
Stroke	86.00 mm
Maximum power	97.4 kW at 5500 rpm
Maximum torque	180 Nm at 4200 rpm
Compression ratio	10.4:1

Table 2-1 Test engine characteristics

The test engine was modified to allow the implementation of several experimental techniques and to control different engine operating conditions. The cylinder head was modified to fit pressure transducers on the third and fourth cylinder for cylinder pressure measurements. In addition, the engine block and the liner of the third cylinder were machined to allow the installation of liner pressure transducers, thermocouples, and silica windows for optical access to the piston-liner interface for oil film thickness

measurements. The implementation of these in-cylinder measurement techniques caused the penetration of the water jacket that surrounds the liner. The problems arising from the penetration of the water jacket, and the precautions taken to address this problem, will be described in Section 2.3.2.

To control the coolant temperature, and thereby the engine thermal conditions, the engine thermostat was removed. The engine coolant from an external coolant tank (capacity of approximately 30 liters) was circulated unrestricted through the engine block. Before entering the engine block, the coolant was cooled in a heat exchanger by city water. Controlling the flow rate of the city water through the heat exchanger regulated the coolant temperature. The city water flow rate was controlled by a regulating valve that could be adjusted to the desired temperature. The heat capacity of the additional coolant slowed the engine's thermal response to changes in the operating conditions.

2.3 Measurement Techniques

An extensive diagnostic system was implemented on the test engine to measure oil consumption, blowby, and the in-cylinder variables oil distribution in the piston-ring-pack, cylinder pressure, land pressures, and liner temperatures. In this section, the applied experimental techniques are described and discussed.

2.3.1 Total Output Measurements

2.3.1.1 Oil Consumption

Typical oil consumption rates of modern passenger car engines are on the order of 10 g/hour. Due to the small amount of oil consumption, its measurement has been always a challenging task for researchers in the automotive industry. However, several oil consumption measurement methods have been developed. Traditional methods such as weight and drain, and continuous weight method require several hours of engine operation. The length of the time required for each measurement introduces also potential interferences with other mechanisms and produces erratic results. For example,

it is well known that the oil consumption rate measurements can be negative due to the dilution of fuel in the engine oil.

Other methods, such as the radioactive tracer methods, have been developed to determine oil consumption by adding radioactive tracers into the oil and measuring the concentration of the tracer in the exhaust gases. The measurement times of these methods are on the order of several minutes, but the handling of the radioactive material requires special equipment and procedures.

One alternative tracer method to measure oil consumption is the sulfur tracer technique. This technique requires high sulfur oil and low sulfur fuel, and monitors the sulfur content in the exhaust gases to determine the engine oil consumption rate. Researchers in the automotive industry have successfully demonstrated the capability of the sulfur tracer technique to measure oil consumption during steady state and transient operating conditions [47][48][49][50][51]. Moreover, this method has the capability to measure the contribution of oil entrained in the blowby gases to total oil consumption. The contribution of the blowby gas to oil consumption can be obtained by determining the difference in oil consumption with and without blowby gas return to the intake system. For this study, the sulfur tracer technique was implemented on the test engine to measure engine oil consumption. The specific requirements of the oil and fuel properties necessary to apply the sulfur tracer technique are described next.

2.3.1.1.1 High Sulfur Oil

By considering typical oil consumption rates for this engine, and the accuracy of the sulfur detector, it was found that the sulfur concentration in the oil needed to be around 1.5% [wt.] in order to have reliable measurements throughout the engine operating range. Oil transport into the combustion chamber is in liquid and vapor form (evaporated oil). As discussed in Section 4.2 the oil evaporation process is in general selective. The major contribution to the total evaporation is from species at the light end. Therefore, a consistent sulfur concentration in the oil is required throughout the oil distillation curve in order to assume that the consumed oil (in liquid and vapor form) in the exhaust has the same concentration of sulfur as in the original oil. Only then, can the sulfur concentration in the exhaust gas be used as indicator for the consumed oil. Lubrizol Corp.

formulated a special high sulfur baseline oil with the desired properties. The sulfur content versus distillation of the baseline oil is illustrated in Figure 2-1. This property was obtained by stepwise distillation of the oil (ASTM D5236) and by measurements of the sulfur contents of each distillate (ASTM D 4294). The relevant oil properties of the Baseline oil are shown in Table 2-2.

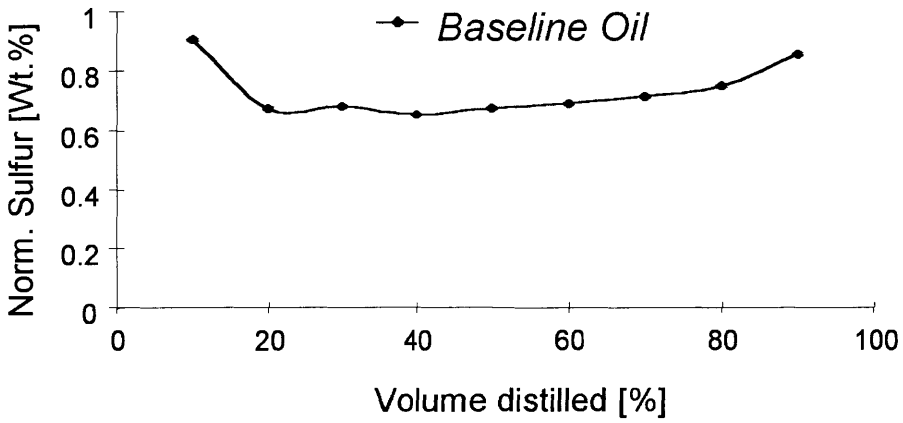

Figure 2-1 Baseline oil sulfur content with distillation

Baseline Oil (Mineral)		**ASTM D**
SAE Viscosity Grade	10W-30	
Sulfur [wt. %]	1.51	1552
Volatility: GCD % off @ 371° C	11.6	
Noack	16.8	5800
Kinematic Viscosity @ 100°C [mm^2/s]	10.77	445
HTHS viscosity [cP]	3.04	4683

Table 2-2 Relevant baseline oil specifications

2.3.1.1.2 Low Sulfur Fuel

In order to utilize the sulfur in the engine oil as the tracer for oil consumption measurements, it is necessary to minimize other sulfur sources. Sulfur in the gasoline can contribute to the sulfur in the exhaust gases, and could mask the actual sulfur-level in the withdrawn sample. To minimize this source of sulfur, a low sulfur research fuel was used with a sulfur level below 2 ppm [wt.]. Table 2-3 summarizes the relevant fuel specifications.

Low Sulfur Fuel	
Sulfur [wt. ppm]	< 2

Table 2-3 Relevant fuel specifications

2.3.1.1.3 Oil Consumption Measurement Setup

The oil consumption measurement setup, as shown in Figure 2-2, consists of four elements. These are the exhaust sampling and analysis section, the air flow meter, the lambda (λ) sensor, and the data acquisition system.

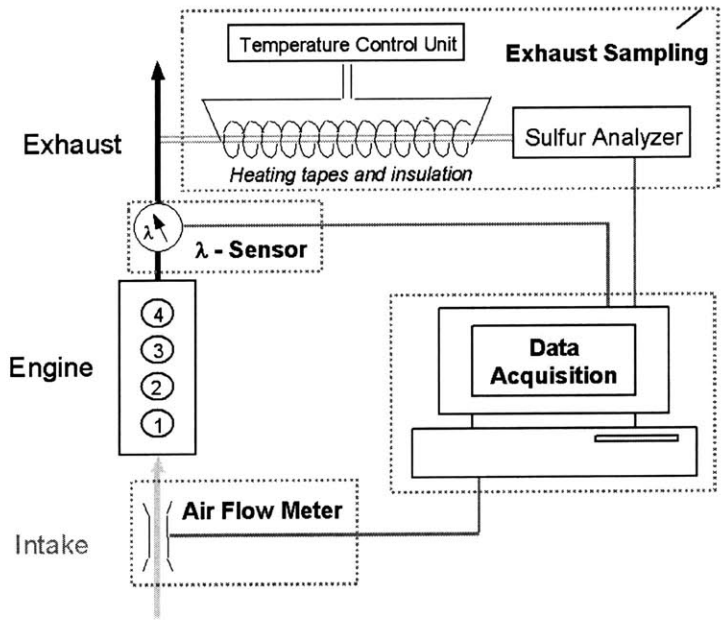

Figure 2-2 Schematic of oil consumption measurement setup

The key element of the system is the exhaust sampling and analysis section. A representative sample from the undiluted exhaust is withdrawn and directed through the sampling line to the sulfur analyzer. The sampling line consists of stainless steel tubing (Grade 314) to ensure resistance to corrosion when exposed to sulfur dioxide (SO_2). An important variable in the design of the sampling system is the sampling line temperature. The transport of the hot exhaust gas stream, which contains particulates, might lead to deposition on cold walls. This process, also known as thermophoresis, could cause plugging of the sampling line. Unburned hydrocarbons in the sample could also condense on the sampling line walls. Both of these phenomena, if occurring during measurements, could result in erratic oil consumption measurements. Therefore, the sampling line was heated with a flexible electrical heater and insulated with fiberglass tape to maintain a high wall temperature that prevents thermophoresis and condensation of hydrocarbons. A temperature control unit regulated the power supply to the heater and maintained the sampling line at a temperature of 300° C.

An Antek® Sulfur-Analyzer (Model R6000 SE) was used to detect the sulfur concentration in the exhaust gas sample. Figure 2-3 illustrates the components of the analyzer in detail. The analyzer is designed as a flow through analyzer. The sample must be conditioned before entering the sulfur detection part of the analyzer. The sample gas is withdrawn by a bellows pump and directed into a furnace for pyrolysis. A controlled flow rate of the pyrolised gas is sent to a second furnace through a fixed restriction transfer tube. Before entering the second furnace, the sample is mixed with additional oxygen to oxidize unburned hydrocarbons, particulates and sulfur compounds contained in the sample. Condensation of water in the cooled detection part of the analyzer could lead to sulfur dioxide absorption and alter the oil consumption measurements. Therefore, after the second furnace, two permeable membrane dryers remove the water in the sample gas before it enters the detector. In the detector, the conditioned sample exhaust gas (oxidized and dried) is mixed with Ozone (O_3) and exposed to ultraviolet radiation in the fluorescence chamber. The UV light brings the sulfur dioxide in the sample to an excited state, which results in a fluorescence emission. A photo multiplier tube detects the fluorescence emission intensity, which has a linear relationship with the sulfur dioxide concentration in the sample gas.

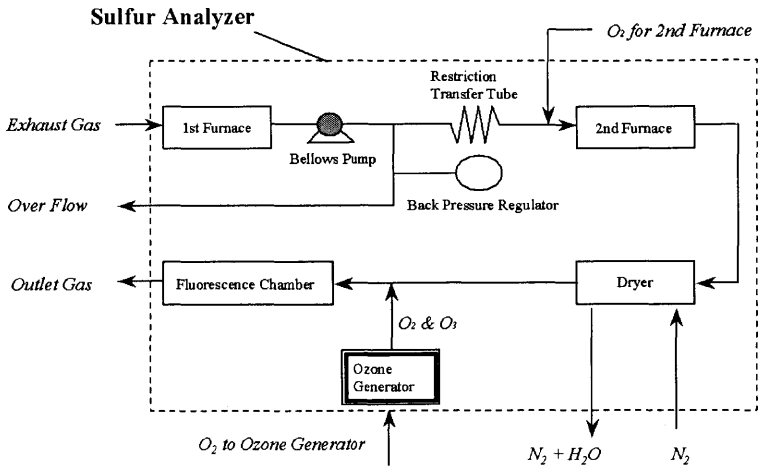

Figure 2-3 Antek® sulfur detector

As discussed above, oil consumption can only be determined by measuring the sulfur content in the exhaust, the airflow rate, and the fuel flow rate. The airflow rate was measured with a laminar flow. A λ - sensor measured the air/fuel ratio relative to the stoichiometric air/fuel ratio in the exhaust system near the exhaust gas sampling location. The fuel flow rate was calculated using the air/fuel ratio measurements, the airflow measurements, and the fuel analysis results.

A LabVIEW based data acquisition program was written to simultaneously take raw data, calculate the oil consumption rate, and display it along with other relevant engine parameters. By displaying the real time oil consumption, the program allows the test conductor to immediately check the data for validity, and to intervene if necessary anytime during the tests. Therefore, the efficiency of taking measurements was improved by combining previously separate steps of data acquisition and analysis.

2.3.1.1.4 Oil Consumption Formula

An oil consumption formula has been derived using the measured sulfur dioxide concentration in the exhaust, the airflow rate, the air/fuel ratio, and the mass fractions of sulfur in the oil and fuel. In this section, the basic assumption and essential relations of the oil consumption formula will be described:

The consumed sulfur mass from the oil can be calculated from mass conservation,

$$\dot{m}_{S,Oil} = \dot{m}_{S,Wet\ Exhaust} - \dot{m}_{S,Fuel} - \dot{m}_{S,Air}\ ; \tag{2.1}$$

where $\dot{m}_{S,Oil}, \dot{m}_{S,Fuel}, \dot{m}_{S,Wet\ Exhaust}, \dot{m}_{S,Air}$ are mass flow rates of the sulfur in oil, fuel, wet exhaust gas, and air respectively. The sulfur content of air is negligible (in the order of 10 ppb), therefore

$$\dot{m}_{S,Air} = 0 \tag{2.2}$$

With

$$\dot{m}_{S,Oil} = \dot{m}_{Oil} * \xi_{S,Oil}, \tag{2.3}$$

$$\dot{m}_{S,Fuel} = \dot{m}_{Fuel} * \xi_{S,Fuel}, \tag{2.4}$$

$$\dot{m}_{S,Wet\ Exhaust} = \dot{m}_{Wet\ Exhaust} * \xi_{S,Wet\ Exhaust}; \tag{2.5}$$

where $\xi_{S,Oil}$, $\xi_{S,Fuel}$, $\xi_{S,Wet\ Exhaust}$ are the mass fractions of sulfur in oil, fuel, and exhaust respectively. Substituting equations (2.2), (2.3), (2.4), (2.5) into (2.1):

$$\dot{m}_{Oil} = \frac{1}{\xi_{S,Oil}}\left[\dot{m}_{Wet\ Exhaust} * \xi_{S,Wet\ Exhaust} - \dot{m}_{Fuel} * \xi_{S,Fuel}\right]. \tag{2.6}$$

From mass conversation and

$$\frac{\dot{m}_{Air}}{\dot{m}_{Fuel}} = L = \lambda * L_{St}, \tag{2.7}$$

where L is the air/fuel ratio, and L_{St} is the stoichiometric air/fuel ratio, it follows that

$$\dot{m}_{Wet\ Exhaust} = \dot{m}_{Air} + \dot{m}_{Fuel} + \dot{m}_{Oil} \approx \dot{m}_{Air}\left(1 + \frac{1}{L_{St} * \lambda}\right). \tag{2.8}$$

The mass fraction of sulfur in the exhaust can be written as

$$\xi_{S,Wet\ Exhaust} = \psi_{S,Wet\ Exhaust} * \frac{M_S}{M_{Wet\ Exhaust}}\ ; \tag{2.9}$$

Where $M_{Wet\ Exhaust}$ is the molecular weight of wet exhaust, M_S is the molecular weight of sulfur (32g/mol), and $\psi_{S,Wet\ Exhaust}$ is the molar fraction of sulfur in wet exhaust. With

$$\psi_{SO_2,Wet\ Exhaust} = \psi_{S,Wet\ Exhaust} \; ; \tag{2.10}$$

where $\psi_{SO_2,Wet\ Exhaust}$ is the molar fraction of sulfur dioxide in wet exhaust. The molar fraction of sulfur dioxide in the wet exhaust may be written as

$$\psi_{SO_2,Wet\ Exhaust} = \psi_{SO_2,Dry\ Exhaust} * \left(1 - \frac{\dot{n}_{H_2O}}{\dot{n}_{Wet\ Exhaust}}\right); \tag{2.11}$$

where $\psi_{SO_2,Dry\ Exhaust}$ is the molar fraction of sulfur dioxide in dry exhaust, and $\dot{n}_{H_2O}$ and $\dot{n}_{Wet\ Exhaust}$ are the moles of water and wet exhaust respectively. Substituting (2.8), (2.9), (2.10), (2.11) into (2.6) results in the final form of the oil consumption formula:

$$\dot{m}_{Oil} = \frac{\dot{m}_{Air}}{\xi_{S,Oil}} * \frac{1}{\lambda * L_{St}} \left(\psi_{SO_2,Dry} * \frac{M_S}{M_{Wet\ Exhaust}} * [1 + \lambda * L_{St}] * \left(1 - \frac{\dot{n}_{H_2O}}{\dot{n}_{Wet\ Exhaust}}\right) - \xi_{S,Fuel} \right) \tag{2.12}$$

2.3.1.2 Blowby

Blowby is the leakage of combustion gases through the piston-ring-liner system into the crankcase. It constitutes combustion gases, unburned mixture, and lubricating oil. Some portion of the entrained oil is present as liquid particles. The blowby gases are in general fed into the intake manifold by a positive crankcase ventilation system to prevent the emission of pollutants in the blowby into the atmosphere. However, as for reasons explained in Section 2.1 it was essential for this study to measure the blowby flow rate into the crankcase. To do so, an accurate flow meter was installed that was based on the Von Kármán-vortex shedding principle. Details of the blowby flow meter are summarized in Table 2-4.

Principle	Von Kármán-vortex shedding
Range	4-100 [l/min]
Accuracy	< 1% of reading

Table 2-4 Blowby meter specifications

The flow meter was not assembled directly into the line of the blowby flow path to the intake system, because of the nature of blowby. The blowby is a pulsating flow with periods when the flow reverses its direction, even though the average flow rate is out of the crankcase. The pulsations are mainly caused by volume changes in the crankcase due to the kinematics of the crank mechanism. The volume displaced by a descending piston corresponds to the swept volume of an ascending piston only during piston reversals. On the other hand, at mid stroke, the total crankcase volume is decreased to a minimum. Figure 2-4 shows the estimated volume fluctuation for the test engine during one engine cycle. The mean gas volume inside the crankcase should be in the order of several liters. This variation of the crankcase volume (~ 0.1 liter) during one stroke generates pressure fluctuation and high gas flows inside the crankcase. The crankcase pressure fluctuations may generate flow pulsations in the ventilation system. These flows can be higher than the actual average blowby flow rate (order of 0.002 liter per cycle; see Section 3.2). The flow pulsation frequency is twice the frequency of the crankshaft and therefore determined by the engine speed.

However, the blowby meter is optimized to measure flows only in one direction. If installed without any modifications into the blowby flow path, the flow meter may indicate higher flow rates than actual due to the flow reversals. Therefore, a damping system was placed upstream of the meter to minimize the flow fluctuations. This system consisted of a large damping tank and hoses connecting the tank to the engine and to the flow meter. The damping system was tested by gradually increasing the volume of the damping tanks and measuring the blowby flow with each damping configuration. No difference was found between the blowby measurements for each configuration, and therefore it was concluded that the damping system had adequate performance for this application.

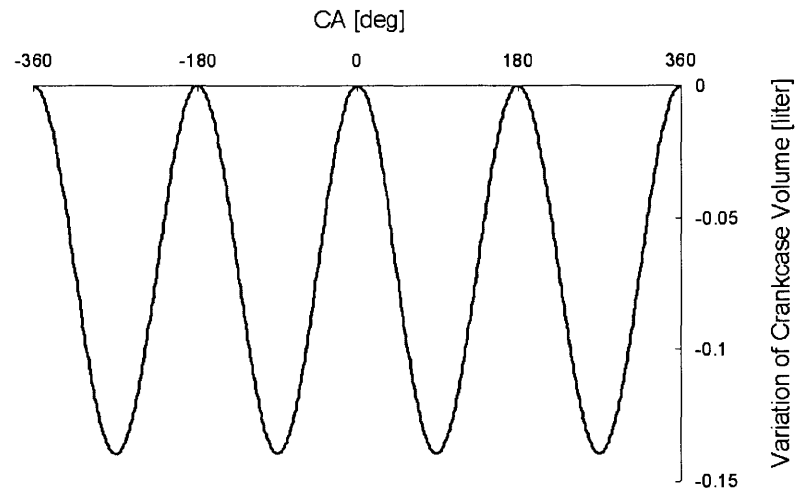

Figure 2-4 Variation of the crankcase volume during one engine cycle

2.3.1.3 SMPS

A Scanning Mobility Particle Sizer (SMPS), produced by TSI incorporated, was used to measure the particle size distribution in the blowby gases at several steady state engine speed and load conditions. The SMPS operates as follows. A vacuum pump draws the measurement sample through an impactor into an Electrostatic Classifier. In the classifier, the sample gas passes through a Kr-85 Bipolar Charger, where the particles in the flow are charged. Then, the sample gas is directed through an annulus, in the center of which is an electrostatically charged tube with a slit at the end that generates an electrical field. The charged particles in the sample flow are drawn towards the central tube through a flow of filtered sheath air. The mobility of the particles in the sample flow is a function of particle diameter, which determines the aerodynamic drag on the particle, and the charge, which determines the force exerted on the particle due to the electrical field. Only particles with a specific mobility are drawn into the slit on the charged tube. The average mobility of the particles, at given flow rates and geometries, are determined by the charge of the central tube. Figure 2-5 shows a schematic of the classification in the annular tube. The classified particles are then counted optically in a Condensation Particle Counter (CPC). To determine the particle size distribution the charge on the

central tube is gradually increased and the particles with different mobility are classified and counted. A software algorithm corrects for the charge distribution of the particles and determines the actual particle size distribution. Additional details of the SMPS system can be found in [27].

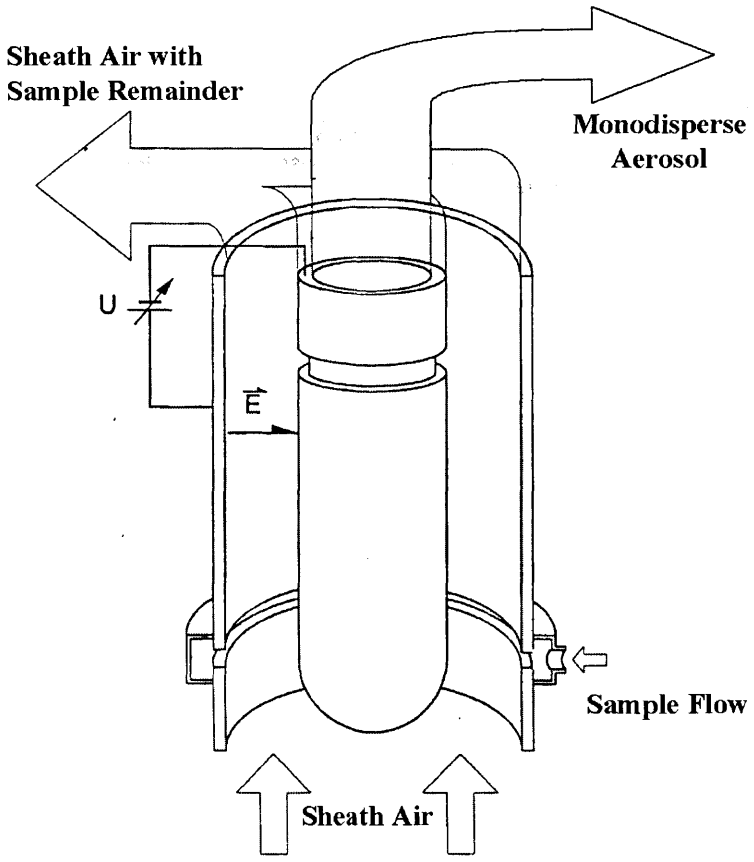

Figure 2-5 Schematic of the classification of particles in the SMPS

2.3.2 In-cylinder Measurements

This section describes the techniques used to measure engine in-cylinder variables and discusses their application on the test engine.

The engine block was modified in the third cylinder to implement the in-cylinder measurement probes. The one-point Laser Induced Fluorescence (LIF) System was applied to gain detailed information of the oil distribution along the piston-ring-pack. Piezoelectric pressure transducers positioned along critical positions on the cylinder liner

provided land pressure traces and transducers mounted to the cylinder head provided cylinder pressure traces. Thermocouples were installed along the cylinder liner to measure liner temperatures. The circumferential positioning of these measurement probes on the engine was primarily determined by the engine accessibility to the test conductor. LIF measurements at different positions can be conducted by mounting the fiber optical cable to the desired LIF window position on the liner. This measurement procedure during engine operation requires continuous engine accessibility, and conditions that allow for physical contact with the engine block. Thus, all LIF windows were installed around the anti-thrust side (intake manifold side) due to the lower component temperatures and the convenient accessibility along the liner. Since the liner pressure and temperature probes require no handling after the installation, these probes were located circumferentially around the thrust-side of the cylinder (exhaust manifold side of engine). Figure 2-6 illustrates the positioning of the measurement probes implemented in the third cylinder.

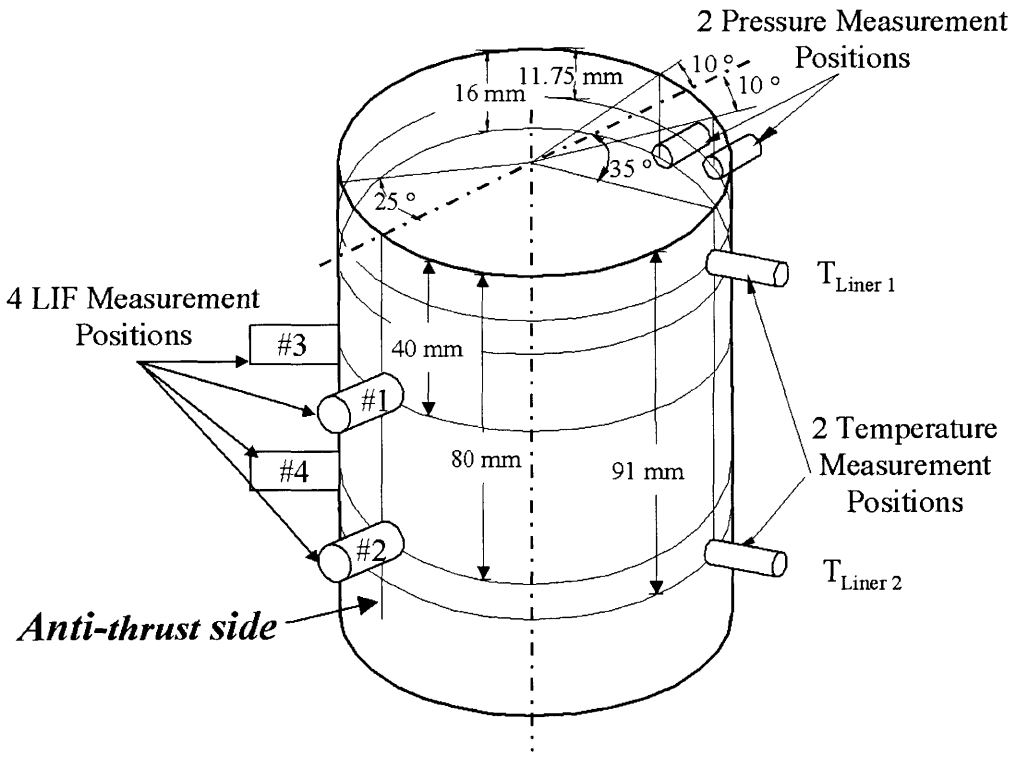

Figure 2-6 Measurement locations of in-cylinder variables

2.3.2.1 Laser-Induced-Fluorescence (LIF) System

Fluorescence can be defined in a simplified description as a three-stage electronic transition process. Certain organic molecules absorb electromagnetic radiation and are excited from the ground electronic state E_0 to an excited electronic state E_1. After excitation, the molecules undergo collisional deactivation with their environment. This results in partial dissipation of their excitation energy to an intermediate electronic state E_1^*. Then the excited molecules return to a lower electronic state and radiation emission occurs. The emitted radiation is known as fluorescence if the return from the excited to the ground electronic state occurs without a significant time delay (longer than1 second). A fluorescence molecule remains in the excited state usually for 10^{-8} to 10^{-9} seconds before returning to the ground state. Due to the partial dissipation of energy in the excited state, the emitted radiation energy is lower than the corresponding absorbed radiation and thus has a longer wavelength.

In this study, the Laser Induced Fluorescence (LIF) System was used to quantify the oil film thickness (OFT) between the piston rings and liner, and to quantify the oil accumulation on the piston lands during engine operation. The LIF System was developed at the Sloan Automotive Laboratory (MIT) and its capabilities were demonstrated in previous studies [28][29][30][32][33]. In these studies, oil was doped with fluorescing dye to increase the natural fluorescence activity of the engine oil to enable the measurements of oil film thickness in the piston-ring-liner system. It was theoretically demonstrated that for low dye concentration and thin lubricant films, the relationship between the film thickness and intensity of the light emitted from the dye was linear. To increase this linear range to thicker films, such as in the piston-ring-pack region, the concentration of the fluorescing dye was minimized. However, the dye concentration was high enough to maximize the fluorescence signal to noise ratio [28].

For this application, the selected fluorescent dye was Coumarin 523 with a concentration of 1.0 * 10-4 mol/liter in the lubricant, as suggested in [28]. The LIF System can be described as follows: The laser beam, produced by a Helium-Cadmium laser (441.6 nm), is directed through a bifurcated fiber optics cable into the LIF focusing probe. In the probe, a conventional lens system focuses the laser light onto the lubricating oil film on the piston and ring surface. The dye molecules solved in the oil

are excited by the laser light and undergo a fluorescence process. The fluoresced light is picked up by the bifurcated fiber optics and directed through an optical filter (495nm) - to block any reflected laser light - to the photomultiplier tube. Figure 2-7 shows a schematic of the LIF setup on the test engine. Table 2-5 summarizes the principal specifications of the LIF technique.

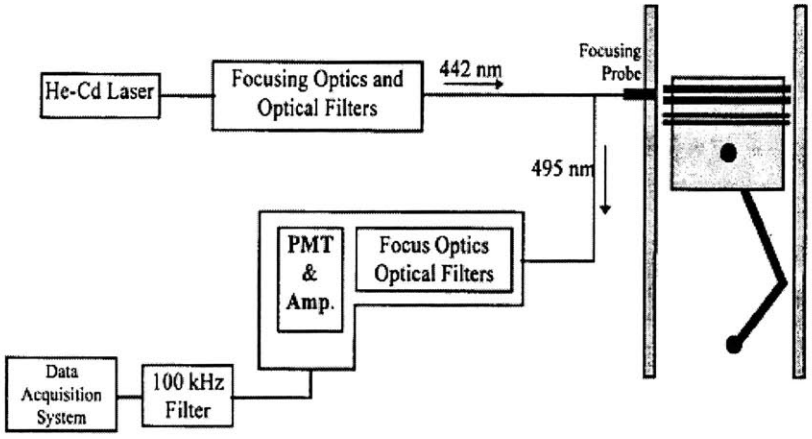

Figure 2-7 Schematic of LIF system setup

Laser	Helium-Cadmium
Power	~ 8 [mW]
Excitation Wavelength	441.6 [nm]
Dye	Coumarin 523
Wavelength of Max. Fluorescence	495 [nm]
Silica window transmission	90 [%]

Table 2-5 LIF specifications

The application of the LIF System requires several modifications to the engine block, liner, and piston. First, the detailed axial and circumferential LIF window locations on the engine liner were determined for optical access into the combustion chamber. It was necessary to position the windows to allow the measurements of the oil distribution on the entire piston belt and upper piston skirt surface. Therefore, two LIF locations were

selected on the anti-thrust line on the same vertical line 40 and 80mm from the top of the liner. In addition, two other probe locations were specified at the same axial position, but 25° clockwise away from the anti-thrust side to investigate any effects of bore distortion and piston secondary motion on oil accumulation on the piston. Figure 2-8 illustrates the axial position of the LIF windows on the liner, and the instantaneous positions of different piston regions as a function of crank angle during the compression and exhaust strokes. As the piston reciprocates through the engine cycle, different regions on the piston pass a window location at different crank angle periods. The instantaneous positions of the piston regions during the intake and exhaust strokes are identical to the expansion and compression strokes, respectively, and thus are not shown.

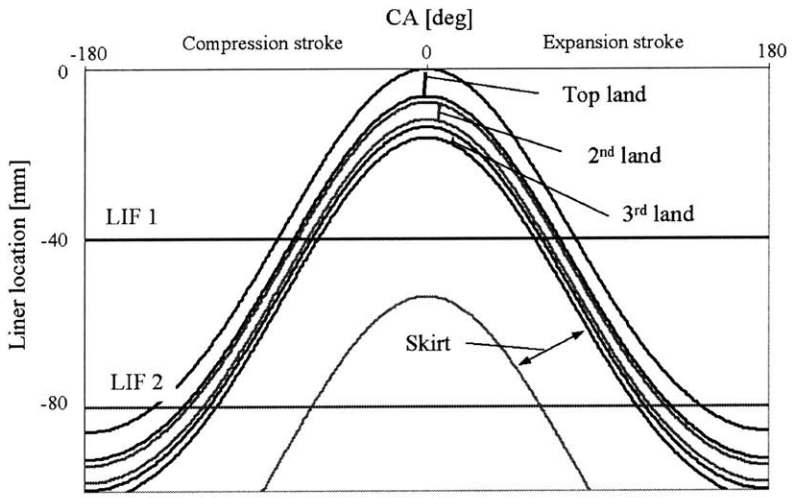

Figure 2-8 Axial position of LIF probes and of different piston regions with crank angle

After the LIF measurement locations were determined the stock engines block and cylinder liner were machined for the installation of the windows. Figure 2-9 shows the details of the engine block after machining.

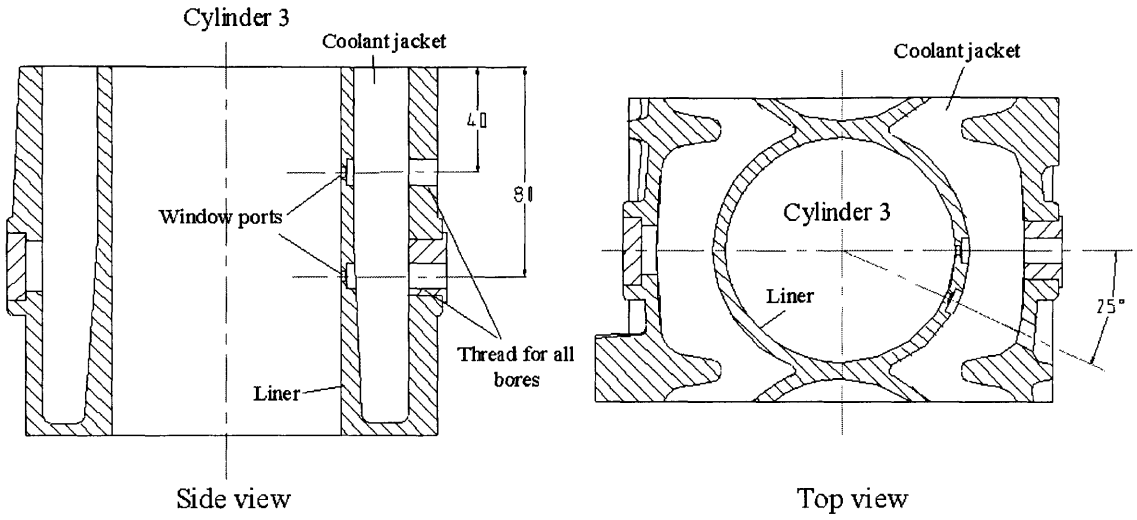

Figure 2-9 Modified engine block for optical access

The windows were inserted and glued into the liner with epoxy glue for high temperatures. The windows were manufactured from silica that has a transmission efficiency of over 90 percent at the LIF operation wavelengths. The window surface facing the combustion chamber was manufactured with a curvature radius of 43.1 mm, which ensures a smooth crossover from cylinder liner to the window surface. The dimensions of the silica windows are shown in Figure 2-10.

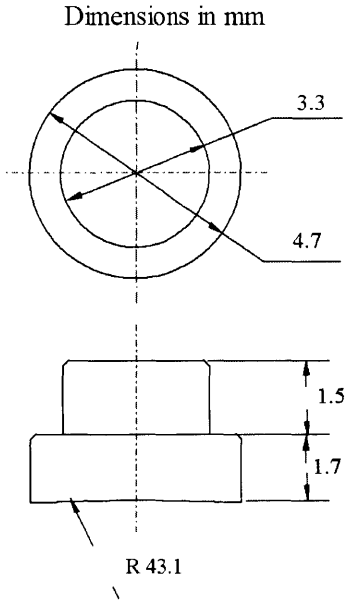

Figure 2-10 LIF window dimensions

After the epoxy was, cured the surface characteristics of the liner with the windows were measured with a stylus instrument (Taylor Hubson Form Talysurf profiler) at ambient conditions. All windows were almost aligned flush with the liner. Figure 2-11 shows the unfiltered primary surface profile measurements along the cylinder liner and window at 80 mm distance from the top of liner at the anti-trust side (Measurement position #2 in Figure 2-6). Appendix A illustrates the measured surface profiles for each window.

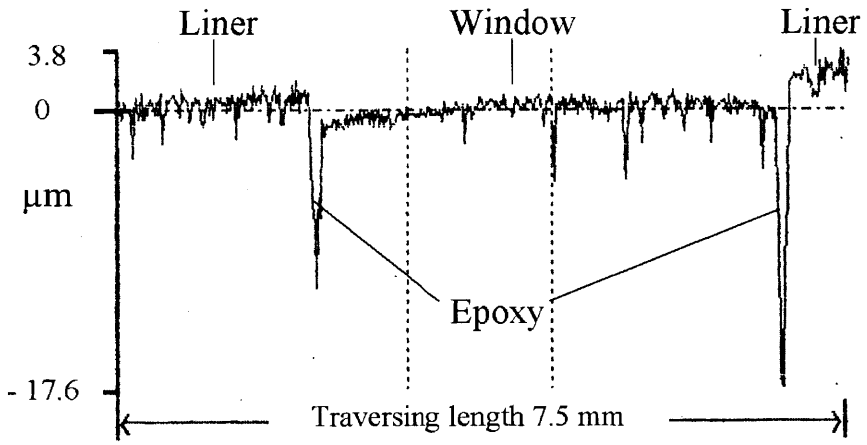

Figure 2-11 Surface profile along liner and bottom window at the anti-thrust side

Housing sleeves were machined and thread connected to the engine block. The main functions of the sleeves are to allow access to the LIF windows, to hold and position the LIF focusing probes with the fiber optics cable, and to seal the engine block from leaking coolant to the environment. The sleeve top was designed to fit into the chamfer on the coolant side of the liner. However, the thread connection to the block could not be tightened very much, since any localized high forces on the liner could cause undesired distortion of the bore. Therefore, to seal the sleeve surface from coolant leakage, a flat o-ring was glued with RTV (Room Temperature Vulcanizing sealant) to the surface of the sleeve top. After curing, a thin layer of RTV was applied on the flat surface of the o-ring and on the area of the sleeve external threads that would seal the engine block after mounting. The sleeve was then mounted to the block and screwed up until resistance was felt indicating contact between the RTV on the tip surface and the liner. The inside of the

sleeve was inspected and any RTV smearing onto the window was removed with cotton tabs.

The focusing probe consists of a probe housing, two optical lenses, and two spacer rings to separate the lenses and to hold them inside the probe housing. The probe is designed to position it inside the housing sleeve. A schematic of the housing sleeve and focusing probe arrangement is shown Figure 2-12.

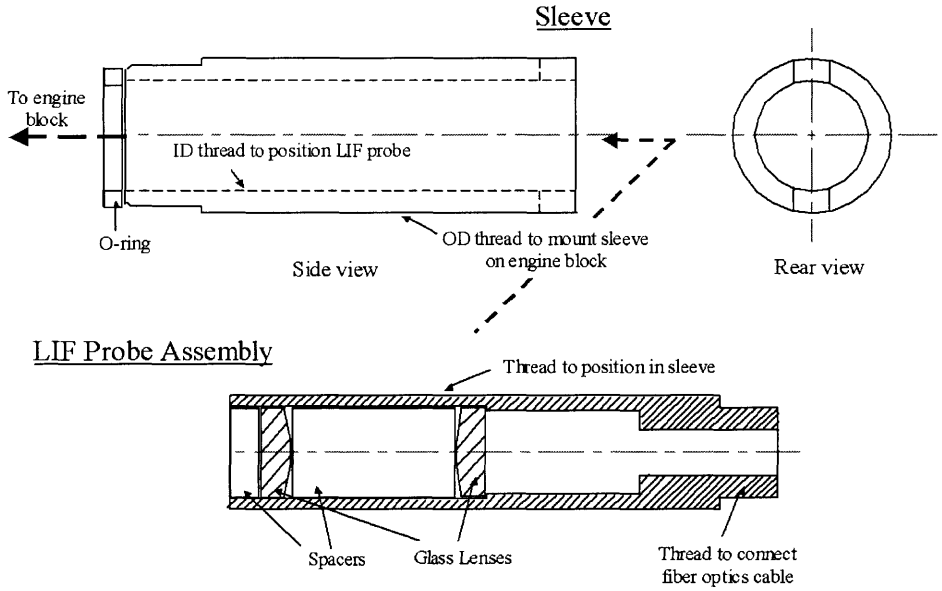

Figure 2-12 Arrangement of LIF housing sleeve and probe assembly

Calibration

Several in-situ calibration techniques have been suggested to convert the acquired LIF data (voltage signal) to a quantitative oil film thickness. All suggested techniques utilize geometrical profile features of the piston-ring-pack such as etch marks on the piston, tool marks on the piston, and ring profiles. In all of these calibration techniques, it is assumed that the region of interest is fully flooded. If this is true, then the oil film thickness and its fluorescence intensity are determined by the geometrical profile. Therefore, the known geometrical profile can be used to scale the LIF data with a certain calibration factor so that the oil film thickness trace fits the micro-geometry of the profile.

This obtained factor is then used to quantify the oil film thickness along the piston and between rings and liner.

The utilized calibration profile must feature certain characteristics. Its characteristic depth (which is equal to the oil film depth if the profile is fully flooded) needs to be in a range of the LIF technique that is linear and has a high signal to noise ratio. On the other hand, the geometrical profile on the piston-ring-pack moves during engine operation between the digitized consecutive data points. Therefore, a minimum characteristic length is required for the profile to be able to trace it. This length depends on the data acquisition rate and on the location of the LIF windows on the liner. The acquisition rate and window location determine the traveled distance of the calibration profile on the piston between two consecutive measurement points.

For this study, the LIF data acquisition rate was 2000 points per crankshaft revolution. Using this rate the calibration profile was able to move a distance of at most 140 μm between two consecutive data points. In order to ensure that there are enough data points (i.e. three points) to trace the oil film on the profile, a characteristic length of 420 μm was necessary. The ring surface profiles could not be used for calibration, because a fully flooded running surface can not be assumed over the entire stroke and the signal to noise ratio is to low due to the thin oil film between ring and liner. Moreover, effects of piston tilt and ring twist on the running surface profile could have impacted the calibration efforts. The piston machining marks on the piston lands and skirt were also unsuitable. Even though the marks have a sinusoidal pattern with a peak to valley height of 10 μm, their distance is about only 300 μm, which is significantly shorter than the required characteristic length.

Therefore, to calibrate the LIF signal two scratch marks with an axial length of 0.5 mm and different depths were machined on the upper part of the piston skirt. The positions and dimensions of the marks are shown in Figure 2-13.

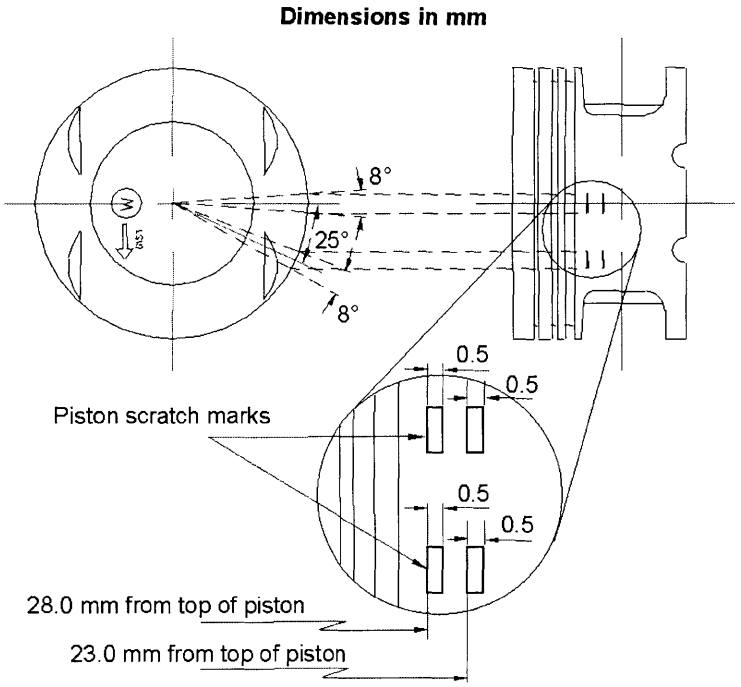

Figure 2-13 Piston scratch mark dimensions

Great effort was directed to achieve a relatively flat groove surface by machining each scratch mark with a new tool. Before reassembling the engine, the piston surface profile was measured with a stylus instrument (Form Talysurf), since the detailed scratch mark depths directly affect the calibration coefficient. Figure 2-14 shows the micro-geometric profile measurements of the piston with the scratch marks at the antitrust side.

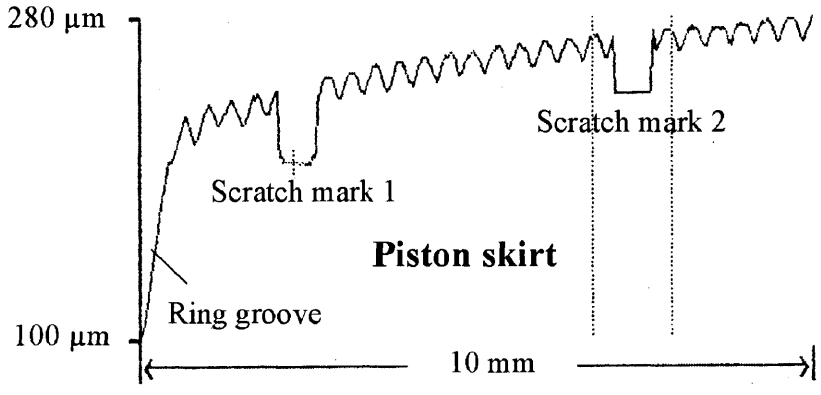

Figure 2-14 Surface profile of piston skirt and scratch marks at anti-thrust side

The LIF calibration was performed with the calibration coefficients obtained during the compression stroke. Figure 2-15 shows a sample LIF traces acquired during steady state engine operation at different times. Each shown trace was averaged over ten consecutive cycles.

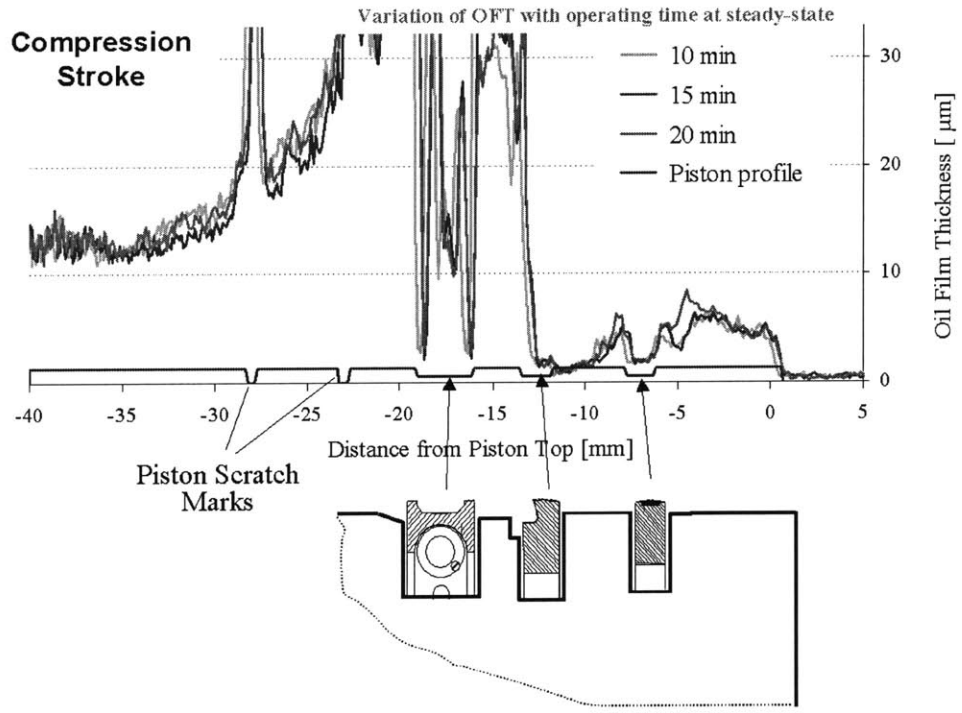

Figure 2-15 Sample LIF traces

2.3.2.2 Cylinder and Land Pressures

The head of the engine was machined to have the capability to measure cylinder pressure traces of two cylinders. The cylinder pressure measurements were taken using water-cooled piezoelectric transducers.

In addition, the liner and engine block were machined at two critical locations, to allow positioning of pressure transducers for the measurement of inter-ring pressures. The detailed pressure transducer positions on the liner can be found in Figure 2-6. These axial locations ensured the measurement of inter-ring pressures for the longest possible crank angle period. One transducer is located just above the TDC position of the scraper ring in order to measure second land pressures during the period of piston reversal

between the compression and expansion strokes. The second transducer was positioned lower on the liner. The distance between both transducers was slightly larger than the width of the piston's second land. This arrangement allowed, for this transducer, the measurement of the second land pressure for the periods just before and after the transducer upper on the liner was exposed to the second land. During the period when the upper transducer was exposed to the second land, the lower transducer provided third land pressure measurements. Therefore, the combination of both pressure transducers provided second land and third land pressures for a period of 62 and 32 crank angle degrees, respectively. Figure 2-16 illustrates the axial positions of both pressure transducers on the liner, and the instantaneous position of different piston regions as a function of crank angle during late compression and early exhaust strokes. The instantaneous positions of the piston regions during the exhaust and intake strokes are identical to the compression and expansion strokes, respectively.

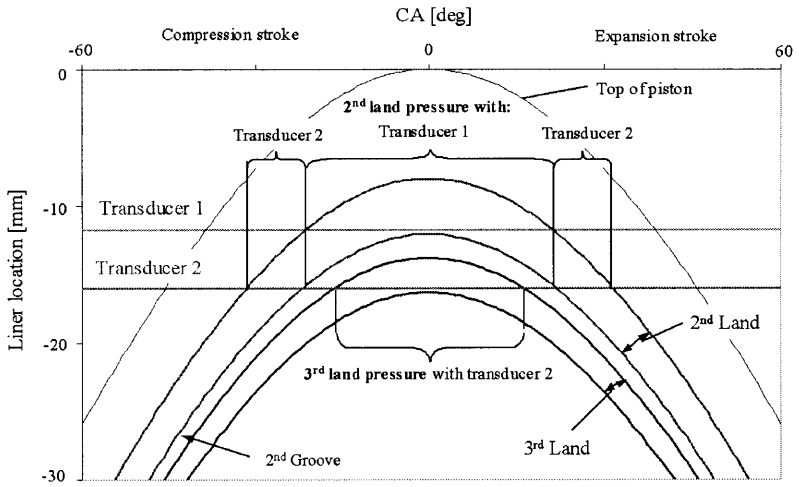

Figure 2-16 Axial positions along liner of different piston region as a function of CA

An adapter was designed to hold the pressure transducers and to seal the cylinder liner and engine block against coolant leakage. Figure 2-17 shows a side view schematic of a pressure transducer adapter mounted to the engine block and liner.

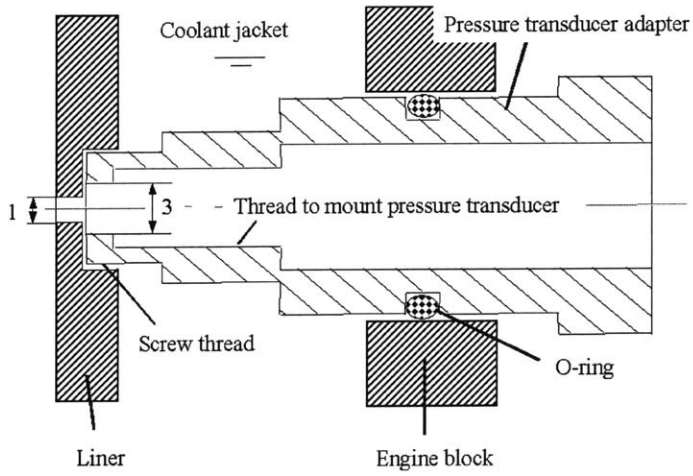

Figure 2-17 Side view schematic of engine with mounted pressure transducer adapter

The holes in the liner and the adapter increase the volume of the clearances between liner and piston, which may alter land pressures and gas flows in the piston-ring-pack from ideal conditions. However, this additional volume was negligible, since its greatest impact on the land clearance volumes was only a 3 percent increase.

Figure 2-18 shows sample second and third land pressure measurements with the two liner pressure transducers during late compression and early expansion strokes at steady state engine operation for 75% load, 2500 rpm.

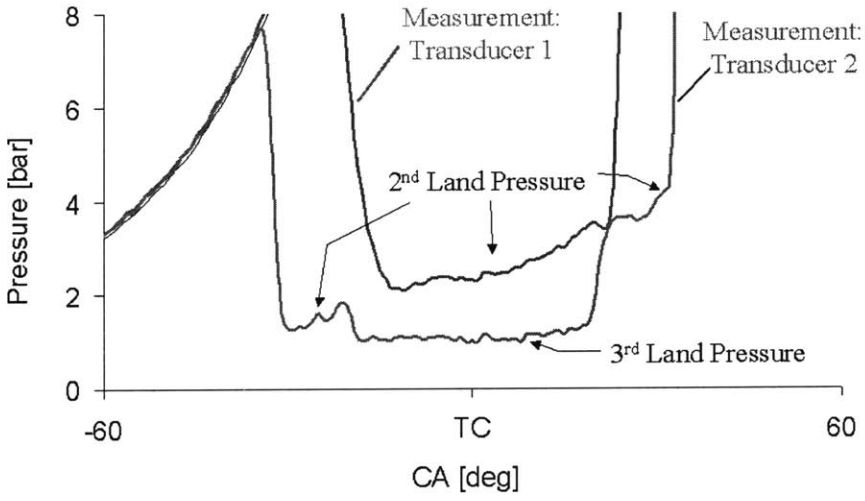

Figure 2-18 Sample second and third land pressure measurements with the liner pressure transducers at 75% load, 2500 rpm

2.3.2.3 Liner Temperatures

As described in Section 2.1, cylinder liner temperatures are believed to influence oil evaporation and thus oil consumption. However, the liner temperatures vary with engine operating conditions, and according to location along the liner. Therefore, the liner and engine block were machined and two fine tip transition joint thermocouples were installed into the liner to measure the local liner temperatures. The ports on the liner were blind holes with a distance of less than 1mm from combustion chamber side of the liner. The temperature measurement locations were at the top dead center position of the scraper ring and at the bottom dead center position of the top ring (see Figure 2-6).

2.4 Experimental Conditions

2.4.1 Engine Operating Conditions

The primary objective of this study was to investigate oil consumption and the contributing major oil consumption sources at a wide range of different engine operating conditions, such as speed, load, and whether the engine operates at steady state. The test engine with its associated experimental setup could be operated between 2000 rpm to 5500 rpm and engine load could be varied by changing the throttle position with a stepper motor from 0% to 100% load.

2.4.1.1 Steady State Engine Operation

Steady state oil consumption, blowby, and in-cylinder variable were measured to gain information about their response to changing speed and load. Oil consumption and blowby maps were created by taking five (0, 25, 50, 75, and 100%) load measurements at different speeds. Engine load was defined by the engine brake torque compared to the torque measured at wide open throttle (100% load), which is shown in Figure 2-19. Therefore, in Figure 2-20 the intake manifold pressure varied slightly for constant load conditions at different engine speeds. It has to be further noted that throughout the thesis, 0% load represents the lowest possible load to operate the engine in a steady condition (around 7 percent of the measured torque at full load).

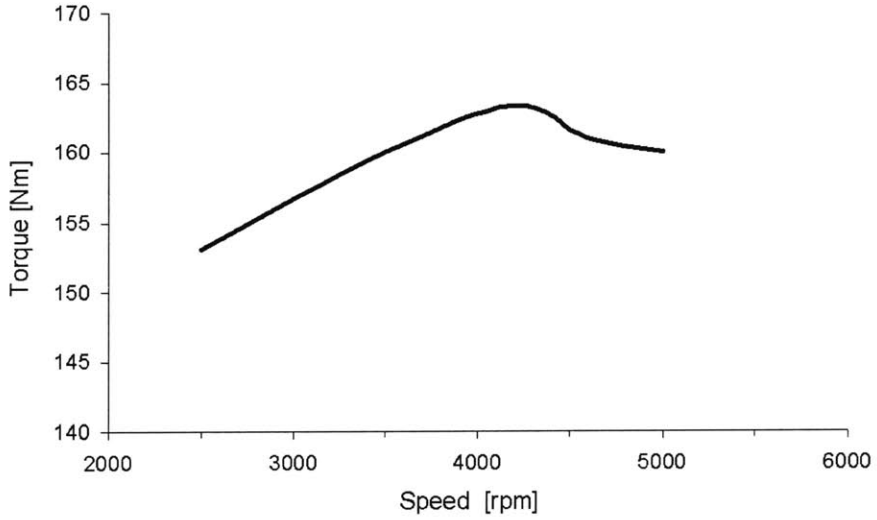

Figure 2-19 Torque at full load (100%) as a function of speed

In-cylinder variables were also measured at almost all investigated operating conditions and used for the oil consumption analysis. The operating region of the test engine, along with the investigated steady state speed and load conditions are shown in Figure 2-20.

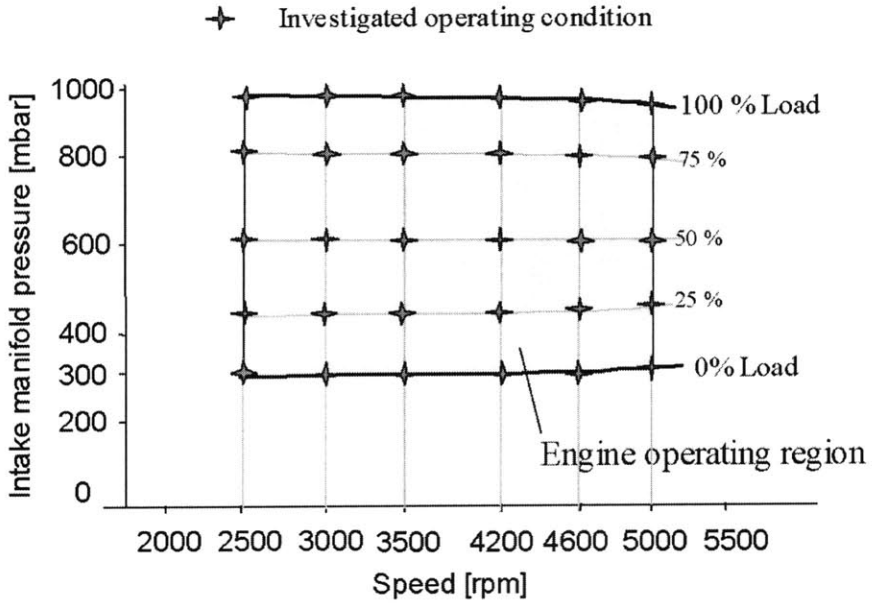

Figure 2-20 Investigated steady state engine operating conditions

Measurements of Blowby Contribution to Oil Consumption

The contribution of oil entrained in the blowby gas to total oil consumption was quantified at several steady state speed and load conditions. These engine speed and load conditions are shown in Figure 2-21.

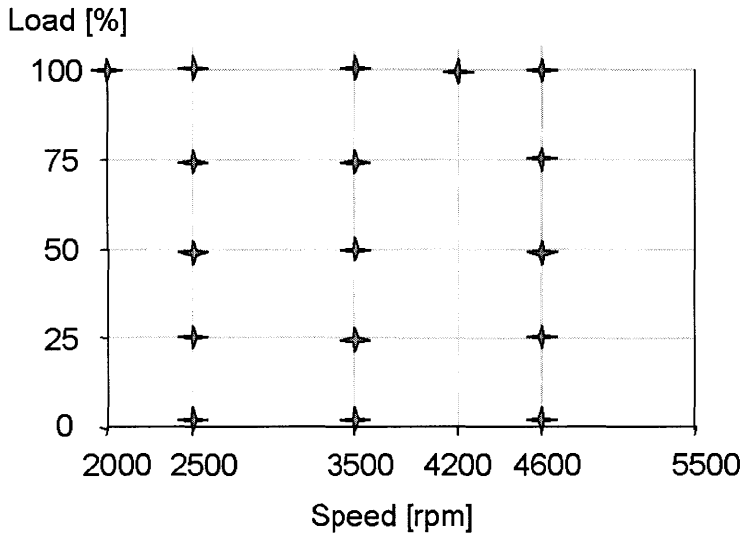

Figure 2-21 Investigated operating conditions of blowby contribution to total oil consumption

2.4.1.2 Engine Transients

In real life, engine performance is determined by its characteristics during transient driving conditions. Therefore, to simulate real driving conditions an extensive study was conducted to measure and analyze oil consumption behavior during engine ramp transients in load. During these transients, the engine load was changed from the initial steady state operating condition by opening or closing the throttle to the final operating condition. A stepper motor controller was used to operate the engine throttle. The stepper motor's shaft and throttle positions were carefully determined for each load at steady state engine operation, prior to the transients measurements. Table 2-6 summarizes the investigated load transients and Figure 2-22 illustrates the ramp transients in load at constant engine speed.

2500 rpm	3500 rpm	4000 rpm	4200 rpm	5000 rpm
0 → 100%	0 → 100%	0 → 100%	50 → 100%	0 → 100%
25 → 100%	25 → 100%	25 → 100%	25 → 100%	
50 ↔ 100%		50 → 100%	50 → 100%	
75 ↔ 100%				

Table 2-6 Investigated load transients at constant speed

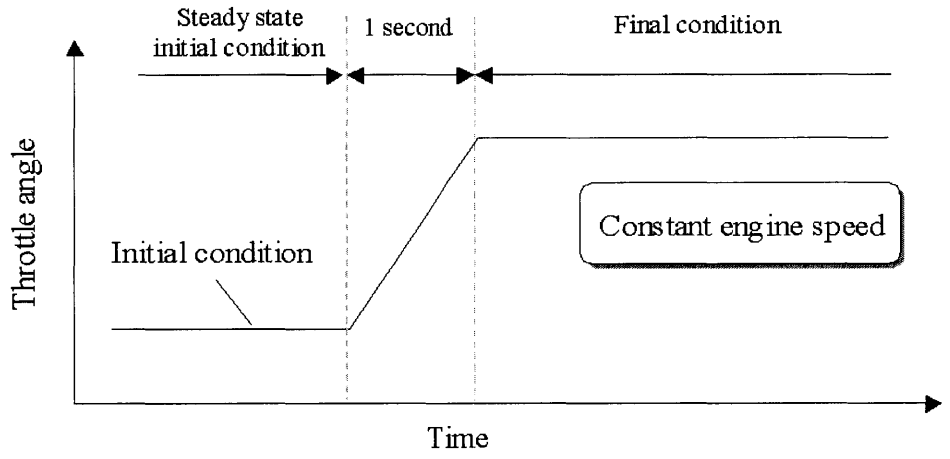

Figure 2-22 Description of the ramp transient experiments in load

2.4.2 Ring-pack Design

The ring-pack design used by the manufacturer was tested as the initial baseline design. All steady state measurements were conducted with the baseline ring-pack. This ring-pack consisted of a rectangular top ring with a barrel-faced running surface, a taper-faced Napier scraper ring, and a U-flex oil control ring, which is divided of about fifty ring segments with gaps between them. The U-flex oil control ring is recognized for its high flexibility and its good conformability to a deformed liner [52]. Figure 2-23 shows the details of the baseline piston-ring-pack design.

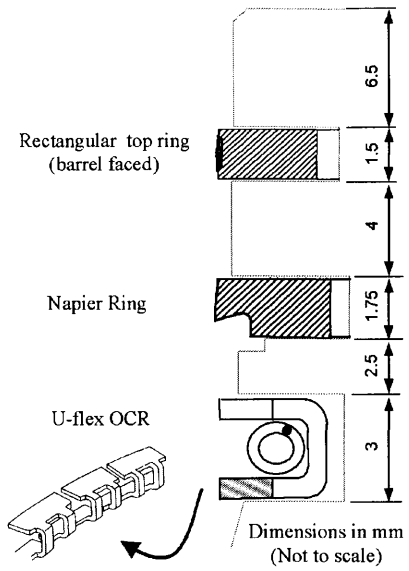

Figure 2-23 Piston and baseline ring-pack geometry

For the engine ramp transient studies the ring-pack was slightly modified: instead of the U-flex oil control ring, a two-piece oil control ring was used. The ring-pack design used for the transient experiments is shown in Figure 2-24.

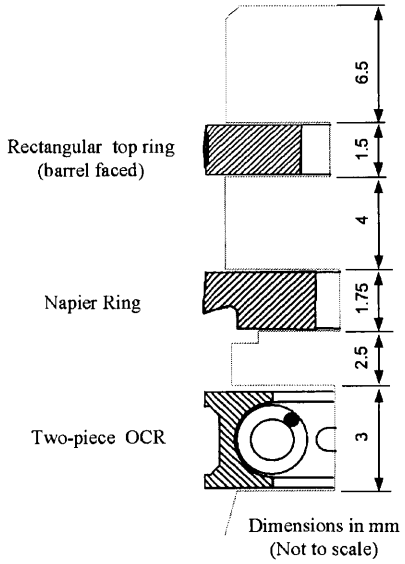

Figure 2-24 Details of the ring-pack geometry used for ramp transient experiments

Chapter 3 Oil Consumption Characteristics during Steady State and Transient Operation

3.1 Factors Influencing Oil Consumption at Different Speed and Load

As discussed in Chapter 1 oil transport and distribution in the piston-ring-liner system is governed by different driving forces such as inertia, gas flow, ring motion, and ring-liner lubrication. These forces, and consequently oil transport, vary considerably with engine operating speed and load. For example, inertia forces due to piston movement can increase by a factor of eight for the investigated engine speed range between 2000 and 5500 rpm. Engine speed, and to an even greater degree engine load, have significant impact on pressure gradients in the piston-ring-pack, and thus on the resulting gas flow rates between different regions of the piston assembly. For example, the blowby flow may increase by a factor of six between no load and full load, due to the variation of the cylinder pressure history with engine load. The cylinder pressure during the intake stroke increases from 300 mbar during no load conditions to 1bar during full load; peak cylinder pressures increase from several bars during no load to greater than 50 bars during full load. In addition, the detailed pressure histories in different regions of the piston-ring-pack and engine speed directly govern ring dynamic behaviors, which affect gas flows, ring-liner lubrication, and ring-groove interaction. The gas flow, pressure distribution, and ring dynamics are therefore coupled.

On the other hand, to advance understanding of the oil consumption phenomena in spark ignition engines, it is necessary to connect oil transport and oil distribution with oil consumption. For instance, the inertial throw off from the top land into the combustion chamber depends mainly on the top land oil accumulation and engine speed. Oil flow to the top land with the reverse gas flow depends on the magnitude of second land pressure and on the distribution of oil on the second land. Oil atomization and entrainment in the blowby gas flow is controlled by oil distribution along the piston and by the blowby gas

flow characteristics through the piston-ring-pack. Therefore, the key for predicting oil consumption is believed to be oil transport in the piston-ring-liner system and its dependence on engine operating conditions. In addition, operating conditions directly influence the thermal loading of engine components, which affects not only oil evaporation, but also the oil viscosity, and thus oil transport and distribution along the piston. Therefore, all oil consumption sources are also expected to vary with engine operating conditions.

Detailed knowledge of oil supply and removal rates in different regions of the piston-ring-pack would not only clarify the oil accumulation characteristics, but could also help in assessing the contribution of key oil consumption sources to total oil consumption. Even though, at low load, evidence supports the mechanism of oil transport through the top ring groove into the combustion chamber as being at least in some degree responsible for oil consumption, our understanding of oil consumption behavior under varying engine operating conditions is limited. The question remains how the different driving forces for oil transport influence the different oil consumption sources with changing engine speed and load.

3.2 Simulation of Piston-Ring-Pack Performance

Before analyzing the data on oil consumption and in-cylinder parameters, it is helpful to consider the analytical tools that were used in this work to evaluate different driving forces for oil transport in the piston-ring-pack. The details of the dynamics of the piston rings, gas flows in various regions of the piston-ring-pack, and ring-liner lubrication were predicted, applying two physics-based models (RINGPACK-OC, FRICTION-OFT) that were both developed at MIT (Sloan Automotive laboratory) [43]. These models require as input the cylinder pressure trace, viscosity properties of the lubricating oil, component geometries and temperatures during engine operation, and oil accumulation in different regions in the piston-ring-pack. However, component geometries and oil volumes inside the ring grooves and on the lands change with engine operating conditions. These unknown parameters were adjusted within a reasonable range, until the predictions from model calculations matched the steady state land pressure and blowby measurements.

The models were applied to two ring-pack designs that were studied in this work as described in Section 2.4.2. Due to the different oil control ring (OCR) designs and operating conditions, each model had to be adjusted for the OCR design and operating conditions individually. The following will describe the adjustments for the U-flex OCR running at steady state operating conditions.

The U-flex OCR is comprised of about fifty ring segments with gaps between them. It is believed that after installation in the piston-liner-system, locally high stresses on the ring may deform the segments (this is also supported by finite element analysis). Consequently, each segment assumes a wavy shape in the piston groove and creates additional gaps between their flanks and the ring groove. This increase of leakage paths around the OCR groove circumference allows more gases to flow from the third land through the OCR ring groove toward the crankcase. These gaps between the segment flanks and the ring groove were also included in the applied computer models by assuming a peak to valley distance of about 30 μm for the wavy segment flank shapes. Figure 3-1 shows a schematic of the believed U-flex OCR segment flank shapes after installation.

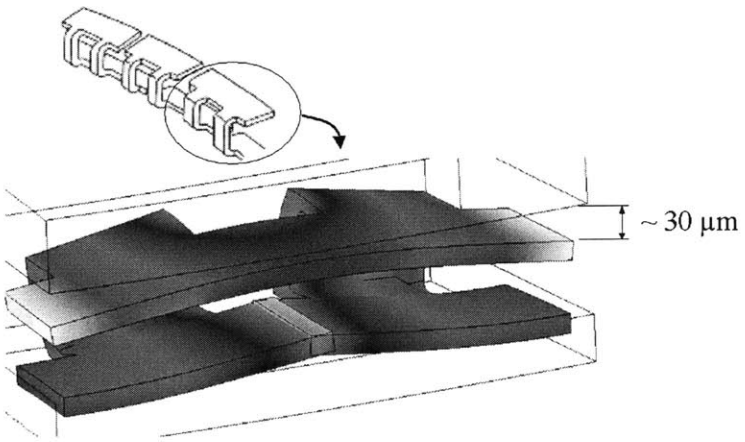

Figure 3-1 Schematic of the believed U-flex OCR flank shape after installation

Figure 3-2 shows the comparison of the predictions from the model calculation with the steady state land pressure and blowby measurements for the baseline ring-pack.

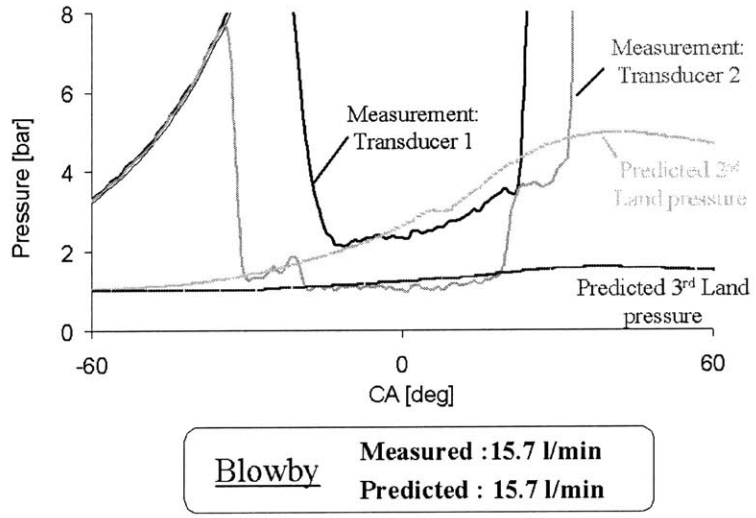

Figure 3-2 Predicted and measured land pressures and blowby at 75% load, 2500 rpm

3.3 Speed and Load Effects on Oil Consumption and In-Cylinder Parameters

In Section 3.1, the effects of engine operating conditions on the driving forces for oil transport and on oil consumption were pointed out. Even though fundamental models for the driving mechanisms have been proposed, a reliable prediction of oil flow and accumulation in the piston-ring-liner system is not possible. This is due to the complexity of the piston-ring-liner-system and the uncertainties of component dimensions during different engine operating conditions. The lack of understanding of oil transport and distribution in the piston-ring-pack is a major reason for difficulties in predicting oil consumption.

Therefore, an experimental test matrix was conducted to investigate the impact of different speed and load conditions on oil transport and distribution in the piston-ring-pack, and the total consumption rate. During these tests, oil consumption, blowby, and in-cylinder parameters were measured. In-cylinder pressure, land pressure and engine blowby measurements were used to analyze the effects of gas flow, ring dynamics, and ring-liner lubrication on oil transport and distribution along the piston and the liner. In

addition, oil distribution on the piston was studied using the one-point LIF technique. All these measurements were conducted at the steady state operating conditions described in Section 2.4.

3.3.1 Oil Consumption Measurements

First, steady state oil consumption measurements were conducted to gain information about the oil consumption pattern of the test engine with changing speed and load, and an oil consumption map (illustrated in Figure 3-3) was created from the measurements. The oil consumption map has several important characteristics. For instance, the measurements showed a clear dependence on engine speed and load. Oil consumption increased with increasing engine speed and load, which is typical for internal combustion engines. Moreover, the consumption rates become more significant at higher speed and load. Severe oil consumption was noticeable at high speed (> 4500 rpm) and high load (≥ 75%) conditions. However, an exception to this general trend was found at low load conditions, where the oil consumption was higher than expected. The dependency of oil consumption on load was found to disappear, as the load was decreased from 25% to 0% load. At 3500 and 4200 rpm, oil consumption was found to increase with a decrease in load from 25% to 0%.

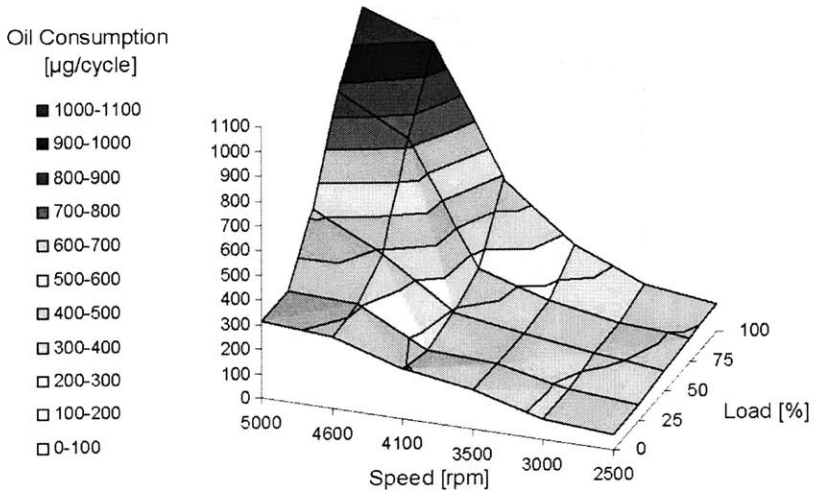

Figure 3-3 Oil consumption at different engine speed and load

3.3.2 Blowby

Having determined the oil consumption pattern, the next step was to investigate the effects of blowby and in-cylinder parameters on oil transport and distribution at different steady state engine speed and load.

3.3.2.1 Blowby Flow Structure

Before analyzing the blowby and LIF oil film thickness measurements, it is helpful to consider the blowby flow features through the piston-ring-pack, since the flow effects oil transport. Blowby gas flow is strongly dependent on leakage paths. If instabilities of the rings are prevented, then the main structure of the blowby flow is believed to be as follows. As the cylinder pressure rises during compression and combustion, the gases in the combustion chamber leak through the top ring gap to the second land. On the second land, these gases flow mainly in the circumferential direction from the top ring gap to the second ring gap. This can be explained using the simulation code RINPACK-OC that computes the land pressure history and gas flow in different regions of the piston-ring-pack. Figure 3-4 shows the measured cylinder and the computed land pressures as well as gas flow rates through the top and second ring gaps during the engine cycle at 25% load, 3500 rpm. During the compression and early expansion strokes, gases flow from the combustion chamber through the top ring gap into the second land due to the pressure gradient across the top ring. As a result, the pressure in the second land clearance increases because of its finite volume, and a pressure gradient evolves between the second and third land regions. This pressure gradient induces a gas flow from the second land through the second ring gap into the third land. During the intake stroke and the late expansion and early exhaust strokes blowby gases may flow back from the second land through the top ring gap to the top land. However, the average of the flows through the top and second ring gaps and the integration of this average through the engine cycle results in a net gas flow from the top to the second ring gap. This gas flows most likely along the circumferential direction of the piston's second land.

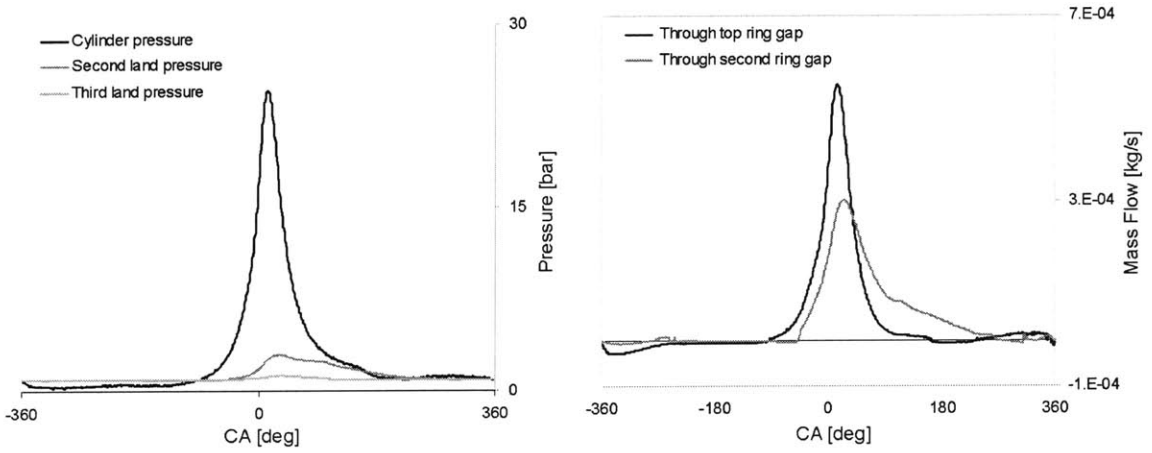

Figure 3-4 Pressures in different regions and gas flows through ring gap at 25% load, 3500 rpm

On the third land, the structure of the blowby flow depends on the oil control ring design. If an oil control ring with a single gap is used, such as the two-piece oil control ring (this ring was used for the transient study), then the blowby gas flow on the third land is believed to be mainly in the circumferential direction from the second ring gap to the third ring gap. However, if a U-flex ring, which is divided of about fifty ring segments with gaps between them, is used, then the blowby flow structure may be different. Moreover, as described in Section 3.2, U-Flex ring segments may assume a wavy shape after installation, which results in additional gaps between the ring flanks and groove surfaces. All these gaps may allow the blowby gases to flow mainly in the axial direction from the second ring gap to the crankcase. Figure 3-5 shows a schematic of the believed net gas flow through the piston-ring-pack with a U-flex oil control ring.

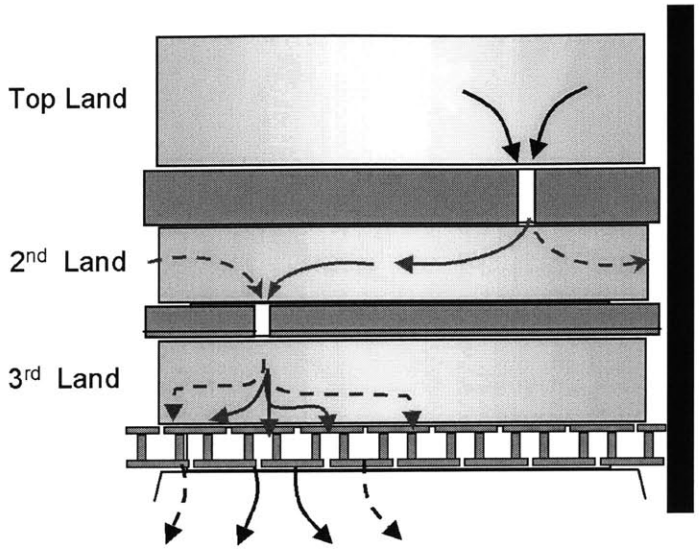

Figure 3-5 Schematic of the main blowby flow path through the piston-ring-pack with a U-flex oil control ring

3.3.2.2 Blowby Gas Flow Oil Dragging

The oil flow and distribution in the piston-ring-pack is believed to be affected by the blowby gas flow oil dragging. Oil dragging is the mechanical action by which the blowby gas, flowing through clearances in the piston-ring-liner system, moves the oil present on surfaces due to interfacial shear stresses. A schematic of the gas flow dragging process is shown in Figure 3-6.

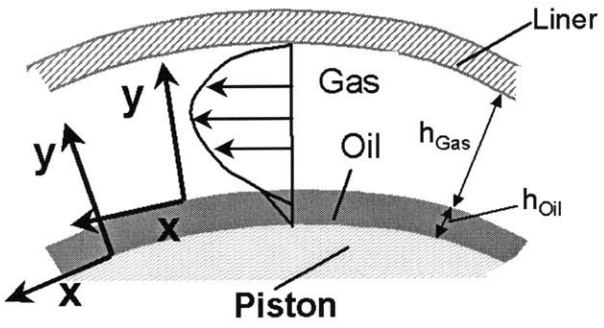

Figure 3-6 Schematic of the transport mechanism of gas flow oil dragging on surfaces

This oil transport mechanism was described and modeled by Thirouard in [46]. The simplified, fully developed one-dimensional Couette flow representation was found to be appropriate for computing the oil flow due to the gas flow dragging action. The Navier-Stokes Equations for the Couette flow reduce to:

$$\mu_{Oil} \frac{\partial^2 u_{Oil}}{\partial y^2} = 0 \; ; \tag{3.1}$$

where μ_{Oil} is the dynamic oil viscosity, u_{Oil} the oil velocity, and y the perpendicular coordinate to the material surface.

The no slip boundary condition at the surface (y = 0) is specified as

$$u_{Oil}\big|_{h=0} = 0. \tag{3.2}$$

At the oil layer surface (y = h_{Oil}) the interfacial shear stress boundary condition is specified as

$$\tau_{Oil} = \left.\frac{\partial u_{Oil}}{\partial y}\right|_{y=h_{Oil}} = \frac{v_{Oil}}{h_{Oil}} \; ; \tag{3.3}$$

where τ_{Oil} is the driving shear stress at the liquid gas interface, and v_{Oil} the oil velocity at the interface ($y=h_{Oil}$).

The shear stress at the interface between the oil and gas flow was estimated by simplifying the blowby gas flow as a fully developed Poiseuille flow:

$$\mu_{Gas} \frac{\partial^2 u_{Gas}}{\partial y^2} = -\frac{dP}{dx}; \tag{3.4}$$

where μ_{gas} is the gas dynamic viscosity and u_{Gas} the gas velocity, y the perpendicular coordinate to the gas flow, and $\frac{dP}{dx}$ the pressure gradient in the direction of the flow.

With the following boundary conditions specified as:

$$u_{Gas}\big|_{y=0} = 0 \text{ and } u_{Gas}\big|_{y=h_{Gas}} = 0. \tag{3.5}$$

The solution of equation (3.4) can be written as

$$-\frac{dP}{dx} = \frac{q_{Gas} * 12 * \mu_{Gas}}{L * h_{Gas}^3}; \tag{3.6}$$

where q_{gas} is the instantaneous volumetric gas flow rate and L the depth of the oil covered surface. The interfacial shear stress is then given as

$$\tau_{Gas} = -\frac{dP}{dx} * \frac{h_{Gas}}{2} \tag{3.7}$$

With equations (3.3), (3.6), and (3.7) the instantaneous oil flow rate due to blowby gas flow dragging can be estimated. In [46], it was found that the average oil flow rate due to gas flow dragging was estimated reasonably well by the following expression:

$$Q_{Oil} = Q_{Gas} * \frac{3 * \mu_{Gas} * \tilde{h}_{Oil}^2}{\mu_{Oil} * h_{Gas}^2} \tag{3.8}$$

where Q_{Oil} is the cumulative oil flow over one cycle [m^3/cycle], Q_{Gas} the cumulative gas flow over one cycle flowing through the clearance of interest [m^3/cycle], and $\tilde{h}_{Oil}$ the average oil layer covering the piston surface of interest.

3.3.2.3 Blowby Measurements

Engine operating conditions drastically change the blowby flow magnitude and possibly the flow paths. Such a change of the gas flow features may have a significant influence on oil transport and oil consumption. Therefore, blowby measurements were taken at different steady state engine speed and load conditions to investigate its operating condition dependence. A common representation of blowby by researchers in the automotive industry is the volumetric blowby gas flow rate per unit time. Figure 3-7 illustrates the variation of the blowby flow rate (liters per minute) with engine speed and load. It is evident that blowby increased with increasing engine load at all investigated speed conditions. The increase of the cylinder pressures history with engine load causes a greater pressure gradient between the combustion chamber and crankcase, which enhances the blowby gas flow through the piston-ring-pack. Moreover, the measurements show that the variation of engine speed at constant load has little effect on the blowby flow rate.

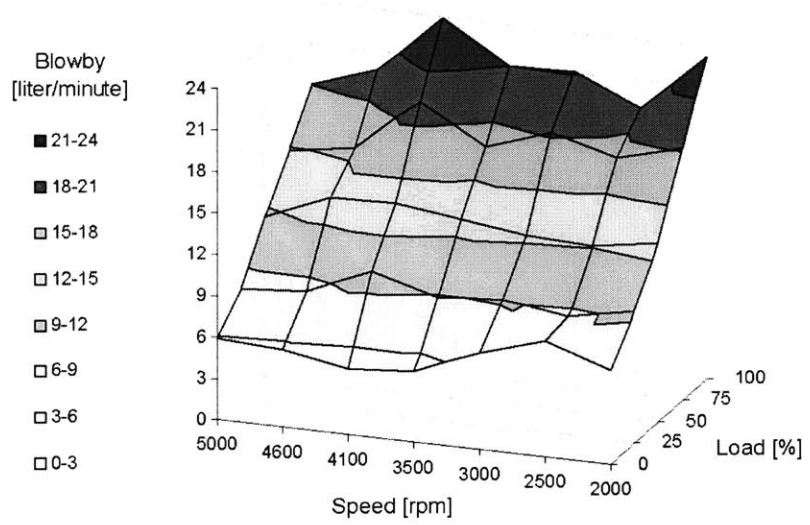

Figure 3-7 Blowby flow rate (liter/minute) at different engine speed and load

However, all driving forces that are believed to control oil transport within the piston-ring-pack, including the blowby gas flow dragging, repeat periodically every cycle, and thus should scale with the engine speed. Therefore, the average volumetric blowby flow per cycle was determined in order to evaluate its impact on oil transport and oil distribution on the piston. Figure 3-8 shows the results for the blowby per cycle at different speed and load conditions.

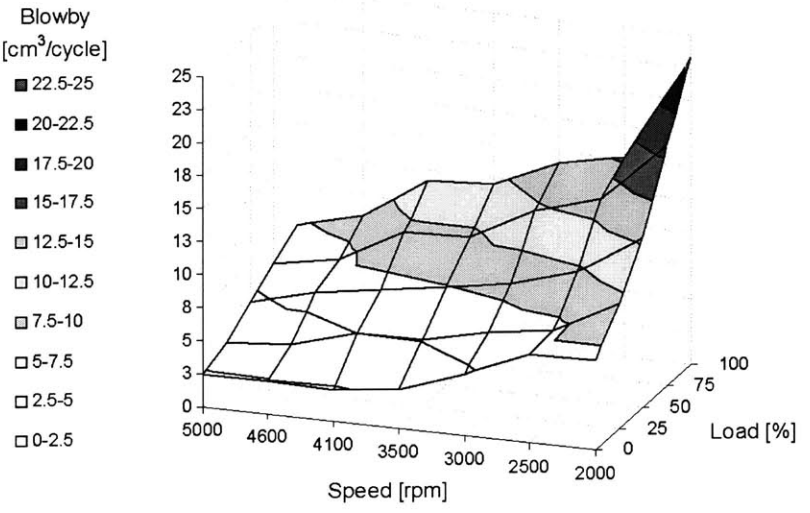

Figure 3-8 Blowby (cm^3/cycle) dependency on engine speed and load

It is clear that blowby per cycle increases with engine load at a constant speed. On the other hand, blowby was found to decrease with increasing engine speed at constant load. This blowby characteristic can be explained as follows. The increase of engine speed reduces the available time for the gases to flow through the piston-ring-pack during one engine cycle. As a result, the amount of gases leaking through the ring-pack, and thus blowby, decreases with increasing engine speed. Consequently, the greatest increase of blowby between the 0% and 100% load conditions was observed at 2000 rpm (the lowest speed investigated). This increase of blowby with engine load was found to be less significant with increasing engine speed. In summary, since oil transport on the piston is governed by, among other mechanisms, dragging of the gas flow, the oil flow rate towards the crankcase should decrease with decreasing engine load and increasing speed. The variation of the blowby flow and the associated driving forces for oil transport, along with engine operating conditions, surely will also have an impact on the oil accumulation and distribution on the piston. These effects of engine speed and load on the oil accumulation will be discussed for different regions of the piston assembly in the following.

3.3.3 Oil Distribution along Piston

Of great interest for oil consumption is the amount of oil on the upper part of the piston. This region of the piston, in particular the region above the second ring (region c in the Figure 1-2), is believed to be a major source for oil consumption. Oil can be consumed by throw off and evaporation from the top land, and by the transport of oil from the second land in the direction of the combustion chamber with the reverse blowby gas flow. The presence of more oil in these upper piston regions should increase the contribution of both oil consumption sources. Therefore, LIF measurements were taken to analyze the dependence of the oil film thickness in the upper piston regions on different steady state engine operating conditions.

The average oil film on each piston land was quantified by integrating the oil film thickness trace along each land, dividing this oil volume by the corresponding land's length for each stroke, and averaging the obtained value for the oil film on each land over

all engine strokes. Figure 3-9 illustrates a sample LIF trace and the piston lands for which the average oil film thickness was determined.

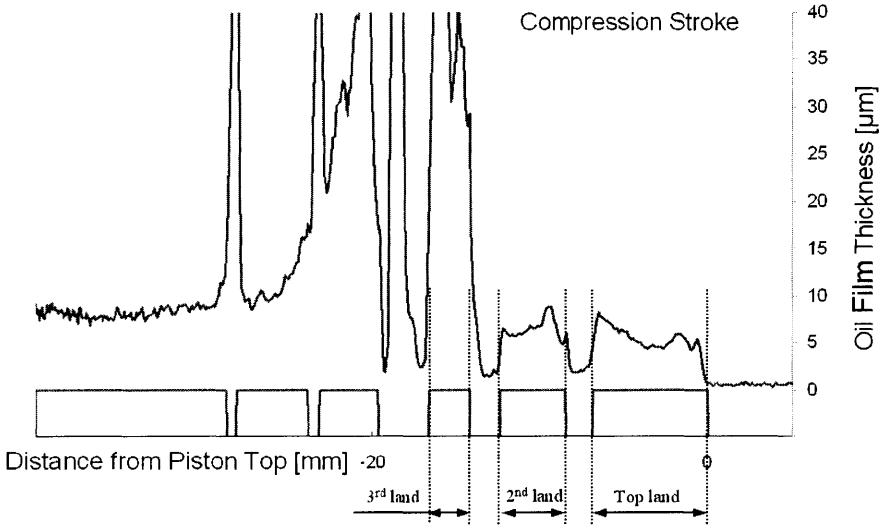

Figure 3-9 Sample LIF trace with control volumes of piston land for averaging

Figure 3-10 shows the measured average oil film thickness on the top two piston lands with engine speed and load. The shown results are from the window on the anti thrust line at mid stroke (measurement position #1 in Figure 2-6). It is apparent that the average oil film on the lands varies with engine conditions. The oil film decreases on both lands with increasing engine load, which should be mainly related to the variation of the blowby flow.

Second land oil accumulation

The oil film on the piston's second land surface is exposed to circumferential blowby gas flow during engine operation. If ring flutter and collapse is prevented, the blowby gases flow mainly through the top ring gap, and along the circumference of the second land to the second ring gap. This gas flow drags the oil on the second land towards the second ring gap due to interfacial shear stresses, and then through the gap to the third land. The increase of blowby with engine load, and the associated higher volumetric gas flow rates in the circumferential direction on the second land (see Figure 3-11), increase the interfacial shear stresses on the oil film. Consequently, more oil is removed from the second land. The dependence of the circumferential gas flow on engine speed and load

(Figure 3-11) was determined using the RINGPACK-OC simulation results. However, the amount of oil that accumulates on the second land depends on the balance of all oil supply and removal rates, including ring squeezing, ring pumping, and the axial oil transport due to inertia.

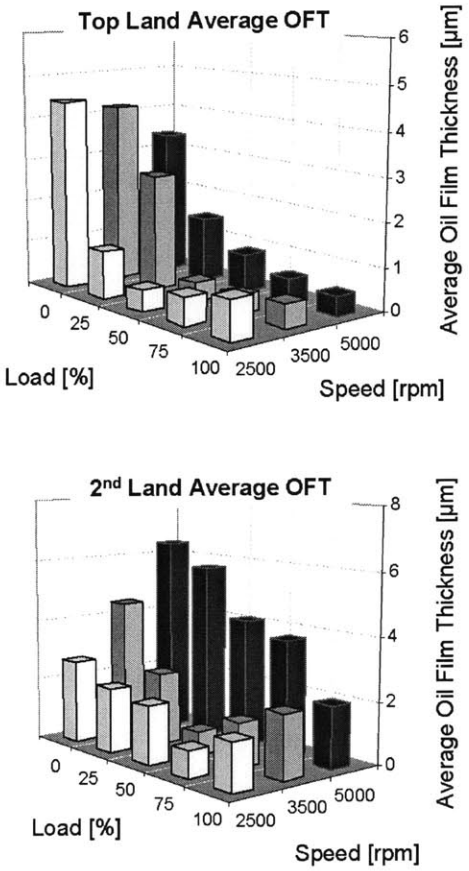

Figure 3-10 Effect of engine speed and load on the oil accumulation on top and 2nd land

In 2-D LIF visualization experiments on a one-cylinder engine (derived from this test engine), oil supply to the second land was found to occur through the second ring groove [46]. Oil transport with the reverse blowby flow through the top and second ring gaps was not observed at the operating conditions investigated in this study (intake manifold pressures >300mbar) and thus was neglected. In [46], oil transport from the second land to the top ring groove due to inertia force was suggested to be a plausible transport mechanism.

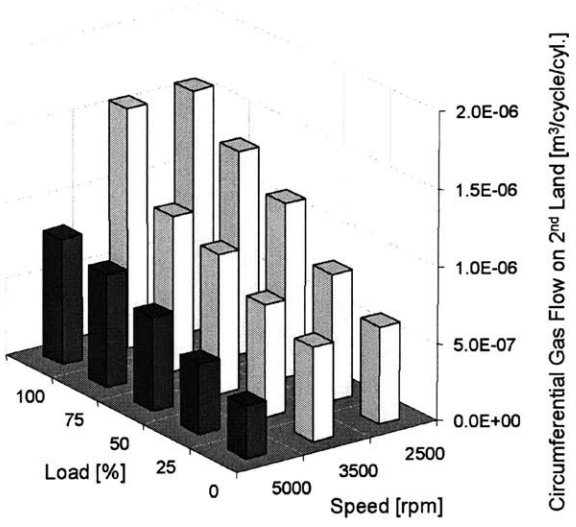

Figure 3-11 Circumferential volumetric gas flow on the second land

The expected oil supply and removal rates from the grooves to the second land depend strongly on engine speed, but they are believed to have a weak dependence on engine load. Therefore, if these oil supply and removal rates to the second land do not vary significantly with engine load, then the gas flow oil dragging should determine both oil transport, and the average oil film on the second land. Increasing engine load increase the circumferential gas flow rates on the second land and therefore according to equation (3.8) the oil removal from the second land. Consequently, the increased oil flow through the second ring gap will decrease the average oil film thickness on the second land as it is observed in the LIF measurements (Figure 3-10).

This simple analysis of the oil film thickness measurement results on the anti-thrust side does not consider any potential circumferential variation of the oil film thickness on the second land. Oil film thickness variations may be caused by the structure of the circumferential gas flow [46]. As shown in Figure 3.5 the gases flowing from the top ring gap to the second ring gap may follow either of two paths. The gas flow rate along these paths depends on the relative position of the two gap locations. The flow rate along a path increases as the distance of this path decreases. Since the circumferential gas flow rates along the two paths vary, the removed oil due to the gas flow dragging varies (because oil flow depends on the gas flow rate according equation (3.8)). On the other

hand, the axial oil supply and removal rates to the second land are believed to occur essentially on the entire piston circumference. Yet, the gas flow along a flow path drags the oil circumferentially to the second ring gap location. According to equation (3.8), the circumferential oil flow also depends on the oil film thickness, which causes an additional variation of the oil film thickness along the flow paths itself. Even if in reality the circumferential second land oil film thickness varies, the main conclusion obtained from the above analysis should not be affected.

Figure 3-10 shows further that the average oil film thickness on the second land increased with increasing engine speed at constant load. However, as shown in Figure 3-11 the circumferential gas flow on the second land also decreases with increasing engine speed at constant load. This gas flow behavior with speed decreases the oil removal rate per cycle from the second land due to gas flow dragging. On the other hand, it is believed that increasing engine speed increases the axial oil transport to higher piston regions, due to the higher inertia forces acting on the oil volume, which may result in higher oil supply rates to the second land [46]. These two effects of increasing speed on the oil flow on the second land result in higher second land oil film thickness.

Top land oil film thickness

The average oil film thickness on the top land was found to decrease with engine load (see Figure 3-10). This behavior can be explained as follows:

Oil accumulation on the top land depends on the balance of the oil supply and removal rates to it. Two mechanisms may supply oil to the top land. First, oil can be supplied through the top ring groove due to oil squeezing caused by the ring's relative motion in its groove. The squeezing of oil to the top land depends, among other factors, on the oil supply to top ring groove, which is governed by the second land oil film thickness, and the oil flow due to inertia forces. Second, oil may be scraped from the liner and supplied to the top land, when the bore is significantly distorted and the ring conformability is dependent on the pressure behind the ring. As mentioned above, in visualization experiments, oil supply through the top ring gap with the reverse blowby flow was not observed at the investigated operating conditions in this study [46].

The supplied oil on the top land is transported either into the combustion chamber, or returned to the second land with the blowby gas flow through the top ring gap. The oil is transported from the top land to the combustion chamber either by the throw off due to inertial forces, or by evaporation into the top land crevice gas flow due to the high top land temperatures. The blowby gas flow moves the oil on the top land through the ring gap to the second land due to interfacial shear stresses. Unlike the blowby flow through the second land, the gases flow only over a small region on the top land near the ring gap due to absence of circumferential gas flow and the higher cylinder pressures. Consequently, oil can be removed only from a small region of the top land. The impact of this mechanism on the top land oil balance depends on the top land oil supply and removal rates, and on the average speed at which the top ring rotates in its groove.

Decreasing engine load increases the oil film thickness on the second land. The higher oil film on the second land with decreasing engine load should also increase the oil transport to the top ring groove, and therefore the oil supply to the top land. On the other hand, decreasing engine load should decrease the oil removal from the top land. The oil return to the second land through the top ring gap decreases due to the lower gas flows and oil evaporation reduces due to the lower top land and crevice gas temperatures. Therefore, this increase in oil supply and decreased removal of oil with decreasing load are the believed reasons for the increase in oil film thickness on the top land.

The increased oil presence on the upper part of the piston during low load conditions is more susceptible to being transported into the combustion chamber by direct oil consumption sources. This may explain the resulting increase of total oil consumption as the engine load was decreased from 25% to 0%. However, for a thorough analysis of the oil consumption pattern other issues that may affect the oil consumption need to be considered, such as variations blowby in gas flow, blowby entrainment, ring dynamics, ring-liner lubrication, and component temperatures. The impact of some of these parameters on the oil consumption sources and the oil consumption pattern of the test engine will be discussed in Section 4.3.

3.4 Analysis of Oil Consumption Behavior during Transients in Load

3.4.1 Introduction

Most prior oil consumption studies have focused on determining and understanding the steady state oil consumption pattern. However, in practice, automotive engines typically operate at non-steady conditions. During transient engine operation, oil consumption can differ significantly from steady state. It is important therefore to understand the oil consumption characteristics during non-steady engine operation. The research work on transient oil consumption was greatly advanced by applying fast-response oil consumption measuring techniques such as the sulfur-tracer technique that was used in this study.

Studies focused on oil consumption behavior during transient engine operation have reported an increase in oil consumption during specific transient conditions. In particular, increased oil consumption values were observed during load transients from low load to high load conditions. Two reasons were suggested as responsible for this oil consumption phenomenon:

(i) More oil accumulated on the liner and top of the piston during low load conditions and

(ii) the subsequent combustion of the accumulated oil [49][50].

Similar higher oil consumption during transients was observed in a heavy duty diesel engine [51]. In [51], the engine oil consumption was measured simultaneously with in-cylinder variables, and the oil consumption phenomenon during the transients was found to be related to the oil transport through the oil control ring.

Oil transport and consumption are affected by in-cylinder variables such as oil accumulation on the piston, ring dynamics, and gas flows. The behavior of these variables during engine transients has not yet been fully analyzed. In this work, a study

was carried out to measure, analyze, and characterize the oil consumption behavior during engine load transients at constant speed. Additional to oil consumption measurements in-cylinder liquid oil behavior along the piston was studied using the Laser Induced Fluorescence (LIF) technique. Land pressure traces and engine blowby were measured to analyze oil transport along the piston and physics-based models that predict ring dynamics and gas flows were used to analyze the transient oil consumption behavior.

Emphasis was placed on the analysis of the oil consumption behavior during transients from low load to full load by combining oil consumption measurements, in-cylinder measurements, and theoretical modeling.

2-D LIF Visualization

Additionally, a one-cylinder visualization engine equipped with a sapphire window was used to verify the conclusions drawn from the studies on the production engine [53]. The one cylinder engine was derived from the production engine and has the same ring-pack and piston design as the production engine.

The window allowed the two dimensional observation of the piston-ring-pack during the entire piston stroke. The visualization setup based on multiple-dye LIF was implemented to generate high-resolution images of the oil distribution in the piston-ring-pack. Using an intensified CCD camera and digitizer, both snapshots and videos of the evolution of the oil distribution could be recorded during engine operation. The observations for this work were limited to qualitative analysis of the liquid oil behavior and a calibration was not attempted. Details of the 2-D LIF setup can be found in [46]. A sample image of the oil distribution in the piston ring-pack is shown in Figure 3-12. In the images, the brighter the regions are, the more oil is present. Thus, the dark rectangular areas represent the locations of the piston rings, since little oil is present between the rings and the liner.

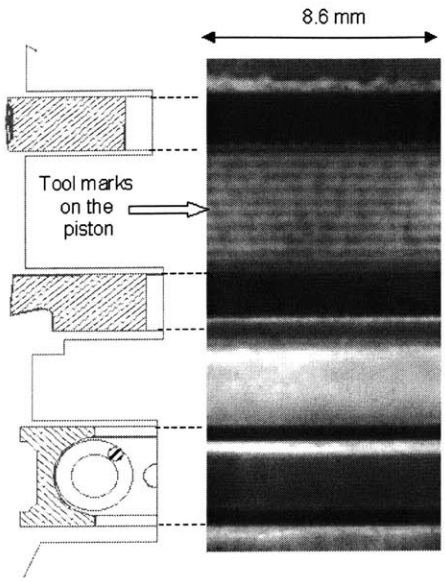

Figure 3-12 Sample 2-D LIF image [53]

Piston-ring-pack

The measurements were conducted with the ring-pack design consisting of a barrel faced top ring, a taper faced Napier (hook) scraper ring, and a two-piece oil control ring. The details of the used ring-pack can be found in Section 2.4.2.

Operating Conditions

Several ramp transient measurements were conducted to investigate the impact of the initial conditions, final conditions, and engine operating speed on oil consumption. First, to understand the effects of engine operating speed, transients in load from no load (0%) to full load (100%) were performed at different engine speeds. Second, the importance of initial and final load conditions on oil consumption was investigated. The ramp transient conditions studied are summarized in Table 2-6. The engine was always operated at steady state conditions before the start of each transient.

3.4.2 Oil Consumption Measurements

Figure 3-13 and Figure 3-14 show the airflow rate, blowby rate, and oil consumption measurements as a function of time before and after the ramp transient for different

engine speeds and initial loads. In these figures, the airflow rate represents the engine load and the start of the ramp transient is marked. One can see that blowby responds to the airflow rate change almost instantaneously.

Figure 3-13 shows load transient measurements from no load (0%) to full load (100%) at two different engine speeds (2500 and 4200 rpm). During these transients, oil consumption reached a peak that is significantly higher than the steady state values and then gradually decreased to the steady state level of the final operating condition. It is appropriate to define transient oil consumption as the extra oil volume consumed during the engine transient to the final operating condition. This extra oil consumption is the difference between the oil consumption trace during the engine transient and the steady state full load value. The shaded area in Figure 3-13 shows this oil volume.

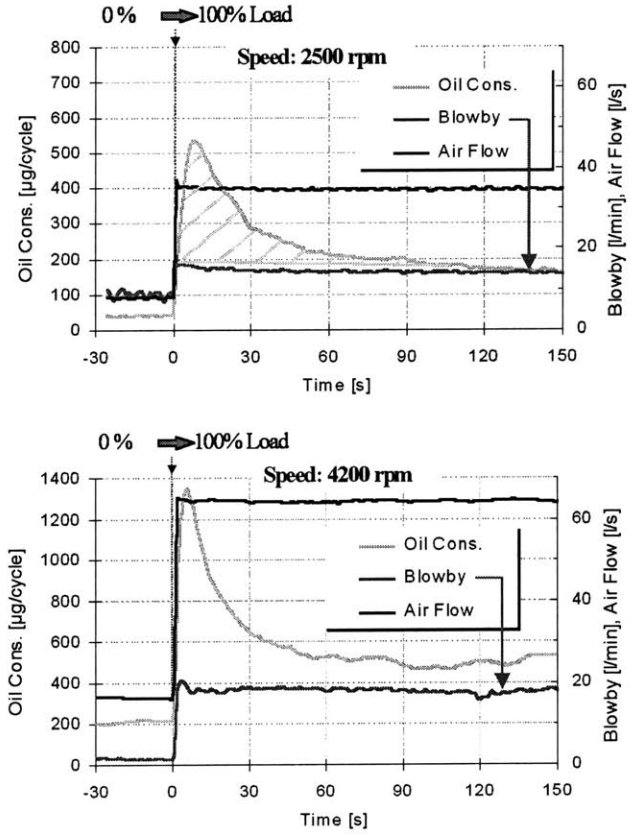

Figure 3-13 Oil consumption and blowby during transient in load (0% to 100%) at different speeds

Further work was conducted to study the importance of the initial load on the transient oil consumption. Figure 3-14 shows the results of ramp transients from different initial loads to full load (100%) at 4000 rpm. It is clear that the increase in oil consumption after the transient is less pronounced with increasing initial load. In the test from half load (50%) to full load (100%), there is no oil consumption spike after the transient and the oil consumption increases gradually from the initial condition to the final operating condition.

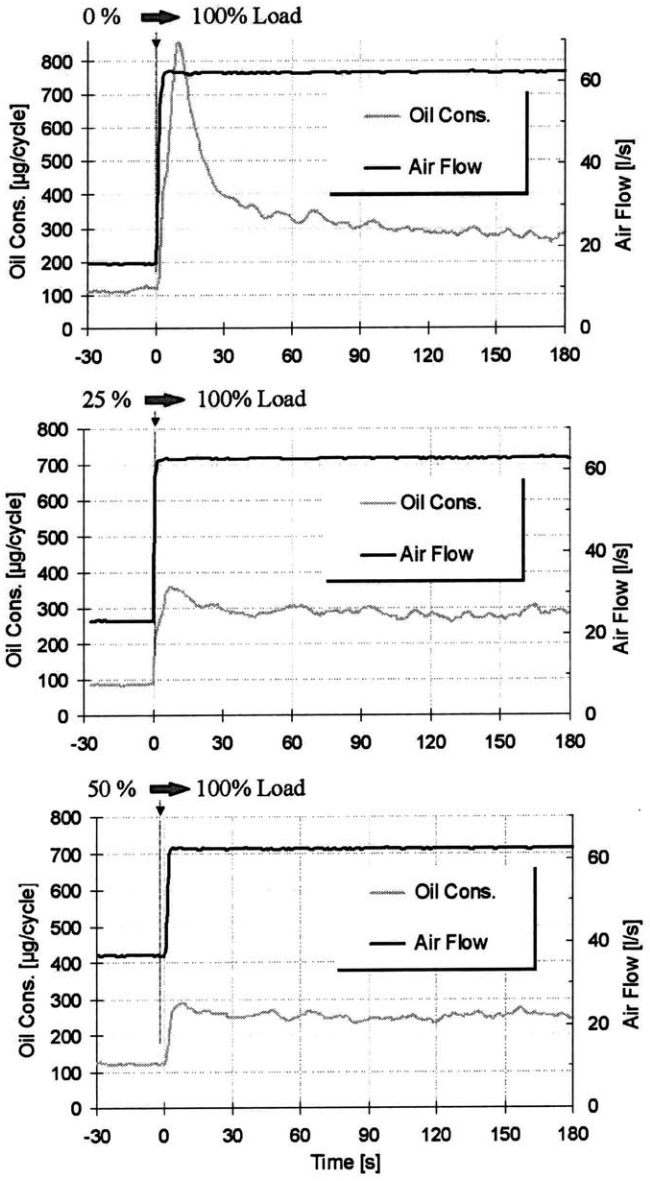

Figure 3-14 Oil consumption during transient in load and the importance of the initial load at 4000 rpm

Effect of blowby recirculation

As discussed in Section 4.1, the blowby gas flow entrains oil in liquid or vapor form and transports this oil to the intake system where it can take part in the combustion process. In order to investigate whether the increase of oil consumption during engine transients was due to increase of blowby oil consumption, measurements at 2500 rpm were repeated without recirculating the blowby gas flow to the intake manifold. Figure 3-15 shows the results of transient oil consumption at constant speed with and without blowby recirculation to the intake system. In both tests, a similar oil consumption peak and evolution can be observed. The influence of blowby on the transient oil consumption is little even though the oil consumption value at the final steady state condition without blowby recirculation is slightly lower than in the case where the blowby gases are recirculated. Therefore, it was concluded that oil entrainment in the blowby gas flow has negligible impact on the transient oil consumption phenomenon.

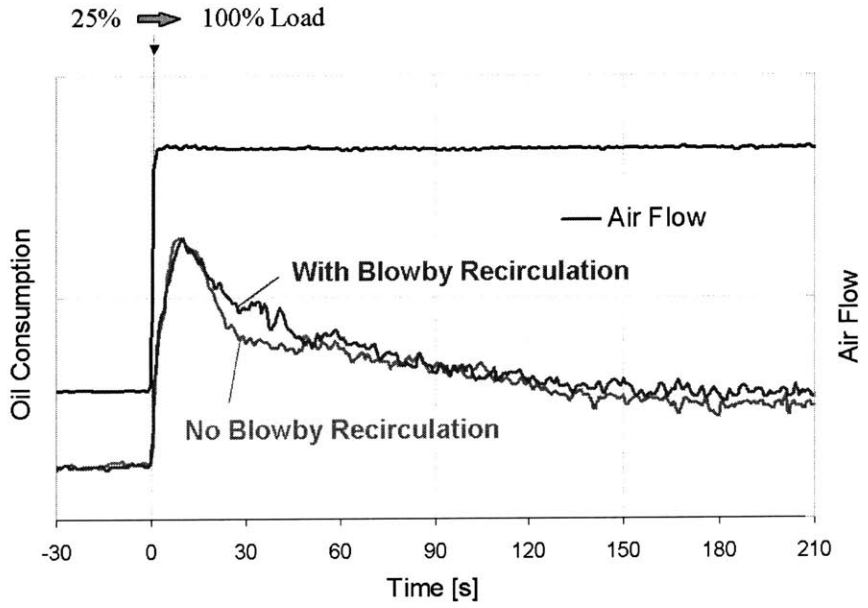

Figure 3-15 Effect of blowby on oil consumption during ramp transient in load

To gain a better understanding of the transient oil consumption, measurements of blowby, oil film thickness on the piston lands, and land pressures were conducted. The impact of these parameters on the transient oil consumption will be analyzed in the rest of

this section. The analysis will focus on the ramp transient from no load (0%) to full load (100%) since it results in the largest transient oil consumption.

3.4.3 Blowby, Land Pressures and Oil Film Thickness

The different ring-pack design used for the transient tests may vary the driving forces for oil transport and distribution in the piston-ring-pack. Therefore, steady state measurements were conducted to study the variation of blowby, land pressure, and oil film thickness with engine operating speed and load conditions.

As pointed out in Section 3.3, oil distribution on the piston lands and inside the ring grooves is largely controlled by the gas flow in different regions of the piston-ring pack. Obviously measuring gas flow between different regions is not possible. Gas flows were evaluated by combining the computer model RINGPACK-OC and the measurements of the following:

- Blowby, the average gas flow to the crankcase, and
- The land pressures when the piston land passes the pressure transducer probes on the liner (see Section 2.3.2)

In applying the models, unknown inputs such as oil volumes inside the piston ring grooves and piston lands were adjusted within a reasonable range until the predictions from the model calculation matched the steady state blowby and land pressure measurements. An example is shown in Figure 3-16. It should be noted that this same procedure was described above in Section 3.2 for the steady state tests. Then, the model prediction on gas flows between different regions was used to analyze the oil transport driven by gas flows, as discussed later in 3.4.4.

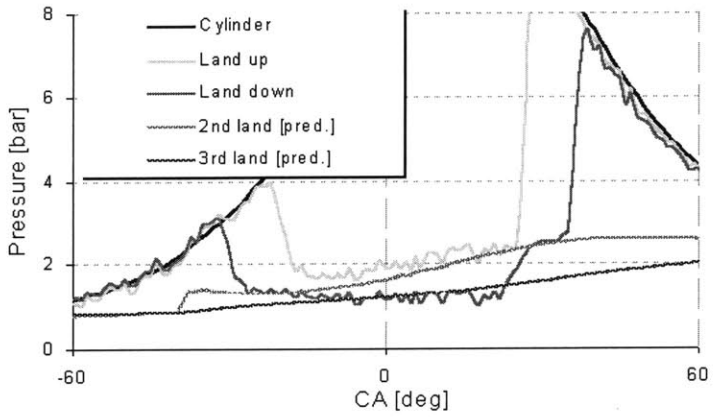

Blow-by: Measured : 3.88 l/min
Predicted : 3.82 l/min

Figure 3-16 Predicted and measured land pressures and blowby at no load (0%), 3500 rpm

Figure 3-17 shows the blowby results during steady state operation at different engine speed and load conditions. It is clear that also with this ring-pack blowby per cycle increases with increasing load throughout the entire speed range.

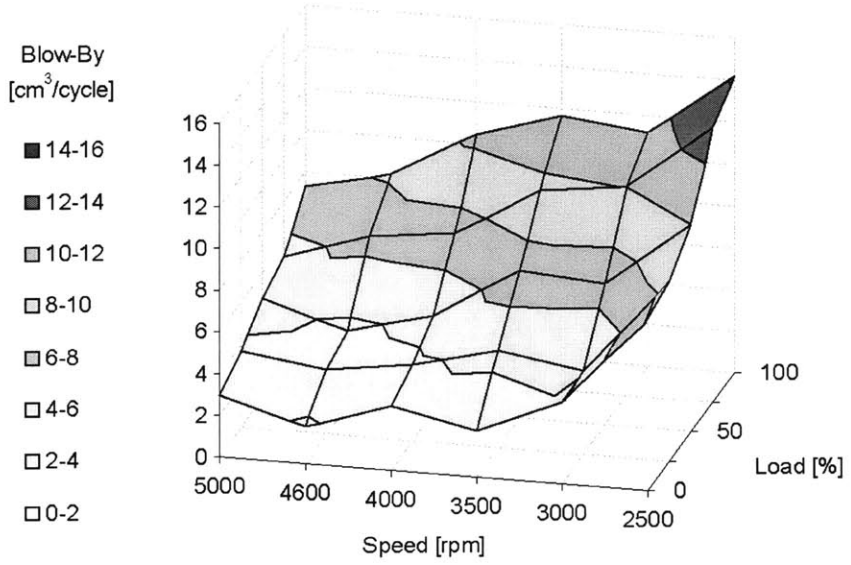

Figure 3-17 Blowby dependency on speed and load with ring-pack used for transient experiments

As discussed earlier in Section 3.3, oil on the piston lands is dragged by the gas flow due to interfacial shear stress. Therefore, decreasing blowby with decrease of engine load results in lower oil flow rate going to the crankcase. As a result, at a constant speed, one expects more oil accumulation on the piston lands with decrease in engine load, which is confirmed by the LIF measurements. The measurements were taken at the anti thrust side at the mid-stroke position (measurement position #1 in Figure 2-6). Figure 3-18 shows the measured average oil film thickness on the piston top land during steady state engine operation at different speed and load conditions. The average oil film thickness was determined by the procedure that was described in Section 3.3.3. It is evident that the average oil film thickness decreases with increasing engine load.

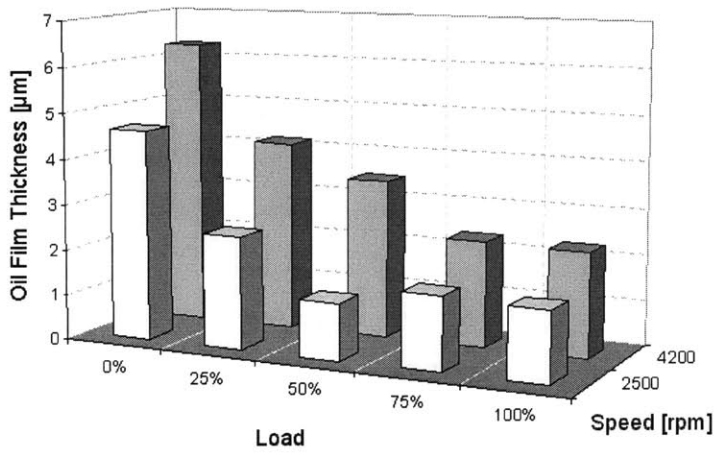

Figure 3-18 Oil accumulation on top land with varying load and speed

With the film thickness on the piston at steady state conditions characterized, the next step was to examine how it evolves after the ramp transient from no load (0%) to full load (100%). In addition to the measurements at initial and final conditions, the oil film thicknesses at two critical moments before the oil consumption is stabilized were measured. First, an LIF measurement was taken one second after the transient (i.e. after the stepper motor controlling the throttle stops at the final position) when a dramatic increase of oil consumption was observed. Then, an LIF measurement was taken two minutes after the transient, when oil consumption stabilizes and approaches the steady state value at full load. Figure 3-19 shows the LIF oil film thickness measurements

averaged over ten consecutive cycles during the ramp transient. The change of the oil film along the piston is shown during the compression stroke at an engine speed of 3500 rpm. It is evident that the oil film thickness on the piston lands decreases during the transient.

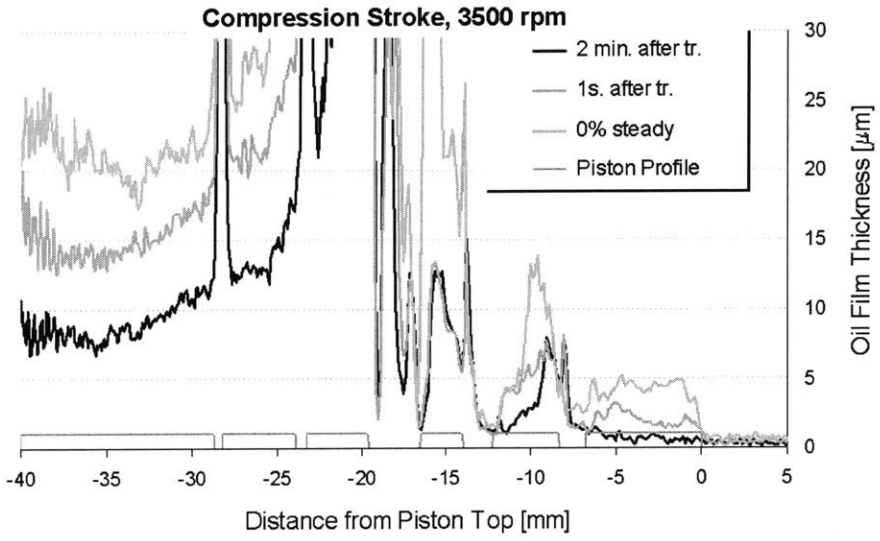

Figure 3-19 Oil film thickness evolution during ramp transient in load from no load (0%) to full load (100%) at 3500 rpm

In Figure 3-20, averaged oil film thickness measurements - over ten consecutive cycles and all engine strokes - on the piston lands are shown at three different engine speeds. The oil film accumulated on the piston lands during low load decreases significantly one second after the transient at all speeds. Thus, the increase of oil consumption immediately after the transient could be due to the oil accumulated on the lands. Furthermore, oil film thickness traces on the piston lands taken two minutes after the transient are similar to the ones acquired at steady full-load conditions suggesting that both engine oil consumption and the oil distribution on the piston have reached a steady state value by this time.

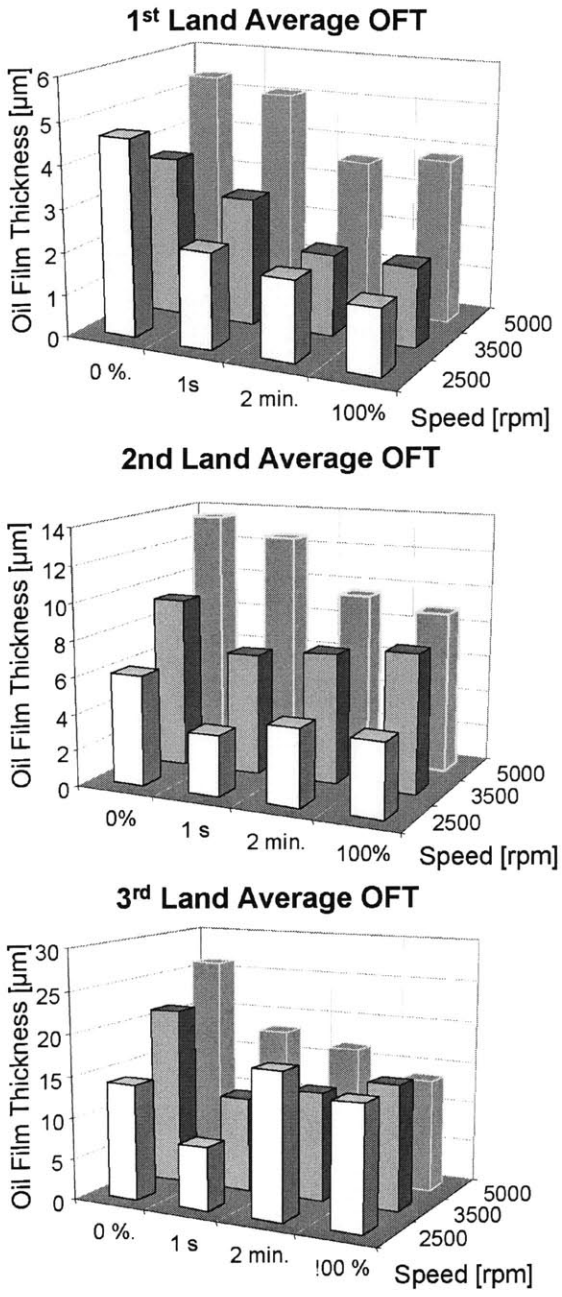

Figure 3-20 Change in oil film thickness after transient in load from no load (0%) to full load (100%) at different speed

During the transient to the final operating condition, gases with higher temperatures flowing into the crevice enhance oil evaporation on the top land. The gas flow into the top land crevice is significantly higher than the flow through the top ring gap into the second land. Therefore it may be reasonable to assume that most of the oil on the crown land enters the combustion chamber with the reverse flow of gases from the top land

crevice, which happens when the cylinder pressure starts to decrease during the engine cycle. The fraction that enters the combustion chamber during the transient from the total oil accumulated on the second and third lands before the transient is not known. However, due to the increase of blowby after the transient, most of the oil accumulated on the third land is probably transported into the crankcase. Assuming a uniform circumferential oil distribution on the lands, the difference between the amounts of oil accumulated before and after the transient on the top two lands can only account for up to 20 percent of the total extra oil consumed. For that reason, only part of the extra oil consumed during the transient in load can be attributed to oil accumulation on the piston lands.

3.4.4 Gas Flow and Ring Dynamics

A possible explanation for the extra oil consumed was suggested using RINGPACK-OC that predicts land pressures, gas flows in different regions of the piston ring-pack, and ring dynamics. As described in Section 3.4.3, steady state cylinder pressure, land pressure, and blowby measurements were used to adjust unknown input parameters for RINGPACK-OC.

Land pressures and blowby depend mostly on engine load. Therefore, during the transients, blowby (Figure 3-13) and land pressures increased almost instantaneously with engine load, while the thermal deformation effects on the clearances in the land and groove regions are of the order of a minute. Consequently, for the calculations the engine transient was simplified by using steady state in-cylinder measurements of the initial and final operating conditions and constant engine geometry inputs. In the following, load transient tests were analyzed at 4200 rpm.

Figure 3-21 shows a comparison of the measured and predicted land pressures at no load and full load conditions respectively. The model predicts second land pressures that are higher than the cylinder pressures, during end of expansion and early exhaust strokes. During this period, the pressure difference can drive oil with the reverse gas flow into the combustion chamber through the top ring gap and eventually groove. The model calculations of the top ring dynamics were used to identify the way oil could be transported into the combustion chamber.

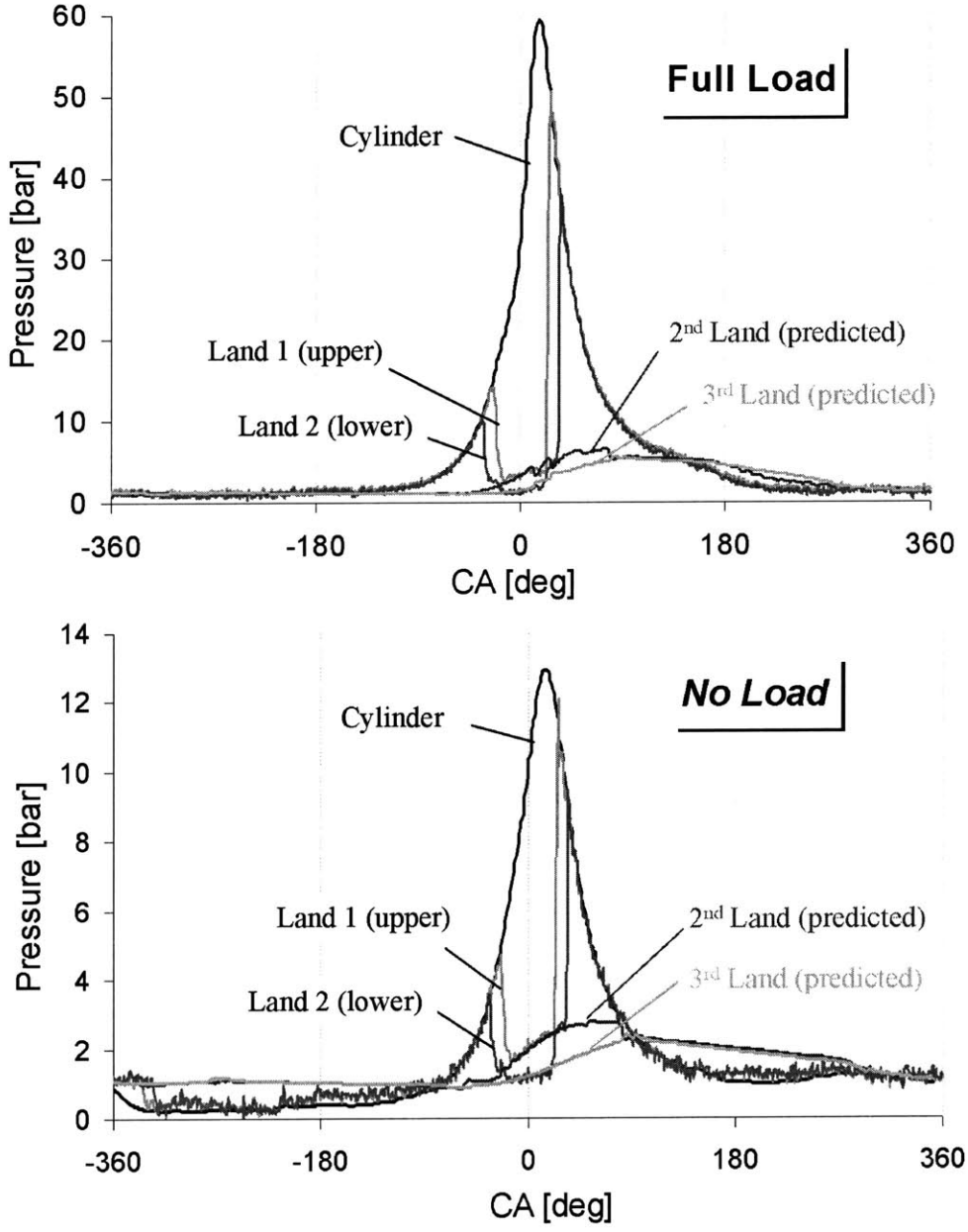

Figure 3-21 Comparison of measured and predicted land pressures at 4200rpm

Figure 3-22 shows the predicted normalized lift of the top ring center of gravity under no load and full load conditions at 4200 rpm. It is evident that top ring dynamics is more pronounced at full load, during the end of expansion and early exhaust strokes. During and after load transients, higher cylinder pressures trigger higher second land pressures. Therefore, during the end of expansion and early exhaust stroke, when the inertia force is downward, significantly higher second land pressures cause the top ring to lose its sealing

ability. Furthermore, the higher second land pressure induces ring flutter in the groove introducing additional leakage paths for reverse blowby gases to flow into the combustion chamber.

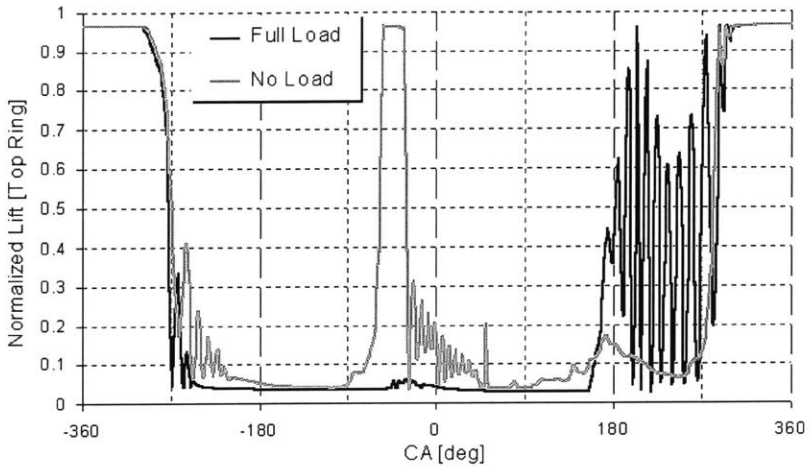

Figure 3-22 Top ring dynamics at 4200 rpm

Ring flutter has been characterized in earlier studies by Tian [43][44][54]. It is a result of the competition between gas pressure and inertial forces on the ring at a certain geometrical configuration with its groove. The top ring in its groove can only flutter and cause reverse blowby gases to flow into the combustion chamber when three critical conditions exist (see also Figure 3-23):

- The inertial force on the ring is pointing towards the crankcase
- The cylinder pressure is lower than the second land pressure and
- The relative angle between the top ring and its groove is positive as shown in Figure 3-23

The relative angle between the top ring and its groove depends on the ring static and dynamic twist, and on the top ring groove tilt. The top ring groove tilt is a result of piston thermal and mechanical deformations during engine operation.

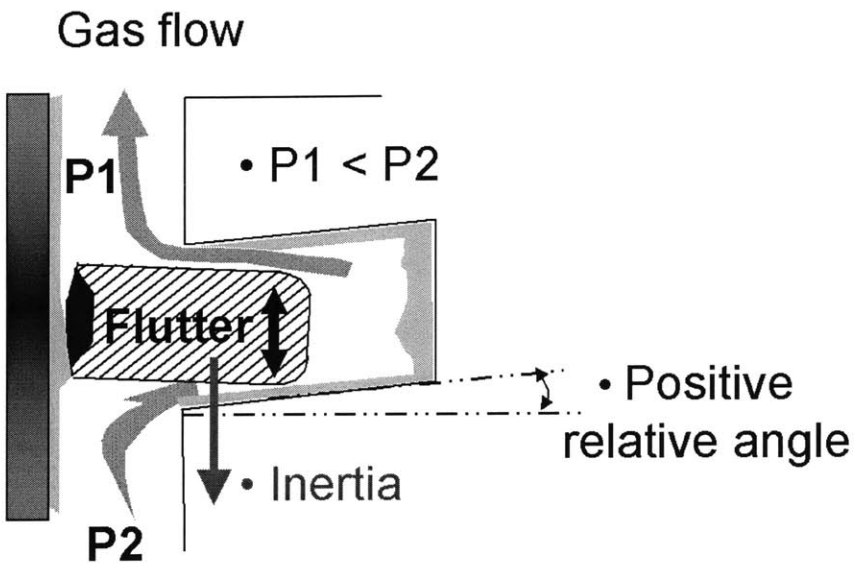

Figure 3-23 Schematic of top ring reverse flutter

If these three conditions exist during engine operation then the following sequence of events start during the end of expansion stroke (Figure 3-24):

As shown in Figure 3-24a, the top ring sits during the expansion stroke with the inner edge on the lower flank of the groove. As the cylinder pressure decreases at the end of the expansion stroke, the second land pressure becomes significantly higher than the cylinder pressures. During this period of the engine cycle, the direction of the inertia force is downwards. However, the net force on the ring is upwards due to the pressure difference across the ring and the ring is pushed to the upper flank of the groove. As a result, the higher second land pressure drives gases from the second land into the top ring groove (Figure 3-24b). Due to the positive relative angle between the ring and its groove, the minimum clearance between these surfaces is now at the outside edge of the groove. The ring seals the groove and the pressure at the back of the ring in the groove balances with the second land (Figure 3-24c). As a result, the net upward pressure force on the ring is decreased due to the smaller effective area exposed to the pressure gradient across the ring. The inertia force becomes dominant and pushes the ring down to the lower flank of the groove. This allows the gases in the region behind the top ring with higher pressure than the cylinder to flow into the combustion chamber (Figure 3-24d). Now the top ring seals again with the inner edge of the lower flank sitting on the top ring groove

and the pressure behind the ring in the groove balances with the combustion chamber (Figure 3-24a). The described sequence of events may start over again for several times until the exhaust stroke. During this period the cylinder pressure, second land pressure, and inertia force decrease. The sequence stops when inertia is reversed and the net force on the ring pushes it to the top flank of the groove at the middle of the exhaust stroke.

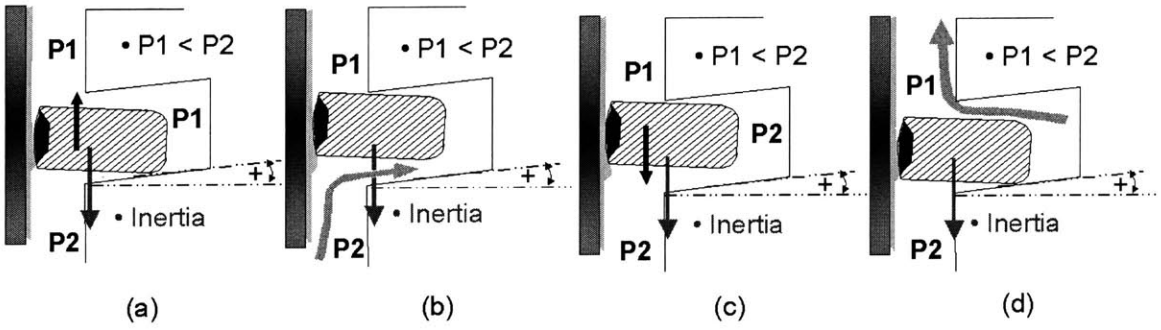

Figure 3-24 Illustration of the sequence of events during top ring reverse flutter

During this sequence of events of the top ring flutter phenomena, due to the pressure difference between the second land and the cylinder, reverse blowby gases flow towards the combustion chamber. The gases flow not only locally through the ring gap but also around the ring through the groove at the entire perimeter of the top ring.

Figure 3-25 shows gas flow rates through the two different paths at full load. It is evident that the gas flow through the top ring gap is negligible compared to the flow through the groove. Since the oil film accumulated on the lands has been found to increase with decreasing load, it is reasonable to assume that the oil present in the ring grooves increases with decreasing load. The reverse flow through the groove has the capability to drive and entrain oil that was accumulated in the top ring groove and second land during low load operating conditions. Subsequently, these gases enter the combustion chamber and temporarily increase oil consumption. The entrainment of oil in the reverse gas flow decreases the amount of oil accumulated in the region around the top ring groove.

The oil consumption data was used to estimate the oil volume consumed during the transient to the final operating condition (shaded area in Figure 3-13). The amount of oil lost during the transients from no load (0%) to full load (100%) was found to vary

between 0.25 to 0.35 grams (by integrating the measured oil consumption rates). The top ring groove of each piston was estimated to be able to hold an amount of up to 0.35 grams (assuming an oil density in the groove of 800 kg/m^3). Therefore, the top ring groove oil filling percentage was assumed 50% as the input for the RINGPACK-OC simulation program. Then the total amount of oil present in the top ring grooves could be around 0.7 grams prior to the transient (4 cylinder engine). Considering the estimates using the oil consumption data (~ 0.35 gram oil loss during the transients) the assumed initial oil filling fraction of the top ring grooves seems to be reasonable if half of this oil is transported into the combustion chamber during the transient.

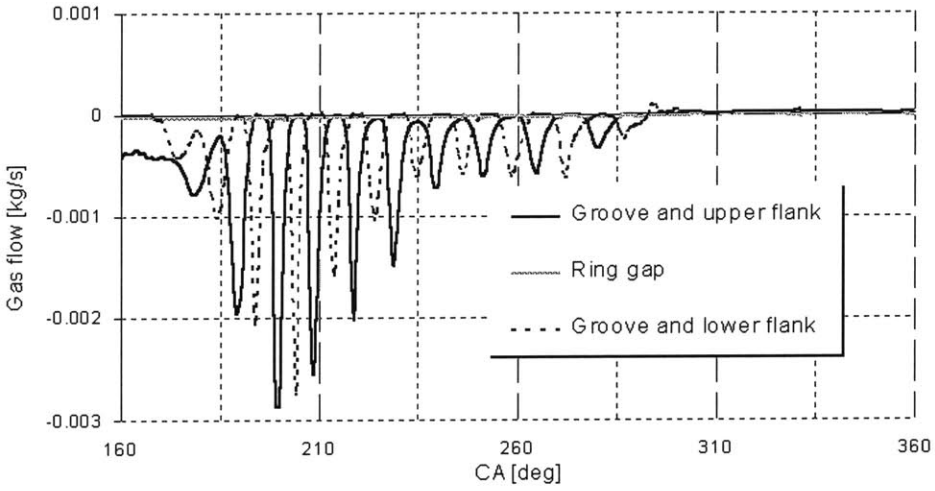

Figure 3-25 Gas flows through top ring groove and gap during reverse flutter at full load (100%), 4200 rpm

Average gas flow rates through the top ring groove and gap into the combustion chamber during the exhaust stroke at no load and full load were computed. The top ring groove oil filling percentage was assumed 50 percent for no load and 20 percent for full load. The results are shown in Table 3-1. In addition, assuming constant oil loadings of 1 percent by weight in the gas flows through the top groove and top ring gap, average oil flow rates into the combustion chamber were predicted. The results emphasize the significance of top ring reverse flutter to oil consumption. An order of magnitude difference in reverse flow through the ring groove is shown in comparing full load case to no load. A comparison with the transient oil consumption trace in Figure 3-13 indicates

that the difference between the observed oil consumption peak, and the steady state oil consumption level at full load, is about a factor of two higher than the predicted oil transport rate with the reverse gas flow into the combustion chamber.

4200 rpm – Full Load	**Through groove**	**Through gap**
Average gas flow (l/min)	-14.3	-1.22
Oil transport (μg/cycle)	- 308.5	- 19.1
4200 rpm – No Load	**Through groove**	**Through gap**
Average gas flow (l/min)	-1.54	- 0.79
Oil transport (μg/cycle)	- 24.1	-12.3

Table 3-1 Average reverse gas flows and oil transport (assuming 1 percent oil loading in the gas) into the combustion chamber at 4200 rpm.

The assumed oil loading was based on top ring groove sampling studies in a diesel engine that suggest 0.5 to 1 percent by weight oil content in the gases in the top ring groove [56]. During that study, gases were sampled continuously from the ring groove. Most of these gases were blown directly from the top land into the groove when the pressures in the top land crevice are high during compression and expansion strokes. In this case, there is little oil available along the flow path for the gas stream to entrain. Along the flow path from second land through the ring groove into the combustion chamber, there is much more oil available to entrain. Thus, the assumed 1 percent loading may underestimate the mass fraction entrained in the gas flow through the ring groove during the transient. However, the exact proportion of oil in the gas is unknown and the described hypothesis assumes a constant oil mass fraction in the gas flow independent of time and load. In reality, the proportion of oil in the reverse gas flow is expected to be higher when more oil is accumulated in the regions around the top ring groove. After the transient, as oil film thickness measurements indicate, oil accumulation on the piston decreases as time evolves. Consequently, oil entrained in the reverse gas

flow declines, which may explain the observed gradual decrease of oil consumption to the steady full-load condition after reaching a maximum.

3.4.5 2-D LIF Observations

To support this hypothesis images were acquired using 2-D LIF on the one cylinder engine. Transient measurements were performed from no load (0%) to full load (100%) at 2500 rpm.

Figure 3-26 shows LIF images before and during the engine transition to the final operating condition. The first image shows the oil distribution on the piston land before the transient. The later images, taken after the transient, clearly show liquid oil outflow from the top ring groove to the top land. Immediately after the transient, liquid oil is transported to the top land around the entire perimeter of the top ring (second image). This observation confirms the presence of oil in the top ring groove during low load and the subsequent transport of oil to the top land. Furthermore, several seconds (~ 12 s) after the transient oil transport to the top land was observed at several locations around the perimeter of the top ring (shown in the third image).

The oil on the top land is probably transported by the gas flow through the groove during top ring flutter at the end of the expansion and early in the exhaust strokes. In summary, the observations in the one cylinder engine support the hypothesis and connect oil consumption and in-cylinder measurements with the modeling results.

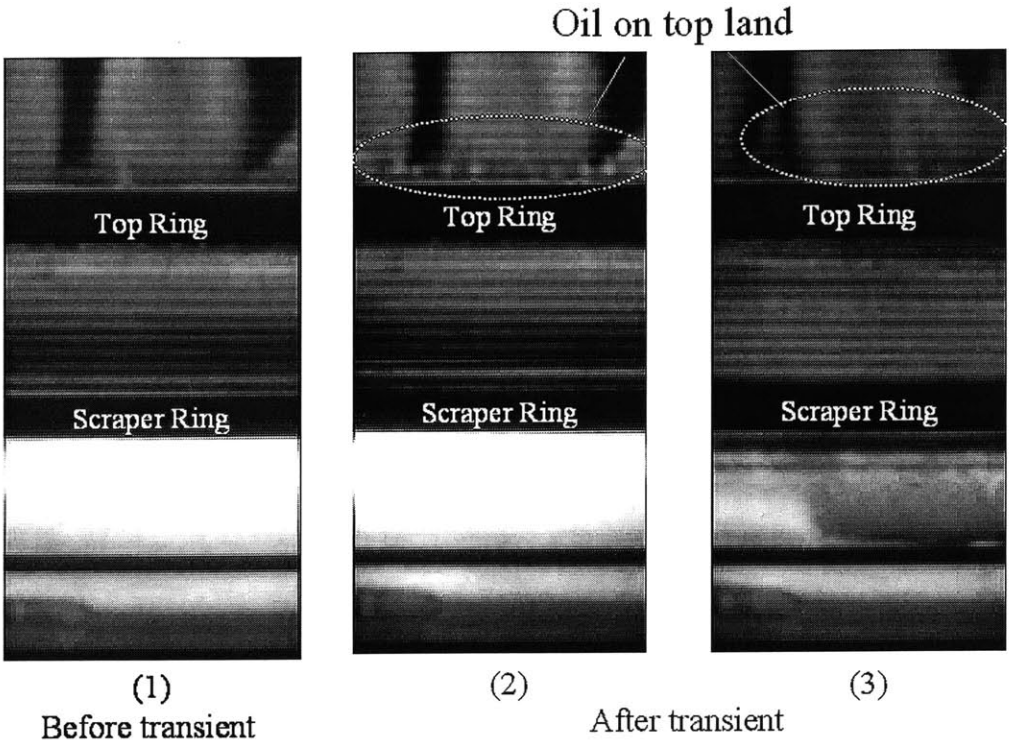

Figure 3-26 Oil flow during transient at 2500 rpm

3.4.6 Summary for Analysis of Oil Consumption during Transients in Load

This section has characterized the oil consumption during ramp transients in load. Oil transport and consumption during transients from low-load to high-load conditions were analyzed by combining oil consumption measurements, in-cylinder measurements, and modeling. Increased oil consumption has been observed during transients from low load to full load. The extra oil consumed during the transient increased with decreasing initial load. Measurements of in-cylinder variables showed that under low load operating conditions, engine oil transport to the upper piston regions was enhanced due to low blowby flow rates into the crankcase. As a result, at lower load conditions more oil accumulated on the piston lands and grooves. After the load transients, the oil accumulated on the piston lands decreased significantly. It was found that the difference of oil accumulation on the lands could not be solely attributed to the extra oil consumed during the transient. Using computer models to predict gas flows in the ring-pack and ring dynamics, a possible explanation was suggested. It was found that the top ring

might lose its sealing ability and flutter during the transient at full load. During top ring flutter, reverse gas flows through the groove, entraining the oil that was accumulated in the groove during low load conditions and driving it into the combustion chamber. This hypothesis was supported by the observations on a one-cylinder research engine with the same ring-pack and engine design when images acquired using a 2-D LIF technique during the same load transients clearly showed liquid oil flowing out from the top ring groove.

Chapter 4 Oil Consumption Sources

All oil consumption sources described in Chapter 1 contribute to total oil consumption during engine operation. The contribution of each source depends on different driving forces for oil transport, and on lubricant properties. For example, oil evaporation is believed to depend largely on component temperatures, lubricant volatility, the transport rate processes of the oil vapor into the cylinder gas, and the supply of oil to regions of high evaporation. The entrainment of oil in the blowby flow depends on oil transport, oil distribution, and the complex flow of gas in the piston-ring-pack. Most of these controlling parameters for oil consumption change with engine operating conditions. Consequently, also the oil consumption rate and the contribution of the different oil consumption sources change with engine operating speed and load.

In this chapter, the contribution of different oil consumption sources to total engine oil consumption is analyzed at various steady state speed and load conditions. The contribution of oil entrained in the blowby gas to total engine oil consumption is experimentally quantified and analyzed. Oil evaporation is then characterized, combining oil consumption measurements, in-cylinder measurements, and theoretical modeling. Finally, the experimental and modeling results are used to separate and assess the contribution of three major oil consumption sources to total oil consumption at different steady state speed and load conditions.

4.1 Blowby

Combustion chamber gases leak past the piston-ring-liner system into the crankcase due to imperfect sealing by the piston rings. This leakage, also referred as blowby, is a non-steady periodic flow containing combustion gases, soot, unburned mixture, and oil in liquid and vapor form. The blowby flow characteristics were described in more detail in Section 2.3.1.2. In modern engines, the crankcase is vented to the intake system and blowby gases are recycled. The oil mist that is entrained in the blowby flow to the intake system subsequently enters the combustion chamber and contributes to total engine oil

consumption. Earlier experimental studies have found that the blowby contribution to total oil consumption could be significant for specific engines and operating conditions [1][7]. In addition to this, the recycled oil in the blowby may form deposits on the intake valves and on compressor blades of turbocharged engines causing engine performance efficiency drops or even, in extreme cases, the failure of these components.

4.1.1 Blowby Contribution to Oil Consumption at Different Speed and Load

Oil from various sources in different regions is entrained in the blowby gas. Along the blowby flow path from the combustion chamber to the crankcase, the gases flow through various regions of the piston-ring-pack and entrain oil. The oil entrainment in these regions is believed to be both in liquid and vapor form. More volatile oil compounds are assumed to evaporate from hot surfaces into the blowby gas stream, and the micron scale liquid oil film in the piston-ring-pack is atomized by locally high velocity gas flows. On their flow path to the crankcase, the gases may flow through the ring gaps, through the ring groove during ring flutter, and through the clearance between ring and liner during ring collapse [43][44]. During most operating conditions, however, ring stability is preserved and the main leakage of consequence is the gas flow from ring gap to ring gap. This gas flow drags the oil on the piston lands toward the ring gaps due to interfacial shear stresses. Experimental evidence from 2-D visualization suggests that this oil atomizes in the ring gap as it flows through, dragged by the high velocity gas flow [46]. A large fraction of this oil is believed to be entrained in the gas stream. The oil transport to the ring gaps was found to depend on the average oil film thickness on the piston lands and on the cumulative volumetric blowby gas flow rate (see Section 3.3.2.2). Therefore, oil distribution on the piston lands and blowby flow are both believed to have a significant impact on oil entrainment in the piston-ring-pack. After passing the piston skirt, the oil-laden blowby gases enter the crankcase and mix with the crankcase gases.

In the crankcase, moving engine parts may reach significant velocities and the piston alternating motion may generate locally high gas velocities. Here, additional oil entrainment can be expected, aided by oil splashing from moving parts, oil leaks from the bearings and the spray jet cooling of the piston. Spray jet cooling is employed in the test engine to reduce the piston temperature by enhancing heat transfer and to supply

additional lubrication for the highly loaded major thrust side of the cylinder liner. To achieve this, oil is being sprayed from a nozzle at the big end of the connecting rod toward the inner side of the piston. Airborne oil in the crankcase from sources described above can reach significant velocities relative to the moving engine parts and the surrounding gas flow. The interaction of airborne oil with the gas flow may cause droplet break-up, forming smaller droplets due to the augmentation of surface tension; the impingement of oil droplets on moving surfaces may also generate smaller secondary droplets due to splash. The resulting small droplets are more likely to be entrained in the crankcase gas flow. In addition, vaporized oil in the blowby may condense along the flow path due to heat losses to the cooler environment, thus creating additional oil droplets. The phenomena described above suggest that the crankcase blowby gases may contain oil droplets from various sources and in different sizes.

Oil entrainment in the crankcase is believed to increase with engine speed. The increased velocities of moving engine parts and of gas flow in the crankcase due to higher engine speeds may enhance the droplet break-up to small droplets and the subsequent entrainment in the blowby flow. In addition, at high engine speed, surface waves in the oil sump could be generated on the oil air interface that may result in additional oil entrainment.

The oil-laden crankcase gases are vented to the intake system. However, before entering the intake manifold the gases flow through an oil separator to minimize oil entrainment and its impact on oil consumption and engine performance. As the gases flow through the separator, oil droplets are removed from the main gas flow and returned to the engine sump. There exist different separator types based on varying separation principles. The test engine in this study was equipped with an inertial baffle separator. A principle schematic of a baffle separator is shown in Figure 4-1. This separator type has prevailed in the automotive industry, driven mainly by an acceptable separation efficiency of small droplets ($< 10\ \mu m$) at a reasonable pressure drop. In addition, the limited space in modern engines, combined with economic factors, contributed to the popularity of the baffle separator in passenger car engines.

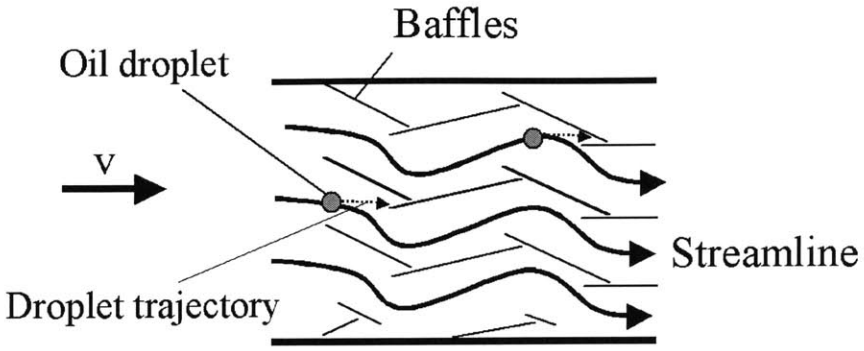

Figure 4-1 Illustration of the inertial separator

The separation principle is based on inertial movements of the disperse phase, relative to the carrier gas streamline. The movement of small droplets (order of 10 μm) in a gas stream is governed by inertia forces and aerodynamic drag. When the exerted aerodynamic drag on the droplet is not able to overcome the inertial forces, the droplets divert from the flow streamline and impact on the baffles. Subsequently, the separated oil drains off from drainage holes to the oil sump. However, not all particles can be efficiently separated from the carrier gas; droplet sizes smaller than a certain diameter may follow the gas flow. This is because inertia forces are proportional to the droplet diameter to the cube (and the droplet velocity), and aerodynamic drag to the droplet diameter (for Reynolds numbers smaller than 0.5). Consequently, with decreasing droplet size, the aerodynamic drag becomes significantly greater than droplet inertia and causes the droplet to follow the gas flow. Therefore, it can be assumed that the probability for droplets to divert from the streamline and impact on a baffle plate increases with their diameter and their velocity. For example, in [57] it is suggested that for a particle of unit specific gravity, inertial effects are unimportant for droplets smaller than 0.2 μm. Larger droplets (dp > 10μm) settle out rapidly due to gravity or are separated efficiently in the separator.

In previous experimental studies, the performances of inertial separators were assessed for different engines and engine operating conditions, and separation efficiency curves were determined. A typical separation efficiency curve range of an inertial

separator is shown in Figure 4-2 [8]. The parameter weight oversize R determines the cumulative weight fraction of droplets above a certain droplet size. It is evident that the separation of fine shares (droplets with dp < 2μm) is inefficient. These droplets constitute about 80 percent of the total droplet mass in the blowby downstream the separator, and therefore contribute significantly to the total oil in the blowby.

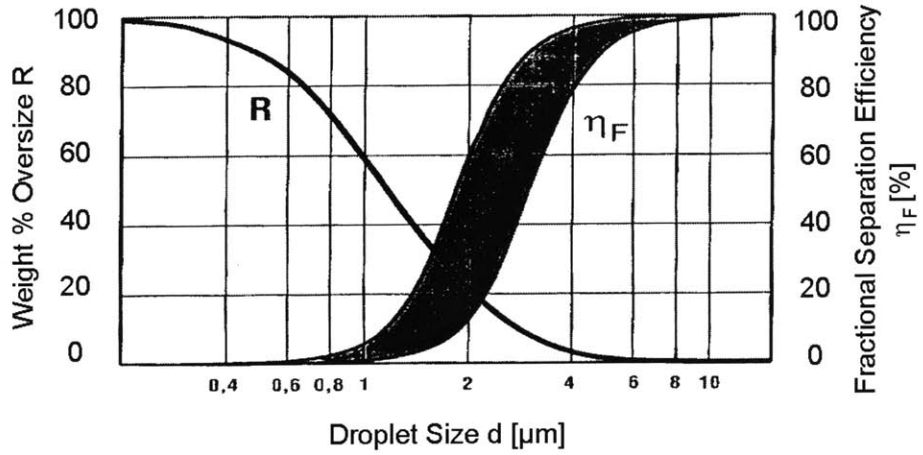

Figure 4-2 Typical efficiency curve of an inertial separator [8]

From the above description, it is apparent that the amount of oil carried to the intake system depends not only on entrainment in the piston-ring-pack and crankcase, but also on the separator performance. All above described aspects for oil entrainment and separation vary with engine operating conditions, such as speed and load. Therefore, the oil transported with the blowby to the intake system, thus contributing to total oil consumption, varies with engine conditions, which emphasizes the complexity of these phenomena.

For the test engine, the contribution of oil in the blowby to total oil consumption was quantified at different engine load and speed conditions. This contribution was obtained by determining the difference in oil consumption with and without blowby gas return to the intake system. In the latter case, the blowby gases were vented to the test cell exhaust trench after passing the oil separator. Figure 4-3 shows the oil consumption rate due to blowby at different steady state engine operating conditions. A close dependence on

engine conditions was found when blowby oil consumption increased with engine speed and load. It should be noted that for the measurements during 0% load at 2500 and 3500 rpm, there was no difference in oil consumption when testing with and without blowby gas return to the intake system. Therefore, it was concluded that at these conditions the contribution of blowby to total oil consumption was negligible.

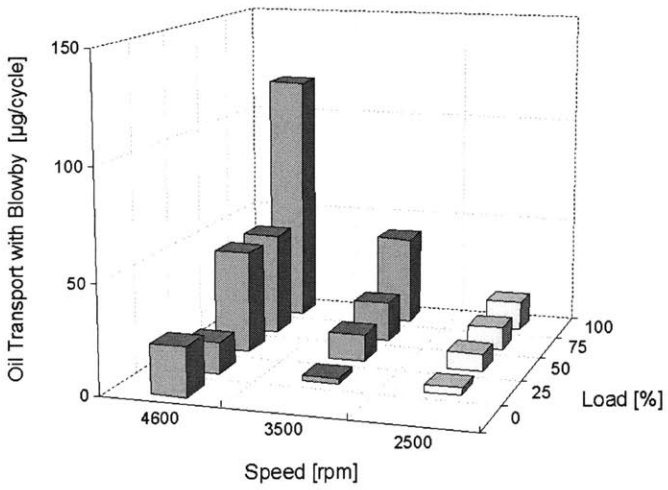

Figure 4-3 Oil consumption due to oil entrainment in the blowby gas flow at different speed and load

As discussed in Section 3.2, steady state total oil consumption and blowby flow rate vary with engine speed and load. Therefore, the data in Figure 4-3 was used to determine the contribution of oil in the blowby to total oil consumption. The relative importance of this oil consumption source was found to increase with engine load reaching significant levels at high load conditions. For the investigated operating conditions, the maximal contribution of the entrained oil in the blowby to total oil consumption was found to be about 16 percent of the total oil consumption at full load (100%) and 3500 rpm. However, there was no consistent trend found with the increase of engine speed at constant load. Figure 4-4 illustrates the blowby contribution to total oil consumption at different speed and load conditions.

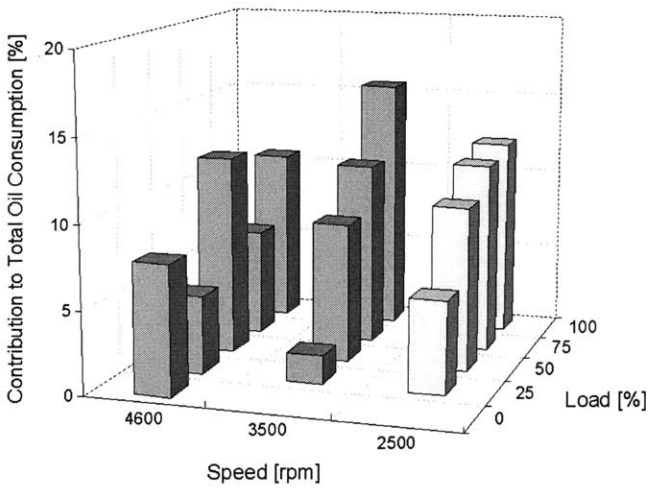

Figure 4-4 Contribution of the oil in the recycled blowby gases to total oil consumption at different speed and load

After quantifying the blowby contribution to total oil consumption, the oil content of the blowby gas (amount of oil carried per volume of blowby gases) was determined. Figure 4-5 illustrates the dependence of blowby oil content on different engine speed and load conditions. It is clear that the blowby oil content increases with engine speed. Increased engine speed may result in an increase of the oil content for the following reasons.

As described above, the amount of oil in the blowby downstream of the separator depends on the oil entrainment in the ring-pack and crankcase, and on the oil separator performance. The atomization and entrainment processes in the piston-ring-pack should be closely related to oil distribution on the piston lands (especially adjacent to the ring gaps), and to the blowby flow feature and rate (per cycle). As described in Section 3.3, steady state blowby and LIF measurements showed that increasing engine speed decreased the average blowby flow, but increased the oil accumulation on the piston top two lands. Therefore, since the oil entrainment in the ring-pack is believed to depend on both blowby and oil accumulation, the impact of higher engine speeds on the atomization and entrainment processes in the piston-ring-pack remains unclear. Yet, higher component temperatures at higher speeds are likely to increase the evaporation of oil into the blowby gas flow. On the other hand, higher gas flows and moving engine part velocities may enhance droplet break-up processes in the crankcase. Consequently, the

entrainment of smaller oil droplets in the crankcase gases may increase with increasing engine speed.

Increasing engine speed may also affect the oil separator's efficiency. Oil separator efficiency and pressure drop both depend on gas flow characteristic and the size and velocity of the entrained droplets. Increasing engine speed has little impact on the average gas flow rate (per unit time), but it increases the frequency of flow pulsations. The impact of speed on blowby pulsation amplitude and on separator efficiency, however, is unknown. The understanding of the impact of engine speed on the separation efficiency requires detailed analysis of gas flow through the separator, which is beyond the scope of this work.

It can be summarized that increasing engine speed is likely to enhance the oil entrainment in the crankcase and piston-ring-pack. This increased entrainment could be the cause for the observed increase of the blowby oil content with engine speed. Even though the oil content in the blowby increases with speed, the relative importance to total oil consumption does not indicate speed dependence.

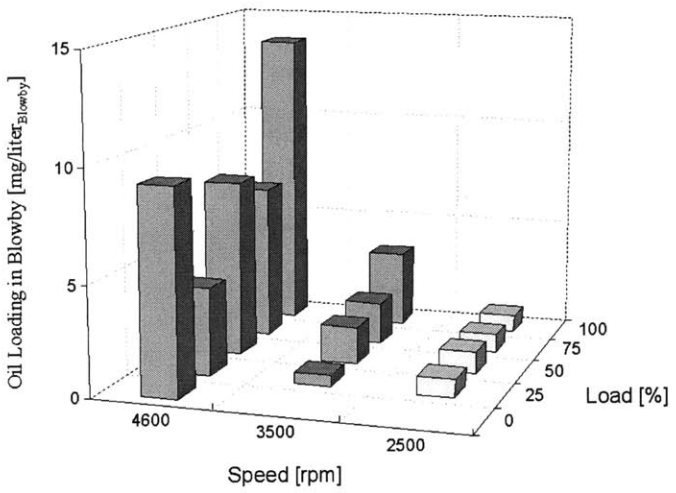

Figure 4-5 Oil loading in the blowby gas flow into the intake manifold system

4.1.2 Particle Size Distribution in the Blowby

The entrained oil in the blowby flow is expected as liquid particles and vapor. Therefore, a study was carried out to investigate the size distribution, size concentration, and volume concentration of the liquid particles in the blowby gas downstream of the oil separator. An earlier study found that the particles in the blowby of different engines exhibited similar mass distributions [9]. Figure 4-6 shows the particle mass distribution results for four different engines that were reported in [9]. In all investigated engines, even though particles up to 6 μm were present in the blowby flow, the particles between 0.5 to 1.5 μm diameter account for the majority of the particle mass.

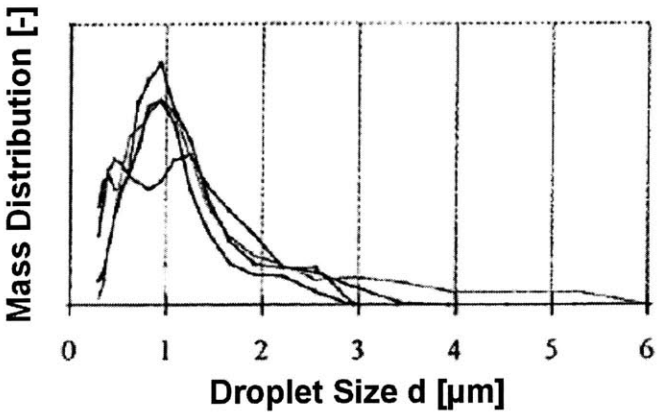

Figure 4-6 Particle mass distribution in the blowby flow of different engines [9]

The Scanning Mobility Particle Sizer (SMPS) was used to measure particle number and volume concentrations. Different steady state speed and load conditions were investigated to obtain information on the operating condition dependence of the particles. The SMPS system has been described in detail in Section 2.3.1.3. The maximal measurable particle size range of the SMPS was set to 20 – 930 nm. Even though the SMPS does not cover the expected entire particle size range in the blowby flow, it can provide useful information on particle characteristics up to 1 μm.

The effect of engine load on the particle size distribution was measured at two engine speeds, namely at 2500 and 3500 rpm. Figure 4-7 shows the effect of engine load on the particle size distribution at 2500 rpm. The concentration of particles with a diameter

larger than 50 nm increased with engine load. Increased load may cause an increase of particles in the blowby, due to the resulting increase in cylinder peak pressures and blowby flow rates. This increase in blowby gas flow through the ring-pack enhances the oil dragging on the piston lands due to interfacial shear stresses. As a result, more oil is dragged through the ring gaps and atomized by the high velocity gap gas flow. The atomized oil is then either entrained in the blowby gas flow or impacts and spreads on the land and the liner. However, since more oil is atomized at higher engine loads, more oil entrainment in the blowby gas flow can be expected. The entrained oil from the piston-ring-pack is believed to be constituted of small droplets (dp < 2 μm). As the blowby gas flows through the oil separator, most of these droplets are expected to escape the separation process and follow the gas flow, because of the separator's low efficiency for small droplets as shown in Figure 4-2. Therefore, increasing engine load enhances oil entrainment in the piston-ring-pack and raises the concentration of the particle size distribution in the blowby.

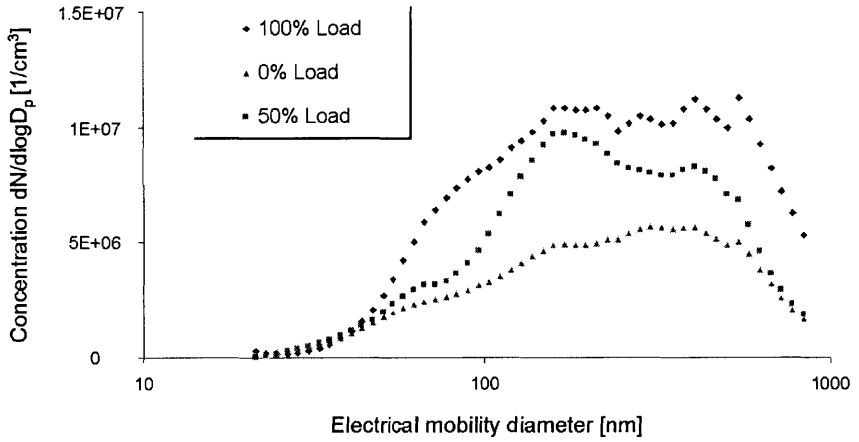

Figure 4-7 Load effect on particle size distribution in the blowby flow at 2500 rpm

Previous studies on the formation of particulate matter in spark ignition engines suggest a strong dependence of particulate matter on engine operating conditions such as engine speed and load. Therefore, the particle size distribution measurements of the blowby gases could include particulate matter in addition to the liquid oil droplets. Changing engine conditions could also affect the formation of particulate matter, and consequently its concentration in the blowby flow. Nevertheless, the contribution of

particulate matter to the particle size distribution measurements of the blowby flow can be neglected for two reasons. First, measurements in the exhaust of a spark ignition engine (Figure 4-8) found an order of magnitude lower particulate matter concentrations than the concentrations in the blowby flow [56]. Second, the size distributions measurements of the particulate matter and blowby gases show different characteristics. In the blowby gas flow, highest particle concentrations were observed for sizes larger than 100 nm. Measurements of particulate matter, however, show a negligible concentration of particulates above 100 nm. Therefore, it should be reasonable to neglect the contribution of particulate matter to the particle size distribution measurements of the blowby gases.

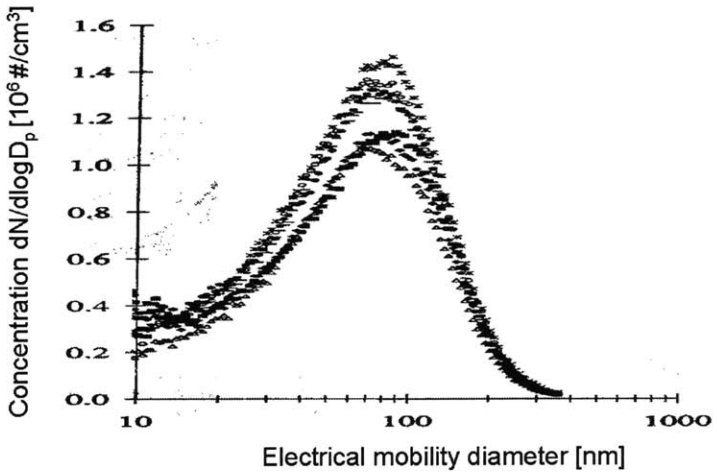

Figure 4-8 Particle size distribution in the exhaust of a spark ignition engine [56]

The impact of engine load on particle number concentrations is reflected in particle volume concentrations, which also increase with engine load. Figure 4-9 shows the variation of the particle volume concentrations in the blowby with load at 2500 rpm. The results for sizes above 930 nm were estimated by assuming spherical particle forms and an exponential decay of the particle concentration distribution curves shown in Figure 4-7. For particle sizes smaller than 300 nm, little difference in the volume concentrations can be found between the different load conditions. However, increased particle volume concentration with engine load is clear for larger particles. Moreover, the difference in the volume concentrations increases with increasing particle size. This is because the

particle volume scales not only with the particle number concentration, but more importantly also with the particle diameter to the cube.

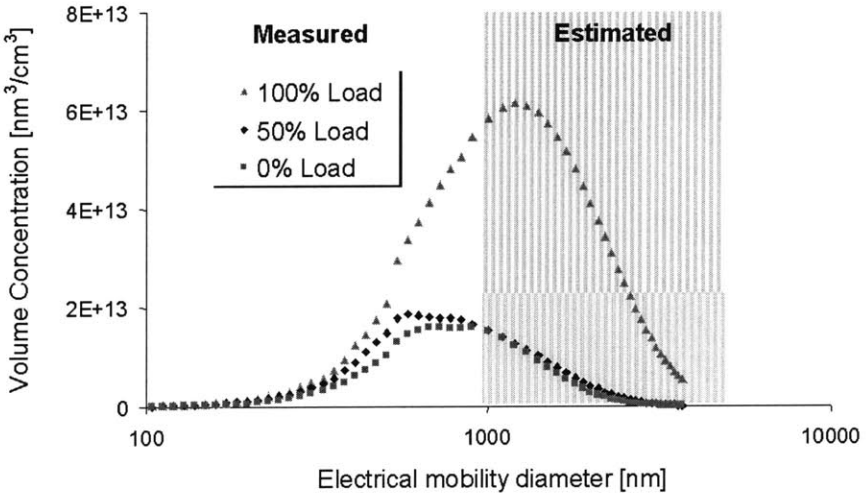

Figure 4-9 Load effect on droplet volume concentration at 2500 rpm

The volume concentration results were used to evaluate the cumulative liquid oil that was entrained in the blowby (summation of all particles up to 1 μm) by assuming that all measured particles are liquid oil droplets. The droplets' mass concentration is directly related to the particle volume concentration by the droplet density. The droplet density was obtained by measuring the blowby gas temperature for the engine conditions of interest and interpolating oil density analysis data of the used oil.

Estimates for the liquid oil entrainment were compared to the measured oil consumption rate due to blowby (shown in Figure 4-3). The proportion of the liquid oil droplets to the total oil in the blowby gas is shown for different engine operating conditions in Figure 4-10. It can be seen that at full load conditions this proportion can account for up to 60 percent of the oil present in the blowby. However, in reality the proportions of liquid oil are likely to be higher since droplets with a diameter larger than 1 μm were not considered. As estimates of the particle volume concentration in Figure 4-9 suggest, droplets larger than 1 μm may significantly increase the total proportion of liquid oil in the blowby.

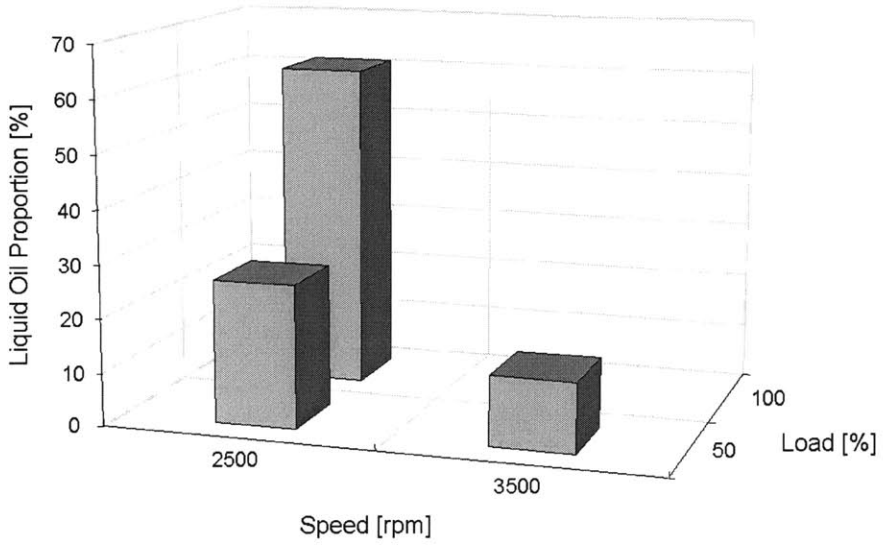

Figure 4-10 Liquid oil particle proportion of total oil in the blowby gases

Additional studies were conducted to investigate the effects of oil evaporation to the blowby oil consumption. For this purpose, blowby oil consumption was measured for varying engine liner temperatures at 50% load and 2500 rpm. A variation of engine liner temperatures may affect the evaporation into the blowby from different sources. As discussed later in Section 4.2, liner temperatures significantly affect the liner evaporation and total oil consumption. Higher liner temperatures increase the thermal conditions in the piston ring-pack, which could affect the evaporation from this region into the blowby. The results showed little impact of varying liner temperatures on blowby oil consumption and thus suggest little contribution of oil evaporation to blowby oil consumption. Therefore, even though evaporation plays an important role to total oil consumption, evaporation does not seem to contribute significantly to blowby oil consumption.

4.1.3 Summary of the Oil Consumption due to Blowby

The contribution of oil entrained in the blowby gases to total engine oil consumption was analyzed by combining measurements of oil consumption, blowby flow, and the particle size distribution in the blowby for different speed and load conditions. Blowby oil consumption was quantified by determining the difference between oil consumption with and without blowby gas return to the intake system. The measurements showed that blowby oil consumption increased with increasing engine speed and load. The

contribution of oil in the blowby gases to total oil consumption, however, was found to increase only with engine load. Its contribution to oil consumption was negligible at low load conditions (below 50% load), but reached significant levels at high load. The maximal contribution of the blowby gases to oil consumption was found to be about 16 percent at 100% load and 3500 rpm. Blowby oil loading increased with engine speed, suggesting an enhanced oil entrainment in either the ring-pack or the crankcase.

Measurements of the particle size distribution in the blowby also showed an increase in particle concentration with engine load. Further analysis of the particle size distribution indicated that a significant portion of the oil in the recycled blowby could be liquid oil droplets.

4.2 Oil Evaporation

Despite much research, there is a lack of understanding and quantification of key oil consumption sources due to the complex nature of the phenomena. One example is the relationship between oil volatility and oil evaporation from the piston-ring-liner system, and its impact on total oil consumption. This section presents an extensive experimental and theoretical study on the contribution of oil evaporation to total oil consumption at different steady state speed and load conditions.

4.2.1 Introduction

Oil consumption is directly related to physical oil properties, such as oil volatility and viscosity. While the viscosity affects oil transport mechanisms on the liner and piston, the volatility directly governs the oil evaporation rate from hot surfaces during the engine cycle. Oil evaporating from the piston-ring-liner system is believed to contribute significantly to total oil consumption, especially during severe operating conditions.

Earlier studies have demonstrated the significance of oil viscosity and volatility to oil consumption [23][24]. There exist also some averaged oil consumption measurements in passenger cars illustrating the effects of volatility and viscosity on oil consumption [59][60][61]. In these studies, the cars were operated for a certain period in a mixed cycle. Empirical formulas, often categorized in engine types, were developed from the

obtained results to correlate oil consumption with oil volatility and viscosity. However, the impact of these physical oil properties on the oil transport and consumption mechanisms is not completely understood. In another experimental study on a one-cylinder hydrogen engine, oil volatility was found to be only critical at elevated liner temperatures [22].

A number of solely theoretical approaches studied the oil evaporation from the cylinder liner of internal combustion engines [40][41][42]. These models were based on the diffusion process of oil vapor through the gas boundary layer on the liner surface. The lubricant was modeled either as a mixture of a number of hydrocarbon species, or as a single species oil. All approaches found a sensitivity of the evaporation process to oil composition and cylinder liner temperature.

The purpose of the described work in this section is to characterize the contribution of oil evaporation on oil consumption in the test engine. For this purpose the coolant outlet temperature, oil volatility, and operating conditions were varied to examine their impact on oil evaporation and oil consumption. The study was carried out by combining oil consumption measurements, in-cylinder measurements, and theoretical modeling.

The dependence of oil consumption on coolant outlet temperature and oil volatility was measured at different engine operating speed and load. Liquid oil distribution on the piston was studied using the one-point Laser-Induced-Fluorescence (LIF). In addition, important in-cylinder variables for oil evaporation, such as liner temperature and cylinder pressure, were measured. A multi-species cylinder liner oil evaporation model was developed to interpret the oil consumption data.

4.2.2 Experimental Methodology and Conditions

4.2.2.1 Oil Specifications

As mentioned earlier the oil transport and consumption are dependent on oil properties such as viscosity and volatility. Several standardized laboratory test methods determine these properties. Since this paper focuses on the volatility of two oils, a brief discussion is presented on test methods that are currently used in the automotive industry

to specify oil volatility, namely the Noack method (ASTM D 5800) and the Gas Chromatography Distillation (GCD) method (ASTM D 6417).

The Noack method quantifies the evaporation loss of lubricating oils in a specified tester and at specified test conditions. The oil sample, heated to 250°C, is exposed for one hour to air with a constant flow rate. The Noack evaporation loss corresponds to the mass of lubricant lost during the test. This method is intended to simulate engine conditions, since the oil surface is constantly exposed to air and the temperature is comparable to temperatures in the upper part of the piston-ring-pack at high engine load conditions.

Although the Noack method is regarded in the industry as a good indicator for oil evaporation, it may not correctly simulate the evaporation processes in the piston-ring-liner system during engine operation. In the Noack test, the liquid film exposed to the airflow is about 3 cm, which is roughly 10^3 to 10^4 times thicker than the average oil film present in the piston-ring-liner system (order of 10 μm on the piston and 1 μm on the liner). During the Noack test the multi-species diffusion resistance inside the oil layer limits the species transport to the liquid-gas interface, whereas the evaporation of oil on the piston and liner is convection limited as discussed later in Section 4.2.5.1. Therefore, the loss of oil, as determined by the Noack method can differ substantially from the actual oil evaporated from the piston-ring-liner system.

For this work, the Gas Chromatography Distillation (GCD) method was found to be more appropriate to characterize the oil volatility and evaporation from the liner. Lubricating oil is a liquid mixture of a number of hydrocarbon species with different vapor pressures and other thermo physical properties. Since the oil evaporation from the piston-ring-liner system is controlled by mass convection, the partial pressure of each hydrocarbon species on the liquid surface affects the rate of evaporation. These partial pressures can be obtained using the GCD method. Unlike the Noack test, the GCD determines the true boiling range distribution of the petroleum fractions at atmospheric pressure. The boiling point distillation curves can then be used to determine the partial pressures of the hydrocarbon species on the surface and therefore to evaluate oil evaporation. It should be noted that the industry uses the percentage of engine oil

volatilized at 371°C, which is obtained from the gas chromatographic distillation, as a common indicator for oil volatility.

BASELINE OIL (MINERAL)		**ASTM D**
SAE Viscosity Grade	10W-30	
Sulfur [wt. %]	1.51	1552
Volatility: GCD % off @ 371° C	11.6	
Noack	16.8	5800
Viscosity @ 100°C [mm2/s]	10.77	445
HTHS viscosity [cP]	3.04	4683

SYNTHETIC OIL		**ASTM D**
SAE Viscosity Grade	0W-30	
Sulfur [wt. %]	1.68	1552
Volatility: GCD % off @ 371° C	3.7	
Noack	13.5	5800
Viscosity @ 100°C [mm2/s]	11.22	445
HTHS viscosity [cP]	3.04	4683

Table 4-1 Relevant oil specifications of the test oils

In this work, two lubricants with different volatility characteristics – different GCD curves (see Figure 4-27) – were used to investigate the impact of oil volatility on oil evaporation and consumption. The relevant oil properties are shown in Table 4-1. While the lower volatility synthetic oil is within the current American Petroleum Institute (API) and International Lubricant Standardization and Approval Committee (ILSAC) specifications (API SL/ ILSAC GF-3), the baseline oil is marginally higher than the specifications.

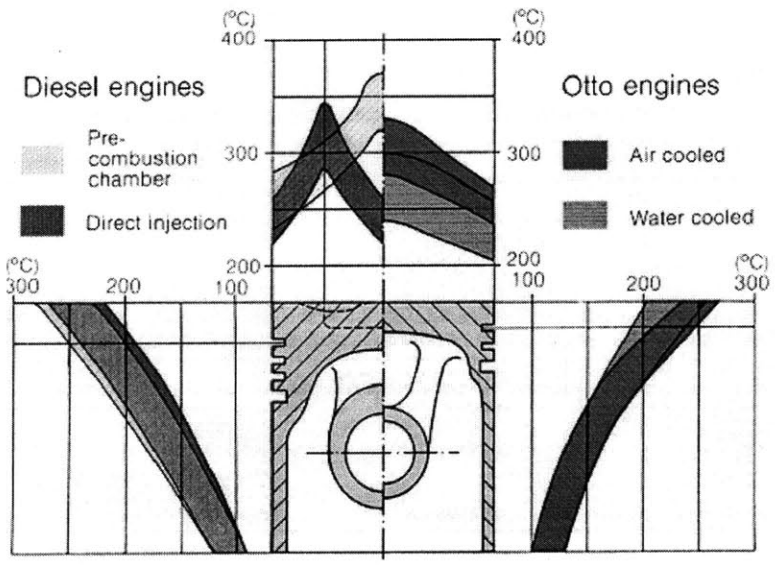

Figure 4-11 Typical operating temperatures on the piston surface at full load [62]

As shown in Table 4-1, the two oils have been formulated with similar viscosity properties to minimize the difference in oil transport along the piston and liner. It must be recognized that viscosity governs in large part oil transport mechanisms to the upper regions of the piston-ring-liner system and therefore affects oil consumption. The low shear viscosity affects different oil transport mechanisms in different regions on the piston surface such as inertia forces due to piston movement, gas flow dragging, and the interactions between the rings and grooves. The HTHS (High Temperature High Shear) viscosity is believed to influence ring and piston liner lubrication, and thus govern the oil transport on the liner.

Even though the test oils low shear viscosities at 100°C are similar, they have different SAE oil classification numbers (SAE 10W-30 and SAE 0W-30). These oils must operate over a range of temperatures (from 100° up to 250°C) because of the temperature gradient along the piston assembly and because of the gradients' dependence on the operating conditions (see Figure 4-11). Moreover, the oil viscosity decreases with increasing temperature. Consequently, any differences between the two oils viscosity at elevated temperatures could affect the oil transport mechanisms along the piston and thus oil consumption. Therefore, further lab analyses were performed on the test oils to examine their low shear viscosities at temperatures above 100°C (ASTM D 445 and SAVLAB LPYC density tests) and the Vogel equation was used to correlate the

measured temperature-viscosity data. The obtained low shear viscosity-temperature relation for both oils is shown in Figure 4-12, which confirms the similarity of the oil viscosities at temperatures above 100°C. Therefore, any difference in oil consumption between the oils should be mainly a result of the difference in their volatilities.

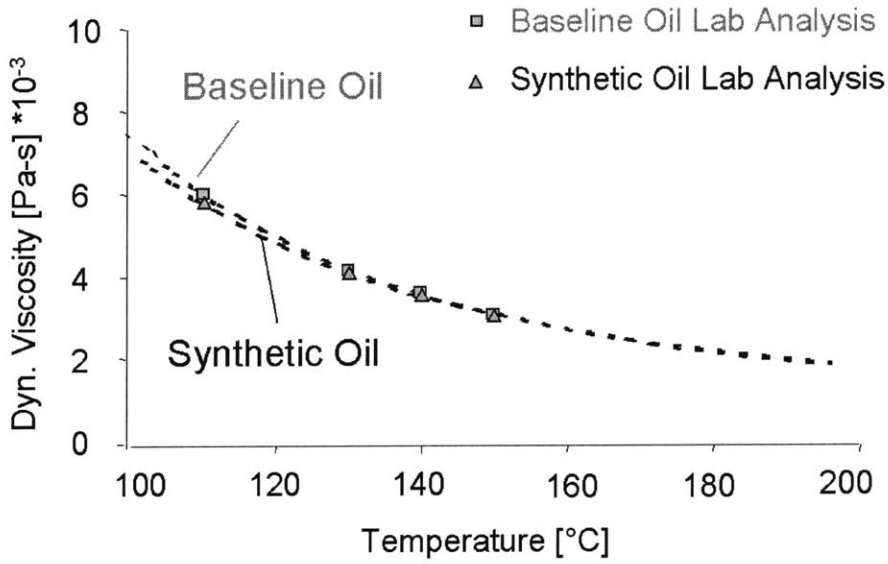

Figure 4-12 Comparison of the viscosity of both test oils

For both oils, the average sulfur concentration by weight (ASTM D 1552) was used to determine the oil consumption rate. This is reasonable if the sulfur in the oil is constant over the entire oil distillation range, as is the case for the baseline oil. Then the consumed oil (liquid and evaporated) in the exhaust has the same concentration of sulfur as in the original oil. However, Figure 4-13 shows that the synthetic oil sulfur content is not constant with the distillation; the sulfur concentration at the 10 percent distillation fraction is significantly higher than the average concentration. This distillation property of the sulfur in the synthetic oil introduces a measurement error, namely an overestimation of the oil evaporation and thus consumption rate. Nonetheless, further analysis using oil evaporation estimations indicated that the introduced error is not significant. The model predictions show that the high volatility oil species (first 6 percent of the distillation curve) contribute to about 80 percent of total oil evaporation. Oil species present in the first 40 percent of the distillation curve contribute to at least 95 percent of the total oil evaporation. In addition, it was found that even at extreme

operating conditions the contribution of oil evaporation to oil consumption does not exceed 40 percent. Using the evaporation predictions with the distillation property of the sulfur in the oil, the introduced error was estimated to be less than 5 percent of the actual total oil consumption value. As a result, this overestimation of the oil consumption rate for the synthetic oil does not affect the main conclusions of this study.

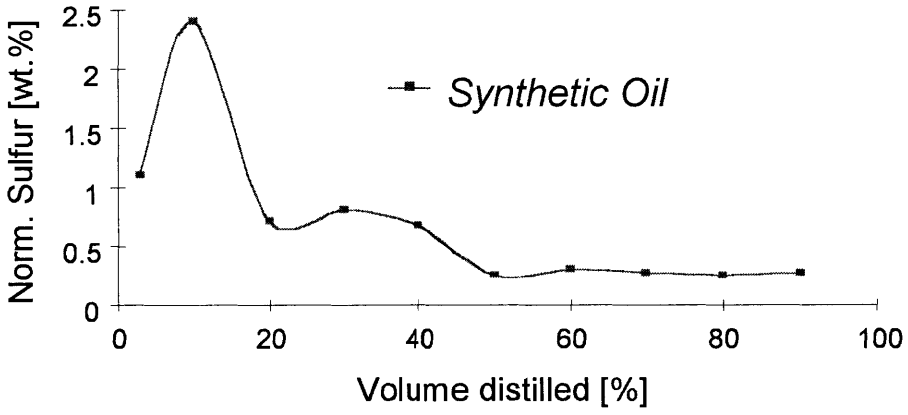

Figure 4-13 Synthetic oil sulfur content with distillation

4.2.2.2 Experimental Conditions

The oil evaporation process is influenced by oil volatility, thermal conditions during engine operation, and gas convection from the film surface. While the oil volatility and engine component temperatures determine the oil vapor pressure in the gas side of the liquid oil-gas interface, the rate of oil vapor convected from the surface is governed by the mass transfer coefficient.

In general, the dependence of oil vapor pressure on temperature is described by an exponential relationship. Therefore, the oil film present in regions with elevated temperature, such as in the upper liner regions, is believed to contribute significantly to the evaporation process. The oil transport mechanisms to regions of high evaporation and thermal conditions in these regions can vary with the engine operation mode (such as engine speed, load and warm-up process). In order to explore thoroughly the contribution of oil evaporation, oil consumption measurements were conducted with varying liner temperatures for both oils at different steady state speed and load conditions.

A linear relationship between cylinder liner and coolant outlet temperatures was observed during all investigated conditions. Therefore, the liner temperature was easily varied by controlling the coolant outlet temperature. For the measurements, the coolant outlet temperature was varied between 55 and 90°C. An example of the relation between the measured coolant outlet and liner temperatures is shown in Figure 4-14 (see Figure 2-6 for the liner temperature measurement locations).

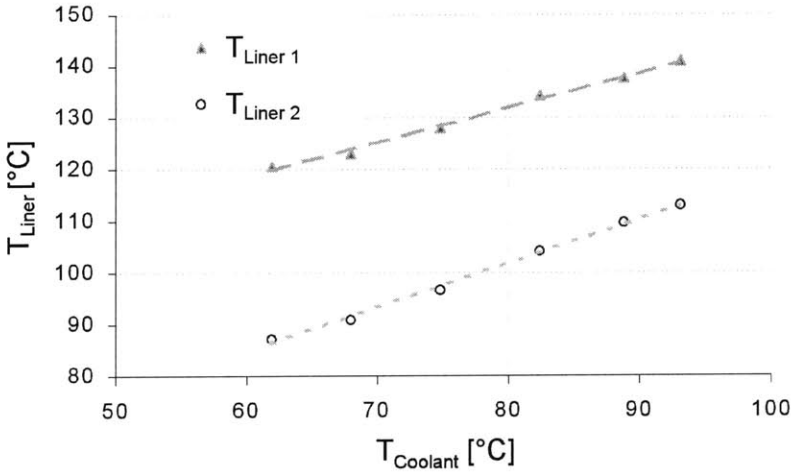

Figure 4-14 Relation between coolant and liner temperatures at 75% load, 3500 rpm

However, heat transfer per unit time and the engine thermal loading increases, as the engine operating speed and load increases. Figure 4-15 shows the relationship between the liner temperature at the location of the scraper ring at TDC ($T_{Liner\ 1}$) and coolant outlet temperature for different load conditions at 3500 rpm.

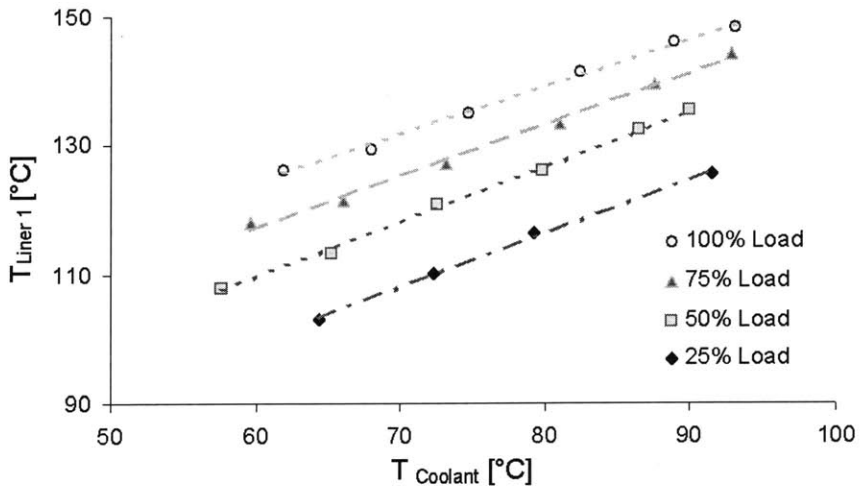

Figure 4-15 Effect of coolant outlet temperature on liner temperature at the TDC location of the scraper ring at different load, 3500 rpm

Additional measurements were conducted for both oils to understand and quantify the impact of oil volatility on oil consumption at different steady state conditions. During these tests the coolant outlet temperature was controlled in the range 81 ± 1.5°C. It is clear that changing operating conditions vary the mass transfer of oil from the surface and the engine component temperatures, which determine the oil vapor pressure on the surface. The mass transfer does not depend on oil composition and the temperature measurements showed little difference between the two oils. Therefore, any difference in oil consumption between the oils should be mainly a result of the difference in their volatilities. All investigated operating conditions are summarized in Figure 4-16.

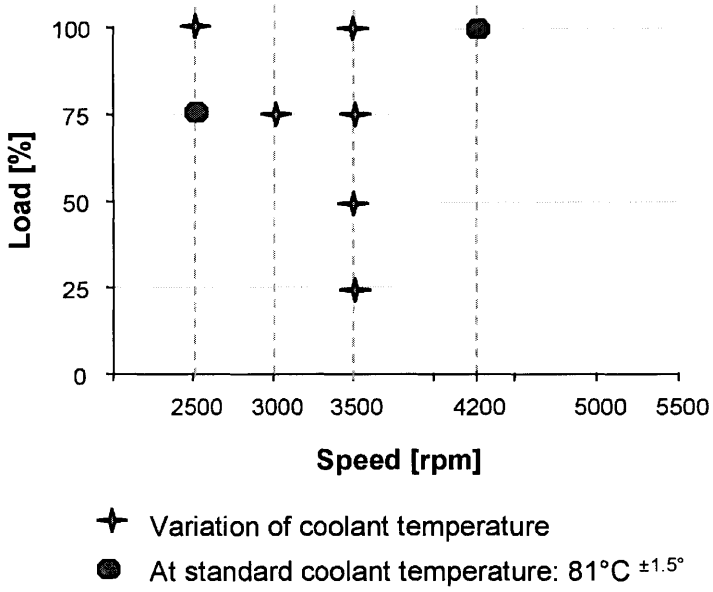

Figure 4-16 Investigated operating conditions (evaporation study)

The testing procedure involved several sequences. First, the engine was filled with fresh oil and was operated 2.5 hours. At the end of this period, the oil consumption value had stabilized. Then the measurements of the total output and in-cylinder variables were conducted. Immediately after the completion of the measurements, the initial oil was drained, the oil filter was changed, and the engine was flushed once with the new oil. Afterwards, the oil filter was changed again before starting the test procedure with the new oil. The engine was always allowed to reach the thermal steady state condition before the start of the data acquisition.

4.2.3 Effect of Cylinder Liner Temperature on Oil Consumption

Figure 4-17 and Figure 4-18 show the total engine oil consumption measurements for both test lubricants as a function of liner temperature (at the TDC location of the scraper ring) for different engine speed and load conditions. Figure 4-17 shows the measurements for low load (25%), half load (50%), and 75% load at 3500 rpm. At all engine loads and for both lubricants, a linear correlation between oil consumption and liner (coolant) temperature was observed when coolant outlet temperatures were increased from 60 to 90°C.

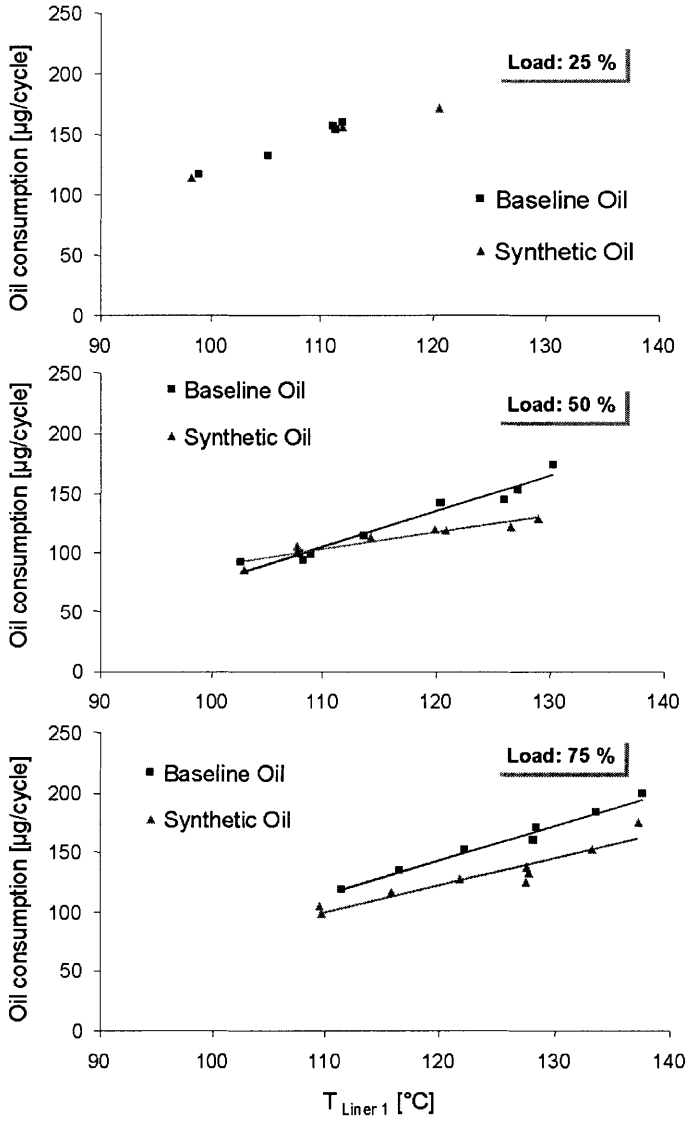

Figure 4-17 Oil consumption dependence on liner temperature at different load, 3500 rpm

For low load (25%), oil consumption increased by about 50% when the liner temperature at TDC of the scraper ring increased from 100°C to 125°C. However, there was little difference found in the oil consumption between the two lubricants at the investigated liner temperatures. As the engine load was increased, a difference of oil consumption between the two oils was observed as shown in the measurements at 50% load, 75% load, and 100% load (Figure 4-17 and Figure 4-18). At these conditions, the baseline oil consumption rate was higher and its dependence on liner temperature was

stronger. Therefore, the difference in oil consumption between the two oils increased as liner temperatures were increased at constant engine load and speed.

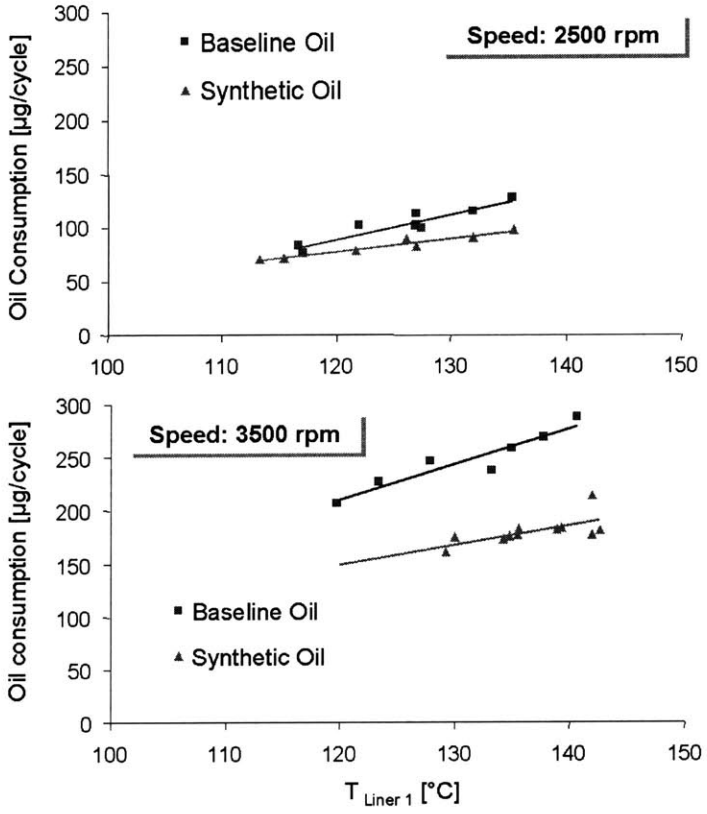

Figure 4-18 Oil consumption dependence on liner temperature at different speed, full load (100%)

Two factors predominantly affect the oil evaporation process when the mass convection coefficient is fixed: the oil volatility, and the thermal loading of hot surfaces in the piston-ring-liner system. If the thermal loading of the engine is also fixed, then the oil volatility should be the main difference in oil consumption between the two oils. Compared to the synthetic oil, the more volatile baseline oil produces higher vapor partial pressure on the gas side of the liquid-gas interface resulting in higher evaporation rates. Moreover, for the baseline oil, there is a stronger exponential relationship between oil vapor pressure and temperature. Thus, as the temperatures increase, the difference in oil consumption between the two oils is also increased.

Furthermore, the measurements indicate that as the thermal loading increases with engine load, the contribution of oil evaporation becomes higher. It can be seen (Figure 4-17) that at operating conditions that have low component temperatures, such as low load conditions, a difference in oil consumption between the two oils could not be observed. As the load is increased, the engine thermal loading becomes more severe and increases the oil evaporation with both oils. Then the difference in the oil consumption rates between the two oils becomes measurable.

Additional measurements were conducted to study the impact of engine speed on oil consumption and evaporation. Increasing engine speed has two primary effects that can cause higher oil evaporation rates. First, the thermal loading of engine components increases as speed increases. Second, higher speeds enhance the level of turbulence in the cylinder and thereby the mass transport in the gas phase (mass convection coefficient). On the other hand, as speed increases the available time for the evaporation process decreases per cycle. Figure 4-18 shows the oil consumption results for both oils as a function of liner temperature at full load and two different engine speeds (2500 and 3500 rpm). Oil consumption was higher with the baseline oil at both speeds. In addition, the linear dependence of oil consumption on liner temperature was stronger with the higher volatility baseline oil as observed in the load studies. Moreover, the difference in oil consumption between the two oils was more pronounced at 3500 rpm due to the higher contribution of oil evaporation to oil consumption. This result suggests that the higher thermal loading and increasing mass convection coefficient with engine speed have a more dominant impact on the evaporation process than the decrease of available time per cycle.

4.2.4 Effect of Oil Volatility on Oil Consumption

The engine is designed to be operated at around 81°C coolant outlet temperature (standard thermal condition). Measurements at this thermal condition were conducted to examine the impact of oil volatility on oil consumption at different steady state speed and load conditions. As oil volatility was reduced, oil consumption decreased at several engine speed and load conditions. Figure 4-19 shows the measured difference of oil consumption (ΔOC) between the baseline oil and the lower volatility synthetic oil at

different speed and load conditions. This difference in oil consumption represents mainly the effect of volatility, since the viscosities of the two oils are comparable. It is clear that the impact of oil volatility on oil consumption increases with engine speed and load.

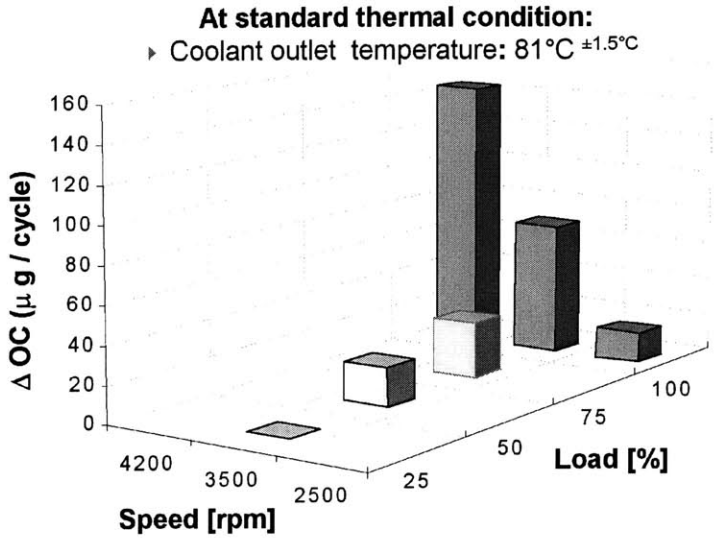

Figure 4-19 Difference in oil consumption due to oil volatility at different speed and load

To further demonstrate the effect of oil volatility, the same data was used to determine the improvement in oil economy due to the reduction in oil volatility – as a percent of the baseline oil consumption. Figure 4-20 illustrates this improvement at different speed and load conditions. Again, a close dependence on speed and load is evident. For example at 4200 rpm and full load (100%), oil consumption was improved by approximately 30 percent due to the reduction in oil volatility, implying a substantial contribution of oil evaporation to total oil consumption at high speed and load conditions.

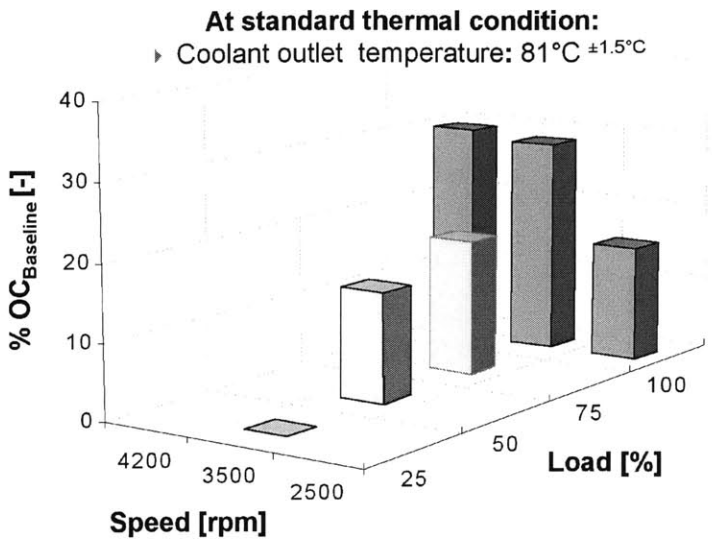

Figure 4-20 Decrease of oil consumption (as percent of the baseline oil consumption) due to reduction of volatility at different speed and load

4.2.5 Estimation of Liner Evaporation

The evaporation of oil from different regions of the engine, such as the cylinder liner, piston, and the oil sump, contributes to total oil consumption. The dominant contribution is believed to be the evaporation from the piston-ring-liner system, as the oil present in these regions is exposed to higher gas flow rates and temperatures.

Oil evaporation from the piston should be mainly from the piston top land, because of the higher temperatures on the top land and of the gases flowing into the crevice. The gas flow rate into and out of the top land crevice is significantly higher than the gas flow through the top ring into the second land volume. Therefore, most of the evaporated oil from the top land enters directly into the combustion chamber with the reverse flow of gases from the top land crevice. This happens when the cylinder pressure starts to decrease during the engine cycle. Oil in vapor form in the reverse blowby gases could also be transported from the second land into the combustion chamber. However, the origin of this oil vapor is believed to be mainly the top land. Oil on the top land evaporates into the crevice gases, and is transported with the gas flow through the top ring gap into the second land. When the second land pressures become higher than the

combustion chamber pressures, a small part of the gas trapped in the second land (containing some oil vapor) is believed to return into the combustion chamber. Since there is no oil available on the second land in the region below the top ring gap, it is believed that little oil evaporates from the second land into the reverse blowby gases. Moreover, as described in Section 4.1.2, measurements of blowby oil consumption indicate the insignificance of oil evaporation from the piston-ring-pack into the blowby flow. Therefore, the contribution of oil evaporation from the piston second land was assumed negligible.

However, after the liquid oil is transported to the top land, it evaporates or oxidizes into the top land crevice gases, or moves from the top land region into the combustion chamber in liquid form due to inertia forces. Therefore, any oil that is transported to the top land region eventually contributes to total oil consumption independent of the volatility of the oil. For this reason, oil evaporation from the piston was not considered in the evaporation analysis. A schematic of the different oil consumption mechanisms from the top land is shown Figure 4-21.

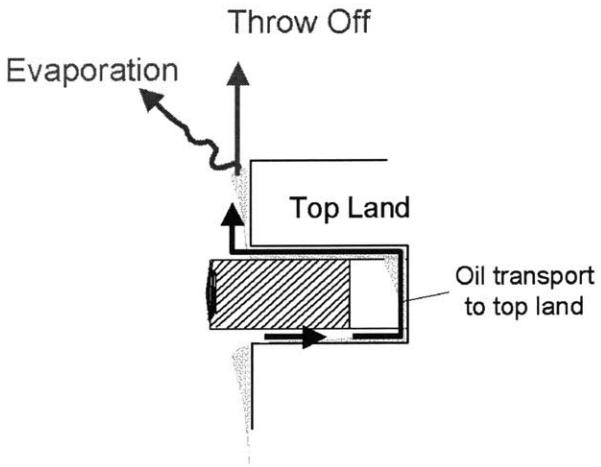

Figure 4-21 Schematic of the oil consumption mechanisms from the top land

As discussed earlier, the oil supply rates along the piston-ring-liner system to the top land should remain unchanged for both test lubricants, which is also supported by the LIF measurements. Figure 4-22 shows the LIF oil film thickness measurements (from the measurement position #1 in Figure 2-6) on the piston for the two oils at 3500 rpm, 75% load, and different coolant temperatures. It is clear that the oil distribution on the piston

is similar for both investigated oils. Therefore, the difference in oil evaporation from the liner should be responsible for the experimentally observed differences in oil consumption between the two oils.

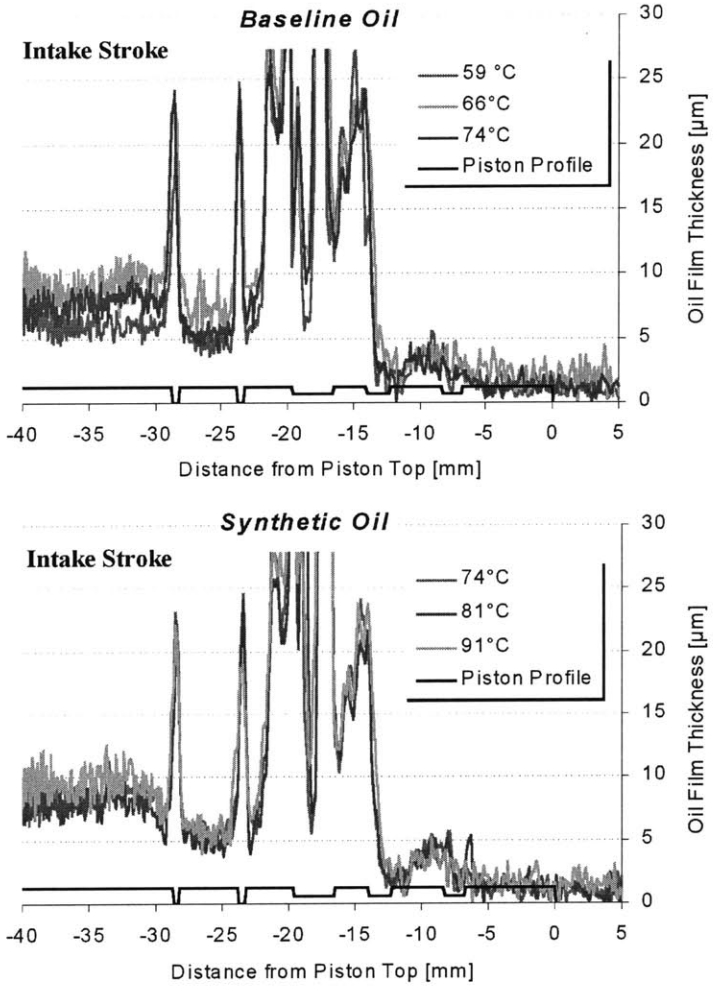

Figure 4-22 Oil film thickness distribution at different coolant outlet temperature at 75% load, 3500 rpm

Here, a simple physics-based multi-species oil evaporation model was developed to predict the evaporation from the cylinder liner, and was used to analyze the observed experimental measurements. In this section, the model is described and the predictions are compared with the experimental results.

The multi-species nature of the oils increases the complexity of the evaporation process of an oil film. Because hydrocarbon species have different volatilities, their rate of evaporation from the film surface differs considerably. The transport of each species through the film to the surface is governed by transient diffusion. Depending on the application, this transport could result in a non-uniform distribution of the hydrocarbon species within the liquid film (see Figure 4-23). Moreover, the composition of the film is unsteady and changes with liner location. This characteristic of the oil film directly influences the oil evaporation, since the vapor mixture in the gas side depends on the liquid oil composition at the interface. An analysis of the oil evaporation process from the engine cylinder liner follows.

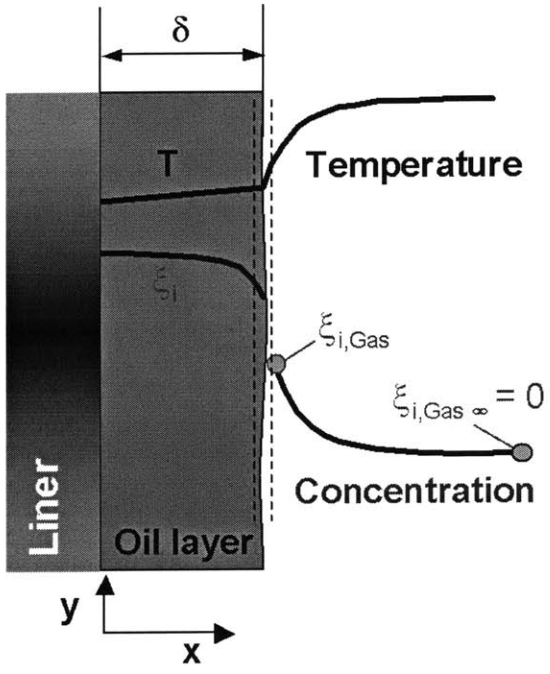

Figure 4-23 Schematic of the liner oil evaporation process

4.2.5.1 Analytical Liner Evaporation Model

The oil evaporation from the cylinder liner can be modeled as a one-dimensional transient diffusion process in the lubricating oil film with a convective boundary

condition. Although the temperature across the liquid-vapor interface is continuous, the oil species concentrations are discontinuous. The concentration on the gas side is determined by assuming thermodynamic equilibrium between the liquid and vapor phases. A schematic of the evaporation process from the cylinder liner is presented in Figure 4-23.

The governing differential equations (diffusion equation) for each oil species in the liquid phase are:

$$\frac{\partial \xi_i}{\partial t} = D_{i,Oil} \frac{\partial^2 \xi_i}{\partial x^2} \; ; \tag{4.1}$$

where ξ_i is the mass fraction of oil species i, $D_{i,Oil}$ the molecular diffusion coefficient for species i in the liquid mixture, x the coordinate perpendicular to the liner (oil layer), and t the time.

The initial condition describing the species mass fraction in the oil layer is specified as

$$\xi_i = \xi_{i,0}, \qquad \text{at t=0.} \tag{4.2}$$

Because the cylinder wall is impermeable to the oil species, a Neumann boundary condition at the cylinder liner surface (x=0) is specified as

$$\left.\frac{\partial \xi_i}{\partial x}\right|_{x=0} = 0 . \tag{4.3}$$

At the liquid-gas interface (x=δ), a mixed boundary condition is specified as

$$-\rho_{Liq} * D_{i,Oil} \left.\frac{\partial \xi_i}{\partial x}\right|_{x=\delta} = g_{m,i} * \xi_{i,Gas} \; ; \tag{4.4}$$

where ρ_{Liq} is the oil density, $g_{m,i}$ the species mass convection coefficient, and $\xi_{i,Gas}$ the mass fraction of the oil vapor species on the gas side of the interface.

To obtain a dimensionless form of equations (4.1)-(4.4), the following dimensionless variables (4.5)-(4.7) are defined:

$$\eta = \frac{x}{\delta}, \tag{4.5}$$

$$\theta_i = \frac{\xi_i}{\xi_{i,0}}, \tag{4.6}$$

$$\zeta = \frac{t * D_{i,Oil}}{\delta^2}; \tag{4.7}$$

where η is the dimensionless coordinate perpendicular to the liner, θ_i the dimensionless liquid species mass fraction, and ζ the dimensionless time. The dimensionless form of the governing equations along with the initial condition and boundary conditions is obtained by substituting the dimensionless variables (4.5)-(4.7) into equations (4.1)-(4.4):

$$\text{DEQ:} \qquad \frac{\partial \theta_i}{\partial \zeta} = \frac{\partial^2 \theta_i}{\partial \eta^2}, \tag{4.8}$$

$$\text{IC:} \qquad \theta_i = 1, \qquad \text{at } \zeta=0, \tag{4.9}$$

$$\text{BC:} \qquad \left.\frac{\partial \theta_i}{\partial \eta}\right|_{\eta=0} = 0, \qquad \text{at } \eta=0, \tag{4.10}$$

$$\text{BC:} \qquad -\left.\frac{\partial \theta_i}{\partial \eta}\right|_{\eta=1} = \left.\frac{g_{m,i} * \delta}{\rho_{Liq} * D_{i,Oil}} * \frac{\xi_{i,Gas}}{\xi_i}\right|_{\eta=1} * \left.\theta_i\right|_{\eta=1}. \tag{4.11}$$

With the definition of the mass transfer Biot number

$$Bi_{m,i} = \left.\frac{g_{m,i} * \delta}{\rho_{Liq} * D_{i,Oil}} * \frac{\xi_{i,Gas}}{\xi_i}\right|_{\eta=1}, \tag{4.12}$$

equation (4.11) reduces to

$$-\left.\frac{\partial \theta_i}{\partial \eta}\right|_{\eta=1} = Bi_{m,i} * \left.\theta_i\right|_{\eta=1}. \tag{4.13}$$

The mass transfer Biot number is defined as the ratio of the oil species diffusion resistance in the liquid to the convection resistance in the gas phase.

Figure 4-24 shows the mass transfer Biot number for two oil species of the baseline oil during the engine cycle at 100% load, 3500 rpm, and 93°C coolant outlet temperature (upper bound). The model predicts maximum mass transfer Biot numbers in the order of

10^{-3} to 10^{-2} during the engine cycle. The small Biot numbers indicate that the diffusion resistance is negligible and oil evaporation is limited by gas side convection. Consequently, it is appropriate to assume a uniform oil composition within the oil film. The problem thus simplifies to a mass convection process with low mass transfer.

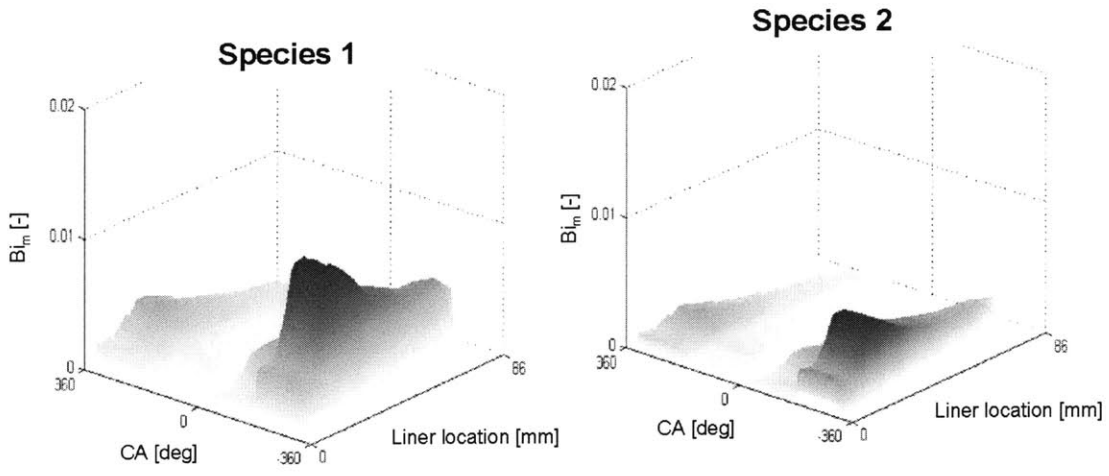

Figure 4-24 Mass transfer Biot number distribution on the liner for the first two species of the baseline oil at 100% load, 3500 rpm, and 93°C coolant outlet temperature

Thus, the approaches in [40][42] were adapted in order to model the mass convection process. The oil film on the liner was modeled as a mixture of a number of paraffins with different vapor pressures and other thermo physical properties. Because of its temperature variation, the liner was discretized into several elements. Instantaneous mass transfer rates were computed for each species with its local properties at each element during the cycle. The time-averaged oil evaporation rate $\dot{M}$ was obtained by integrating the results over time and over the part of the cylinder liner exposed to the in-cylinder gases during the cycle, and by summing the fluxes of the different oil species:

$$\dot{M} = \frac{2\pi R}{T} \sum_i \int_0^T \int_0^{L(t)} g_{m,i}(y,t) * \left(\xi_{i,Gas}(y,t) - \xi_{i,\infty}\right) dy\, dt\,; \tag{4.14}$$

where R is the cylinder radius, T the cycle period, L(t) the instantaneous axial length of the bore area that is exposed to the in-cylinder gases, $g_{m,i}(y,t)$ the instantaneous local

mass transfer coefficient of species i, $\xi_{i,Gas}(y,t)$ the instantaneous local vapor mass fraction of oil species i in the gas phase of the liquid-gas interface, and $\xi_{i,\infty}$ the vapor mass fraction of oil species i in the cylinder gases (which is assumed to be zero).

The mass transfer coefficient $g_{m,i}$ is obtained by using the Chilton-Colburn analogy between heat and mass transfer, expressed as

$$g_{m,i} = \frac{h}{c_p Le_i^{2/3}}, \text{ and} \tag{4.15}$$

$$Le_i = \frac{k}{\rho c_p D_{i,Gas}}; \tag{4.16}$$

where h is the instantaneous spatially averaged heat transfer coefficient, ρ and c_p the gas density and specific heat capacity, respectively, Le_i the Lewis number of oil species i, k the thermal conductivity of the gas, and $D_{i,Gas}$ the diffusion coefficient of species i through the gas.

The heat transfer coefficient for the combustion chamber surface is evaluated by using the semi-empirical Woschni correlation (see Appendix B) [62]. Some researchers have modified the constants within the Woschni equation to improve the fit between modeling and data. For this study, the evaporation modeling predictions were found to fit reasonably well with the measured data without any modification of the constants, as presented later in this section.

To evaluate the mass transfer coefficient, several temperature dependent cylinder gas properties are needed which depend on temperature. The bulk temperature of cylinder gas was evaluated by combining a zero-dimensional cycle simulation program with measurements of the cylinder pressure and liner temperatures. Unknown parameters, such as burn rates, were adjusted within a reasonable range until the pressure predictions from the cycle simulator matched the measured steady state cylinder pressure traces. The cylinder gas bulk temperature was then obtained from the temperatures of the burned and unburned gases. A typical profile of the cylinder pressure measurement with the computed cylinder gas bulk temperature is shown in Figure 4-25.

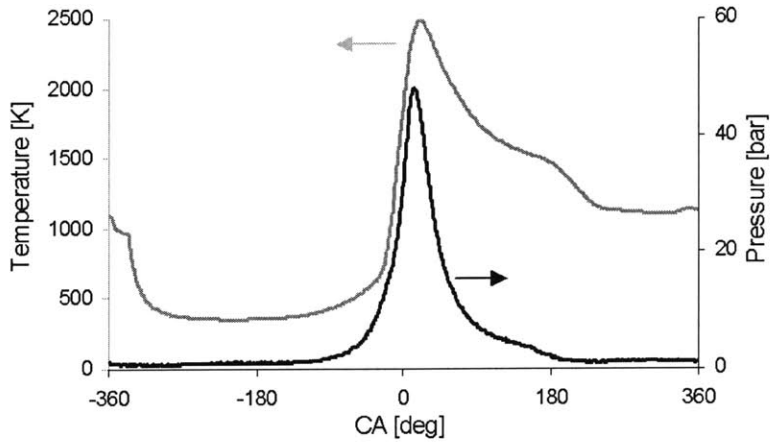

Figure 4-25 Typical cylinder pressure measurement with computed bulk gas temperature

Then the average temperature of the local liner and the predicted cylinder gas bulk temperature were subsequently used to evaluate the temperature dependent gas properties. The temperature measurements on the liner were used to estimate the temperature distribution on the liner with an expression based on the square root of the distance from the TDC of the top ring [65]:

$$T(y) = \sqrt{(T_{TDC} - T_{BDC}) * \frac{y}{s}}; \tag{4.17}$$

where y is the liner location relative to the TDC location of the top ring, T(y) is the liner temperature, TTDC and TBDC are the liner temperatures at the locations of the top ring at TDC and BDC, respectively, and s is the engine stroke. Figure 4-26a illustrates the variation of the liner temperature distribution for different load conditions at 3500 rpm and standard coolant outlet temperatures (~ 81°C) and Figure 4-26b for different coolant outlet temperatures at 100% and 3500 rpm as determined by the procedure explained above.

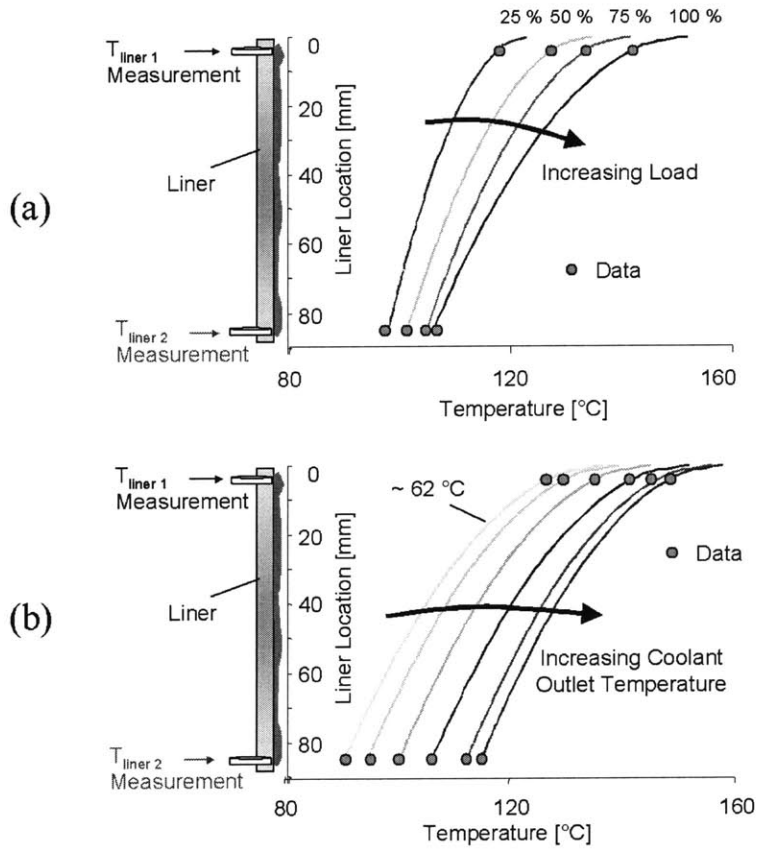

Figure 4-26 Variation of the liner temperature distribution for different load conditions at 3500 rpm, standard coolant outlet temperature (a); and for different coolant outlet temperatures at 100% load, 3500 rpm (b)

The binary diffusion coefficients $D_{i,Gas}$ for each oil species were estimated by using the Wilke-Lee relation [66].

In general, the oil species mass fraction is discontinuous across the phase interface (see Figure 4-23). Thermodynamic equilibrium is assumed at the vapor-liquid interface, and the species mass fraction in the gas phase $\xi_{i,Gas}$ is obtained by using Raoult's law:

$$\psi_{i,Gas} * p = \psi_{i,Liq} * p_i^0 . \tag{4.18}$$

Here $\psi_{i,Gas}$ and $\psi_{i,Liq}$ are the mole fractions of the oil species in the liquid and gas phase, respectively, p is the bulk cylinder gas pressure, and p_i^o is the pure-species saturated vapor pressure of species i. It should be noted that p_i^o is obtained from pure hydrocarbon vapor pressure data and is a function of temperature [67].

The liquid phase mass fraction and boiling points of each oil species must be specified. This information was obtained from atmospheric boiling point distillation curves. These curves were determined using High Temperature Simulated Distillation (HTSD) tests (also based on GCD as described in DIN 51435-2 and draft ASTM). Figure 4-27 shows the distillation curves of the fresh oils used for this study.

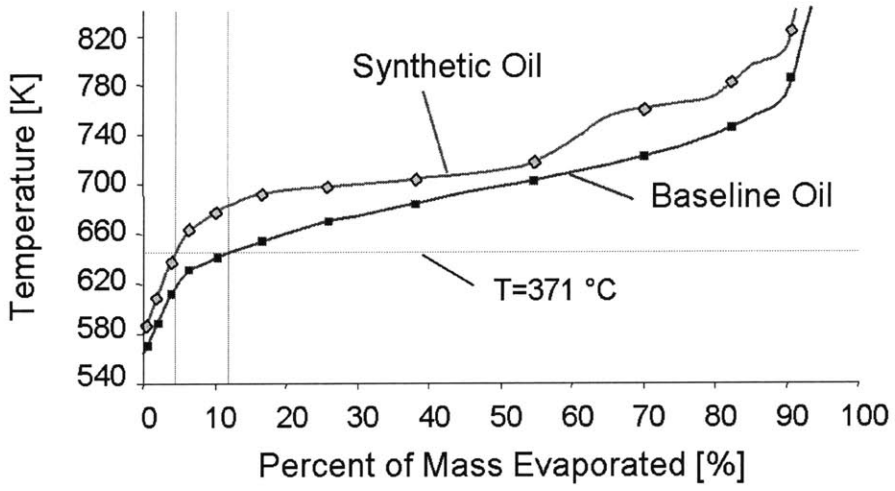

Figure 4-27 Distillation curves of baseline and synthetic oil

The oil film thickness on the liner was predicted at the anti-thrust side using the simulation code Friction-OFT [68][43]. A typical plot of the oil film thickness left on the liner after the intake and expansion strokes is shown in Figure 4-28. The binary diffusion coefficient $D_{i,Oil}$ for species i through the oil film (used for the mass transfer Biot number) was estimated using the Wilke-Chang method as described in [66].

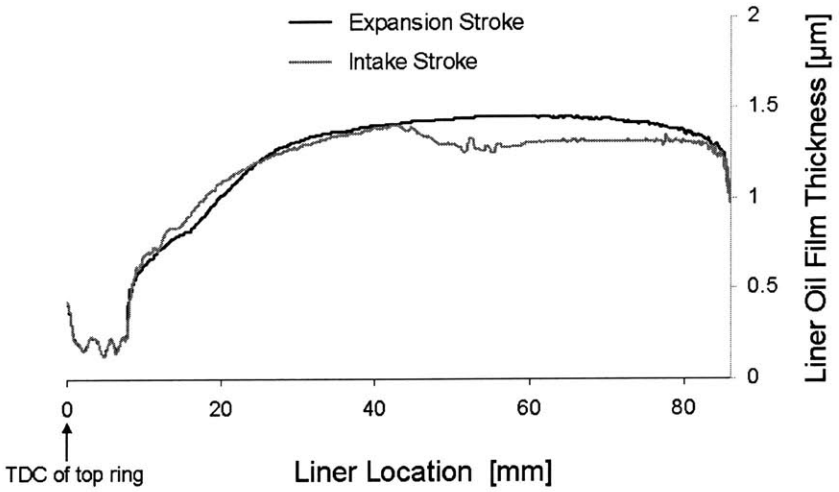

Figure 4-28 Typical trace of the oil film thickness left on the liner after the intake and expansion stroke

4.2.6 Analysis of Model Results and Comparison with Experiments

Figure 4-29 shows the predicted oil evaporation rate from the cylinder liner for both test oils as a function of liner temperature under 75% load conditions at 3500 rpm. The evaporation rate rises with liner temperatures for both lubricants. Moreover, as observed in the experiments, the more volatile baseline oil exhibits a higher evaporation rate and a stronger dependence on liner temperature.

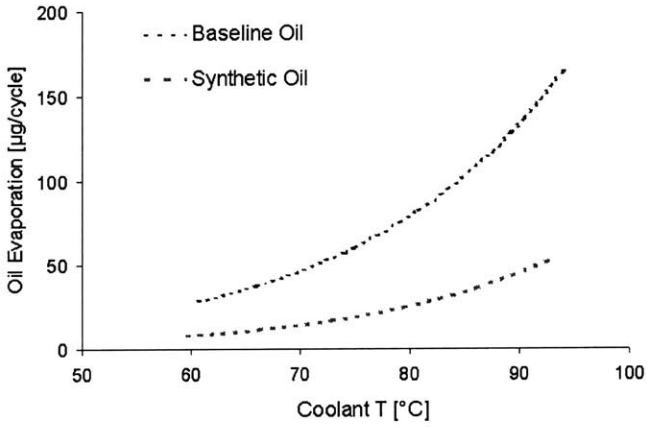

Figure 4-29 Oil evaporation dependence on liner temperatures at 75% load, 3500 rpm

Figure 4-30 shows the experimentally obtained total oil consumption results and the oil evaporation predicted by the model for both oils as a function of liner temperature under different load conditions at 3500 rpm. It should be noted that the axis that represents the evaporation results was shifted to compare it with the total oil consumption data. For the synthetic oil, the predicted rate of change of oil evaporation with liner temperature is similar to the measured rate of change of oil consumption for all load conditions.

For the baseline oil, the dependencies of the measured oil consumption rate and the predicted liner evaporation rate on liner temperatures are comparable when the liner temperatures are low. Moreover, at low liner temperatures, the difference between the liner evaporation rates of the two oils is comparable to the measured difference in oil consumption for the 100% load and 75% load conditions. Under the 50% load condition when component temperatures become lower, the oil consumption rate approaches the same value for the two oils. The model, however, predicts a small difference between the liner evaporation rates of the two oils.

At higher liner temperatures, the evaporation predictions for the baseline oil show a stronger dependence on liner temperature than the oil consumption measurements. This discrepancy between the model and experimental results for the baseline oil can be attributed to the assumptions of the model on oil supply.

The evaporation model assumes an infinite supply of oil species on the entire liner when the piston passes by during compression and exhaust strokes. However, in reality the oil supply to the liner is limited. In particular, the top of the liner in the region between the TDC location of the oil control ring and the TDC location of the top ring [55]. Since the oil control ring and piston skirt never travels in this region the oil supply can be either from the piston lands or along the liner due to ring-liner interaction. As discussed in Section 3.3.3, LIF measurements indicate that there is little oil accumulation on the piston top and second land at the investigated operating conditions. Therefore, oil flow from the piston lands to the top of the liner is unlikely, and the ring-liner interface is probably the only oil source of consequence. Therefore, the oil supply to the top of the liner may depend mainly on the lubrication conditions of the top two rings and the availability of oil before they enter this region, as described in [55]. In addition, the

lubrication conditions are affected by the piston dynamic tilt, because it determines the position of the rings relative to the liner and thus the ring running surfaces. Consequently, this variation of the ring lubrication conditions causes a variation of the oil supply along the liner circumference.

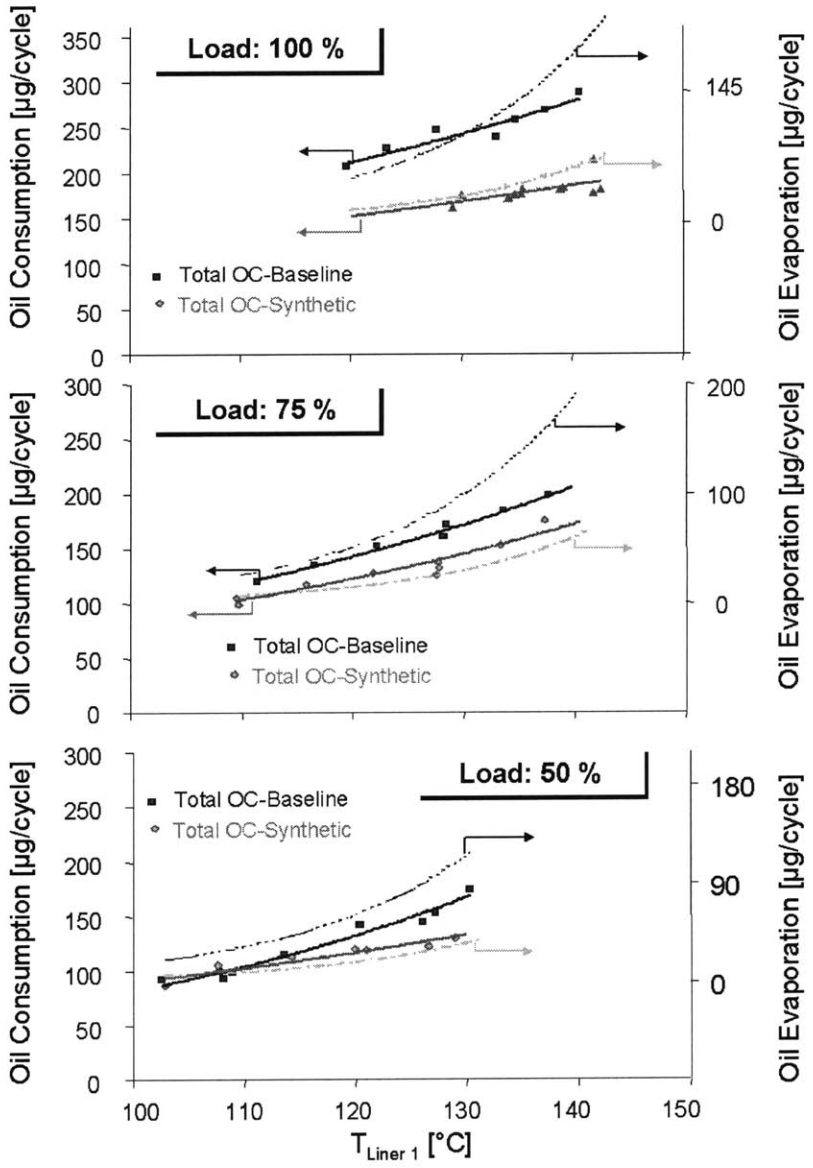

Figure 4-30 Total oil consumption and predicted liner evaporation dependence on liner temperature at different load, 3500 rpm

Another source of the variation in oil supply comes from the assumed initial oil film on the liner. An example of this is given in the following using the simulation code

FRICTION-OFT. The oil film thickness results that were used for the evaporation model (one example is shown in Figure 4-28) were based on the assumption that there is initially a certain amount of oil in the region above the TDC location of the oil control ring. However, when the initial oil film thickness was assumed zero, the top ring was found to be incapable of transporting oil to the region above the TDC of the oil control ring. Figure 4-31 shows the result for the oil volume (per unit length in the circumferential direction) of the oil between the top ring and the liner for the minor thrust side at 100% load and 3500 rpm. It is evident that the oil volume diminishes when the top ring enters the region above the TDC location of the oil control ring. This lack of oil supply is also reflected in the liner oil film thickness predictions after the intake and expansion strokes (also shown in Figure 4-31). Clearly, there is no oil available on the top of the liner.

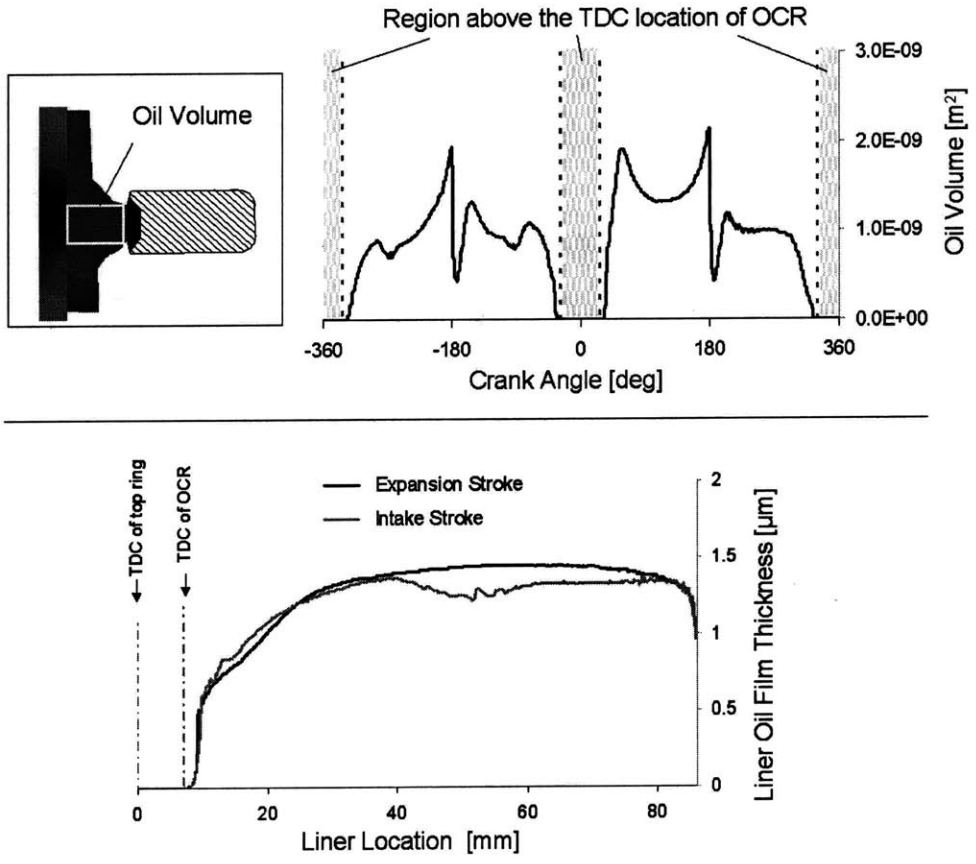

Figure 4-31 Oil volume held by the top ring and liner oil film thickness after downstrokes at the minor thrust side for 100% load, 3500rpm

On the other hand, the region above the oil control ring at TDC displays the highest evaporation rates since it experiences the highest thermal loading as it is exposed to the cylinder gases for the longest period during the cycle. For example, the evaporation model results at 3500 rpm, 100% load, and high liner temperatures show that roughly 50 percent of the oil evaporation from the liner occurs in this region. Furthermore, because the evaporation process depends on the oil species partial pressures, the greatest contributors to total evaporation are the species from the light end of the distillation curve. Figure 4-32 shows the predicted cumulative total evaporation and the cumulative evaporation of the four lightest oil species. The results are normalized by the total oil evaporation rate during one cycle. The lightest oil species was found to contribute around 35 percent to the total oil evaporated. The four lightest constituents, which represent the first 6 percent on the oil distillation curve, contributed almost to 80 percent of the evaporated oil.

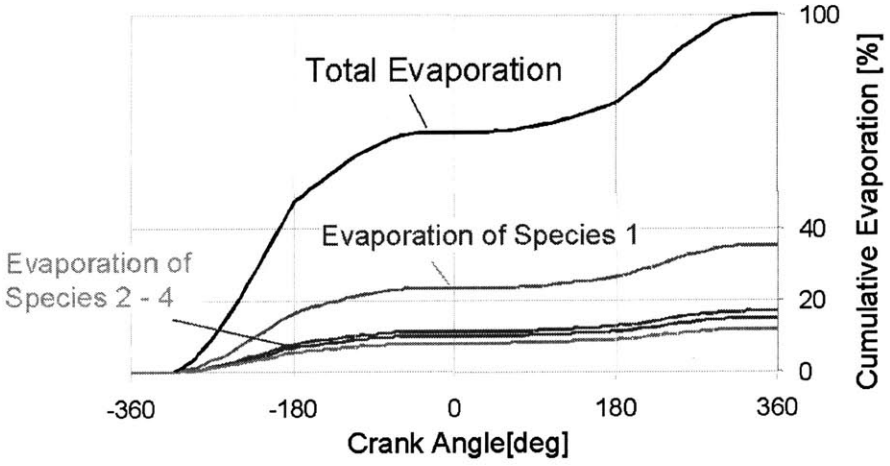

Figure 4-32 Cumulative total oil evaporation and proportions of the lightest four species during one engine cycle at 100% load, 3500 rpm, and 93°C coolant outlet temperature.

Therefore, because of the limited oil supply and the selective evaporation of lighter species at severe operating conditions (high load and high liner temperatures) it is likely that the fresh oil from the sump may not be able to refresh the oil over a large region of the liner in each cycle. This explanation is supported by a study on an SI engine at relatively low liner temperatures (between 45 - 80°C when oil evaporation from the liner

is expected to be low), which showed that the oil layer on the cylinder liner could not be refreshed completely [69].

At high liner temperatures, it is reasonable to assume that the more volatile species of the baseline oil on the liner deplete due to high evaporation rates. Then the oil composition on the liner may change and differ from the oil composition in the sump. This change in composition of the oil on the liner is governed by the piston skirt and ring-liner lubrication associated oil transport rates along the liner, and by the instantaneous evaporation rate from the liner. Since the oil on the liner has a less volatile composition than the initially assumed fresh oil composition in the model, the evaporation rate is overestimated by the model. Therefore, the illustrated modeling results in Figure 4-30 for the baseline oil represent an upper bound estimate for the oil evaporation rate from the liner.

To illustrate the impact of oil composition variation along the liner, the liner evaporation rates were recomputed for the baseline oil at 3500 rpm and 100% load. At low liner temperatures, the fresh oil composition was assumed to hold for the entire liner. At high liner temperatures, the liner was divided into two regions with different oil compositions. Below the TDC location of the oil control ring, the fresh oil composition was used. Above the TDC location of the oil control ring, however, a depleted oil composition was assumed. Figure 4-33 shows the light ends of both distillation curves that were used for the two liner regions. The new evaporation predictions are also shown in Figure 4-33 along with the total oil consumption measurements at different liner temperatures. Unlike the results in Figure 4-30, here the predicted rate of change of liner evaporation with liner temperature clearly follows the measured rate of change of oil consumption. This confirms the assumption that the depletion of the light ends in the region above the oil control ring at TDC may indeed change the slope of the evaporation curve at high liner temperatures. These results strongly imply that the variation of oil consumption with liner temperature at constant speed and load conditions is due to the increase of the oil evaporation rate from the liner.

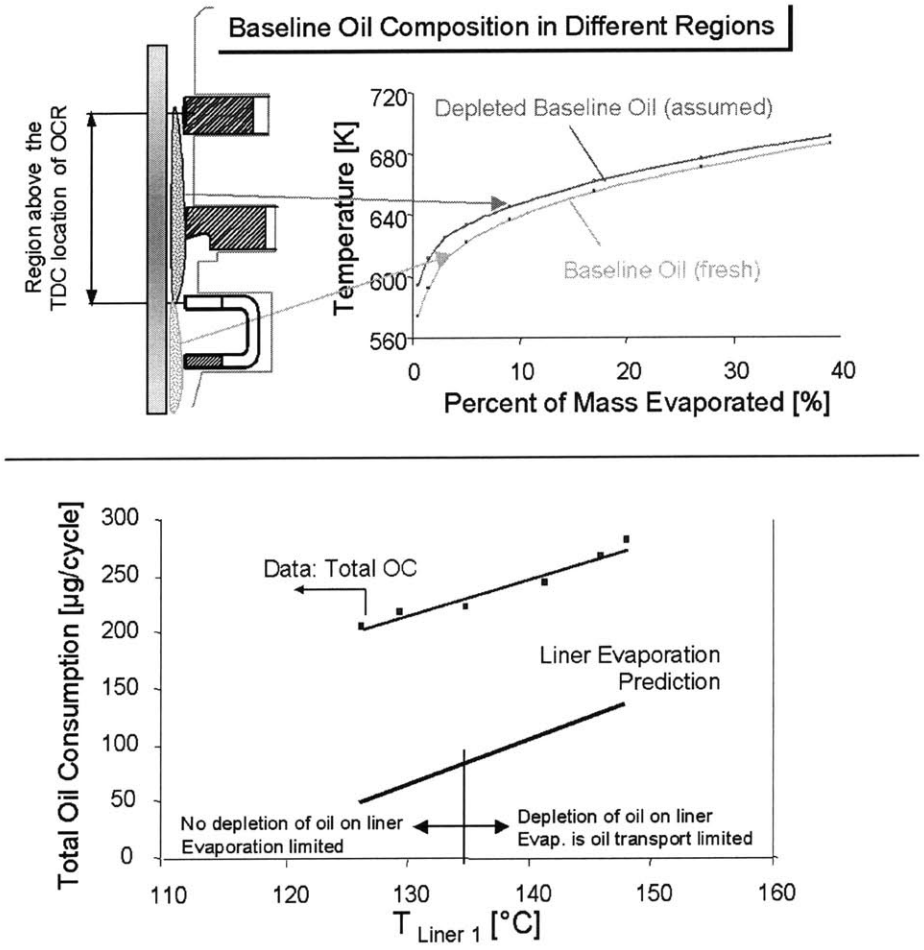

Figure 4-33 Effect of the liner oil composition variation (baseline oil) on the evaporation at 100% load, 3500 rpm

The above discussion demonstrated the strong effect of liner temperature on oil consumption at different steady state speed and load conditions. The effect of different engine operating conditions on the variation of oil consumption with liner temperature was subsequently investigated. For this purpose, the total oil consumption measurements and evaporation results obtained from the model were plotted against liner temperature on a single graph for 50, 75, and 100% load at 3500 rpm (Figure 4-34). The results indicate a dependence of total engine oil consumption on liner temperature (thermal loading). Oil consumption increased with increasing liner temperature for both the baseline and the synthetic oil. The stronger dependency of the more volatile baseline oil on liner temperatures is also evident. The predicted rate of change of oil evaporation with liner temperature is similar to the measured rate of change of oil consumption.

There is also a strong correlation between predicted liner evaporation rates and liner temperatures. This indicates that the evaporation process is less dependent on engine load, which can be explained as follows. A variation in engine load affects both the oil species mass transfer coefficient and the species vapor mass fraction in the liquid-gas interface, which together govern the liner evaporation process (see equation (4.14)). While the mass transfer coefficient increases with engine load, the vapor mass fraction decreases with load due to the higher pressures in the combustion chamber. Therefore, when load is varied, the competition of these two controlling parameters results only in a small variation of the evaporation rate. It should be noted that the total engine oil consumption data includes the blowby contribution to oil consumption, which varies between the engine loads shown in figure (see Section 4.1.1). This blowby variation is the likely cause of the weaker correlation coefficients for the experimental data.

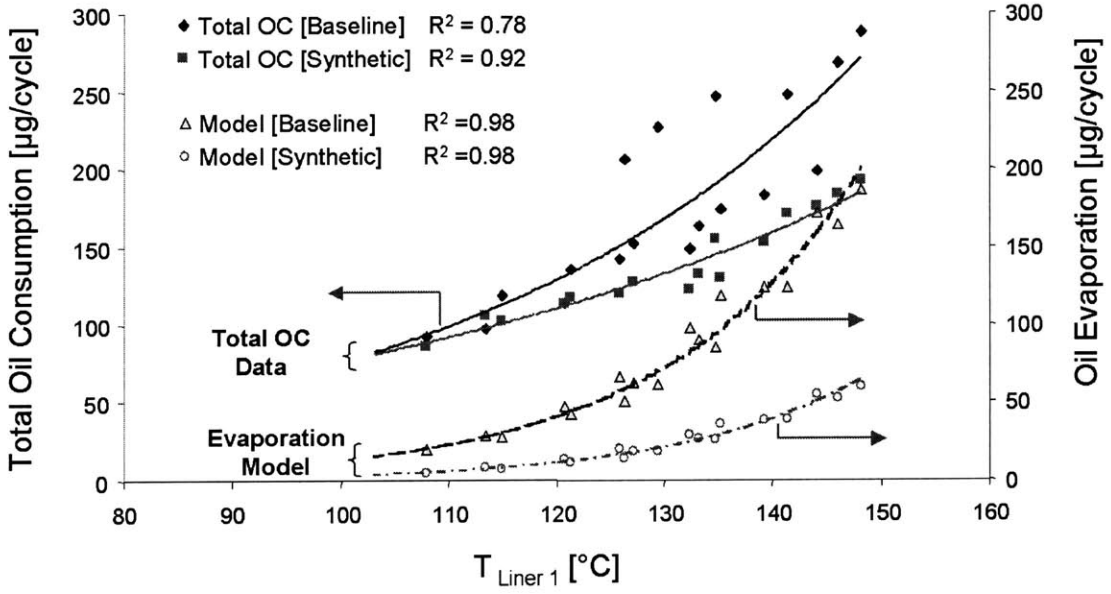

Figure 4-34 Measured total oil consumption and predicted liner evaporation dependence on liner temperature at different load (50%, 75%, and 100%), 3500 rpm. Exponential curve fit to each data set and corresponding R^2 correlation coefficient shown.

Further work was conducted to examine the dependence of oil consumption on liner temperatures at 2500 rpm. This change of speed is expected to affect the evaporation rate by increasing the available time for evaporation during one engine cycle and by

decreasing the mass transfer coefficient. The dependencies of oil consumption and liner evaporation on liner temperatures are shown for the synthetic oil in Figure 4-35 for 50, 75, and 100% load at 2500 pm. Please note that the axis that represents the evaporation results was shifted to compare it with the total oil consumption data. Again, a direct correlation between oil consumption and liner temperature exists. There is also good agreement between the experimentally obtained oil consumption and the evaporation predictions.

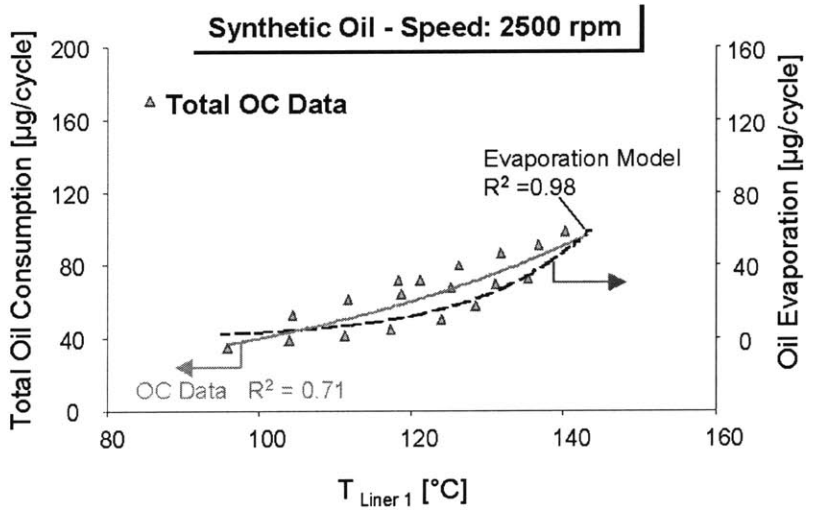

Figure 4-35 Measured total oil consumption and predicted liner evaporation dependence on liner temperature for synthetic oil at different load (50, 75, and 100%), 2500 rpm. Exponential curve fit to each data set and corresponding R^2 correlation coefficient shown.

4.2.7 Summary of the Oil Evaporation Study

This study has characterized the impact of oil volatility and coolant outlet temperatures on oil evaporation from the liner at different steady state engine speed and load conditions. For two oils with different volatilities, the dependence of oil consumption and evaporation on coolant temperatures was analyzed by combining oil consumption measurements, in-cylinder measurements, and theoretical modeling. A linear relationship between cylinder liner and coolant outlet temperatures was obtained and oil consumption was found to increase with liner temperature for both oils. At operating conditions between half load (50%) and full load (100%), the dependence of oil

consumption on liner temperature was stronger with the high volatility baseline oil. In addition, the influence of oil volatility on oil consumption was analyzed at standard coolant outlet temperatures at different steady state engine loads and speeds. The measurements showed that the impact of oil volatility on oil evaporation and consumption increased with engine speed and load.

It has been demonstrated in this work that the gas side convection process limits the oil film evaporation process from the cylinder liner. A multi-species liner evaporation model was developed to interpret the oil consumption measurements. Oil evaporation from the liner was found to increase with liner temperature for both oils investigated. For the low volatility synthetic oil, the predictions of the dependence of the evaporation rate on liner temperatures closely followed the experimentally obtained oil consumption trends. The high volatility baseline oil generally showed higher levels of evaporation and a stronger dependence on liner temperatures than observed in the experiments. This discrepancy occurred because the model ignores the depletion of the lighter oil species from the liner. The high evaporation rates combined with insufficient oil replenishment altered the oil composition on the liner. This change in composition resulted in lower oil evaporation rates than predicted. The model predictions thus provide an upper bound estimate for the evaporation rates of the high volatility baseline oil.

In summary, the evaporation predictions implied that oil evaporating from the liner was responsible for the experimentally obtained relationship between oil consumption and coolant outlet temperature. Moreover, for engine loads above 50% load oil consumption was found to depend directly on the liner temperatures and the liner oil evaporation rate.

4.3 Contribution of Different Sources to Total Oil Consumption

Understanding the contribution of the different oil consumption sources to total oil consumption is essential for the development of analytical tools to predict oil consumption in spark ignition engines. Moreover, the analysis and quantification of major oil consumption sources at different engine conditions will provide insights into the main causes of high oil consumption.

In this section, the relative importance of three different oil consumption sources to total oil consumption was assessed for the baseline oil by combining the experimental and theoretical results obtained in the previous sections. Specifically, the contributions of oil evaporation, oil entrained in the blowby gas flow, and oil flow into the combustion chamber (through the piston system and valve guide) to total oil consumption were quantified and analyzed at different steady state engine speed and load conditions.

4.3.1 Separation of Three Different Oil Consumption Sources

All of the oil consumption sources described in Chapter 1 contribute to total engine oil consumption. The relative importance of these oil consumption sources at different operating conditions depends on the variation of the driving forces for each source. In this section, a description is provided as to how the contributions of the three major oil consumption sources were separated at different engine operating conditions.

Steady state total engine oil consumption measurements were used in conjunction with the results of the studies on the blowby contribution and oil evaporation to separate and assess three different oil consumption sources. The contributions of oil evaporation, oil entrained in the blowby gas flow, and oil flow into the cylinder through the piston system and valve guide were quantified. The variation of these oil consumption sources under different steady state engine speed and load conditions was analyzed. This was done for the baseline oil at the standard thermal operating condition (~81°C coolant outlet temperature). Figure 4-36 illustrates a schematic of the separated oil consumption sources.

For each investigated engine operating condition, it was assumed that the sum of all three oil consumption sources would result in the experimentally obtained total oil consumption. As discussed in Section 3.3, total oil consumption measurements were conducted at a wide range of engine speed and load conditions. The results of Section 4.1.1 were used for the contribution of blowby to total oil consumption. The procedure used to determine the contributions of oil evaporation and of oil flow into the cylinder for each operating condition is described in the following.

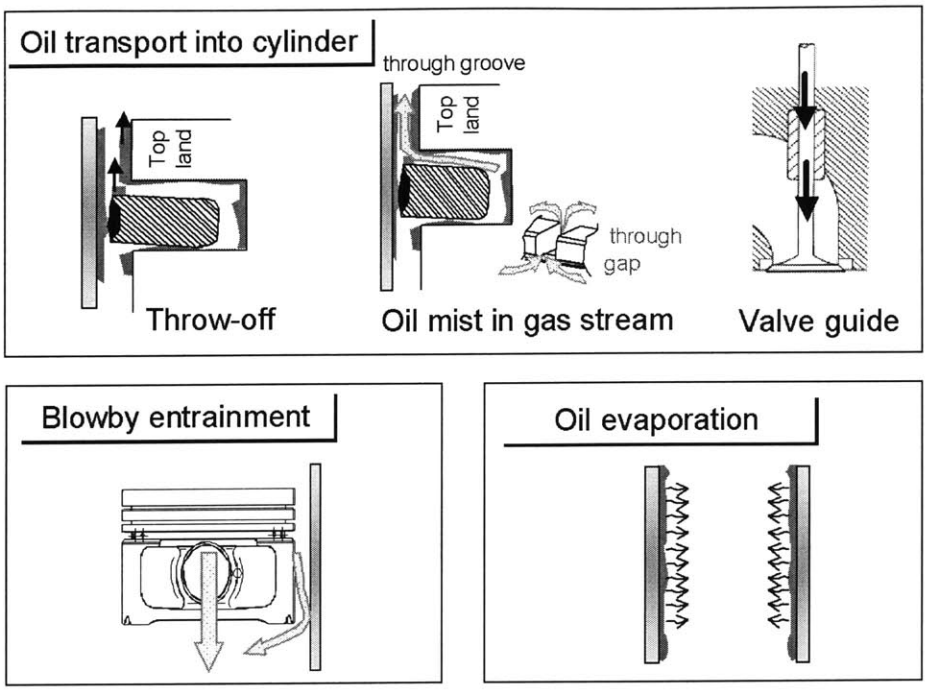

Figure 4-36 Illustration of the separated oil consumption sources

Contribution of oil evaporation

The contribution of oil evaporation to total oil consumption for the baseline oil was determined by combining oil consumption measurements and predictions of the in the previous section proposed liner evaporation model. As discussed previously, the evaporation model overestimated the evaporation of the baseline oil. However, good agreement was obtained between the evaporation predictions and the oil consumption measurements at the different engine operating conditions that were investigated for the low volatility synthetic oil. Consequently, it was assumed that the liner evaporation model holds for the synthetic oil. The evaporation rate for the baseline oil was estimated by adding the measured difference in oil consumption (Δ OC) between the baseline and the lower volatility synthetic oil to the evaporation predictions for the synthetic oil. This difference in oil consumption (Δ OC) accounts for the additional evaporation of the baseline oil due to its higher volatility than that of the synthetic oil. This approach is possible because the oil consumption due to oil transport is assumed to not vary between the two oils since their viscosities are comparable (see Section 4.2.4 and Figure 4-19). The difference in oil consumption (Δ OC) is mainly due to the difference in liner

evaporation between the two oils. There may also be small differences in evaporation from other regions, such as within the piston and crankcase. However, as described in the Sections 4.1 and 4.2, the latter sources for oil evaporation seem to have little impact on the difference in oil consumption between the two oils. Therefore, at a given steady state engine operating condition, the total evaporation rate of the baseline oil was determined by the sum of the experimentally obtained difference in evaporation between the baseline and synthetic oil (Δ OC) and the estimated evaporation for the synthetic oil.

Contribution of oil transport

The amount of oil transported directly into the combustion chamber through the piston ring-pack and the valve guides was deduced by subtracting the contributions of oil entrained in the blowby flow and oil evaporation for the baseline oil determined by the above described procedure from the measured total engine oil consumption rate. In the later analysis of the oil consumption sources, it was assumed that the oil transport into the cylinder is solely due to the oil flow along the piston ring-pack. This assumption is a simplification; especially during low load conditions, when there is also a large pressure difference between the intake port and valve housing that could cause loss of oil through the inlet valve guides. This oil consumption source is not distinguishable from the oil flow through the piston with this experimental setup. However, the test engine is equipped with spring loaded flexible lip seals, which positively seal to the valve guide and the valve stem outside diameter. The effective sealing ability of this type of seal has been reported in [1]. Moreover, to keep the contribution to oil consumption from the valve guides at a minimum, the valve stem seals of the engine were frequently checked (approximately every 100 hours of engine operation) and replaced if necessary.

A schematic of the described separation of the different oil consumption sources is shown in Figure 4-37.

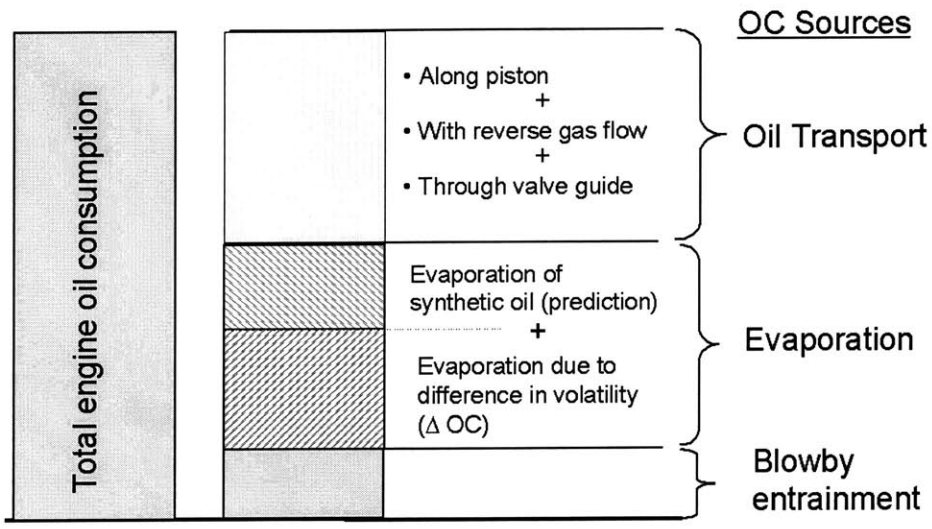

Figure 4-37 Schematic illustrating the separation of the three oil consumption sources

4.3.2 Variation of the Oil Consumption Sources with Engine Load

Figure 4-38 shows the variation of the three oil consumption sources for the baseline oil with different steady state engine load conditions at 3500 rpm as determined by the procedure that was described above. In the figure, the oil consumption rate of each source during one engine cycle along with the total oil consumption rate is shown.

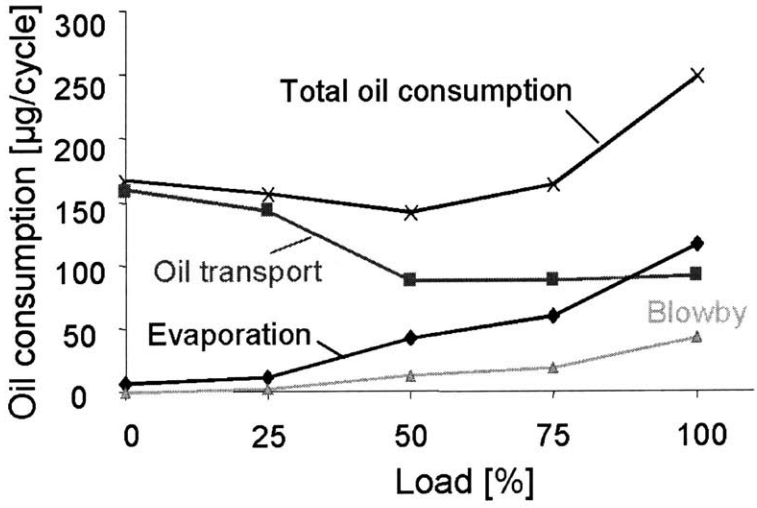

Figure 4-38 Effect of engine load on different oil consumption sources and on total oil consumption at 3500 rpm for the baseline oil

As pointed out in Section 3.3.1, total engine oil consumption initially decreases as engine load is increased from 0% load to 50%. Oil consumption then increases to a maximum as the engine load is further increased. This characteristic of oil consumption to exhibit two operating regions with distinct trends is a result of the variation of the three oil consumption sources, which show significantly different characteristics at different loads. The impact of the variation of engine load on the separated oil consumption sources is described below.

Oil Transport

The rate of oil transport through the piston-ring-pack into the cylinder is highest at 0% load. This consumption source decreases progressively as engine load is increased to 50% load. However, there is no noticeable variation of this source as load is further increased from 50% to 100% load.

Engine load affects cylinder pressures during the intake stroke and the peak cylinder pressures, which govern the gas flow structure through in the piston-ring-pack and blowby. Decreasing engine load generally decreases the blowby flow, and therefore the oil removal from the piston to the crankcase due to interfacial shear stresses also decreases. This results in more oil accumulation at various regions in the piston-ring-pack. The dependence of blowby and of oil accumulation on engine load in the top two piston lands at the minor thrust side was demonstrated in Section 3.3.2. The presence of more oil on the second land with the decrease of engine loads may result in an increase of the oil transport along the piston into the cylinder via different paths. More oil may flow to the top ring groove and from there to the top land. The oil could also be transported through the top ring gap with the reverse gas flow from the second land, when the second land pressure becomes greater than the cylinder pressure. The variation of engine load also has a considerable influence on this transport mechanism, because it determines both cylinder and land pressures.

The volumetric reverse gas flow rates from the second land through the top ring gap were predicted using RINGPACK-OC for different steady state engine load conditions at 3500 rpm. Figure 4-39 shows the results for the gas flows through the top ring gap during one engine cycle. The positive flow direction is defined as the flow from the top

land to the second land and thus negative gas flow rates indicate phases of the engine cycle when gases flow from the second land to the top land.

There exist two periods during the engine cycle when gases may flow from the second land to the top land due to negative pressure gradients across the top ring. The cylinder pressure may become smaller than the second land pressure during the intake stroke and during the late part of expansion and early exhaust strokes. Decreasing engine load causes an increase of the reverse gas flow through the top ring gap during the intake stroke due to the lower cylinder pressures. In addition, decreasing engine load also increases the crank angle period during which gases flow into the cylinder due to the pressure difference across the top ring. The reverse flow during late expansion and early exhaust stroke is less prominent and the impact of engine load is small. Therefore, it can be concluded that the overall reverse gas flow rate through the top ring gap increases as engine load is decreased.

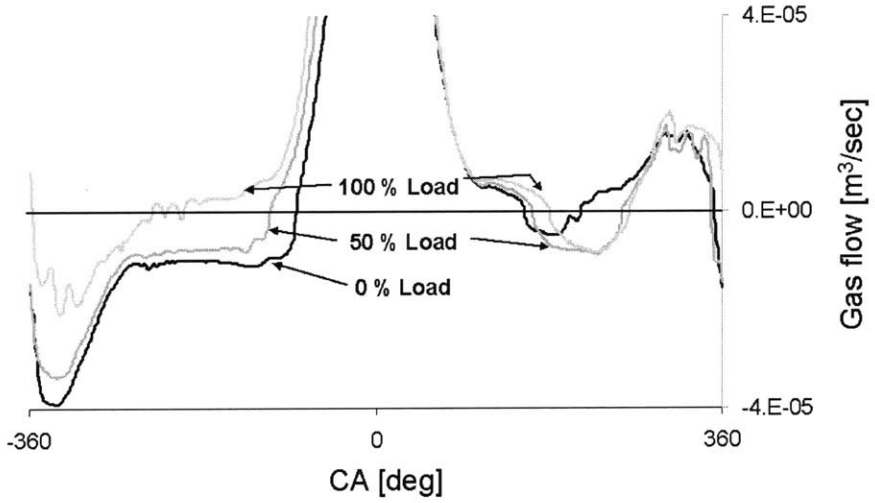

Figure 4-39 Reverse gas flow through top ring gap at different engine load

In [46] a one-dimensional model was proposed for the average oil flow through ring gaps (details of this model are described in Section 3.3.2.2) and the following expression was suggested:

$$Q_{Oil} = Q_{Gas} * \frac{3 * \mu_{Gas} * \tilde{h}_{Oil}^2}{\mu_{Oil} * h_{Gas}^2} \tag{4.19}$$

where Q_{Oil} is the cumulative oil flow over one cycle [m^3/cycle], Q_{Gas} is the cumulative gas flow flowing through the clearance of interest over one cycle [m^3/cycle], h_{Gas} is the clearance between the oil layer on the land and the liner, and $\tilde{h}_{Oil}$ is the average oil layer covering the piston surface of interest. According to equation 4.19, the above explained combination of increased oil accumulation on the second land, combined with the increase of reverse gas flows through the top ring gap with decreasing engine load, may result in greater oil flow rates into the cylinder.

This oil flow through the top ring gap was estimated for different engine loads at 3500 rpm using the computed average reverse gas flow rates through the top ring gap, the average clearance between land and liner, and the steady state LIF oil film thickness measurements (see Section 3.3.3). 2-D LIF observations of the top ring gap area during low load show that the oil accumulation adjacent to the gap is thicker than the average oil film thickness results [46]. This variation of the oil film distribution can affect the oil dragged through the top ring gap by the reverse gas flow. To illustrate the effect of the increased oil film thickness near the gap, the oil flow through the top ring gap was calculated using artificially elevated average oil film thickness (the measured average oil film thickness was multiplied by a factor of two).

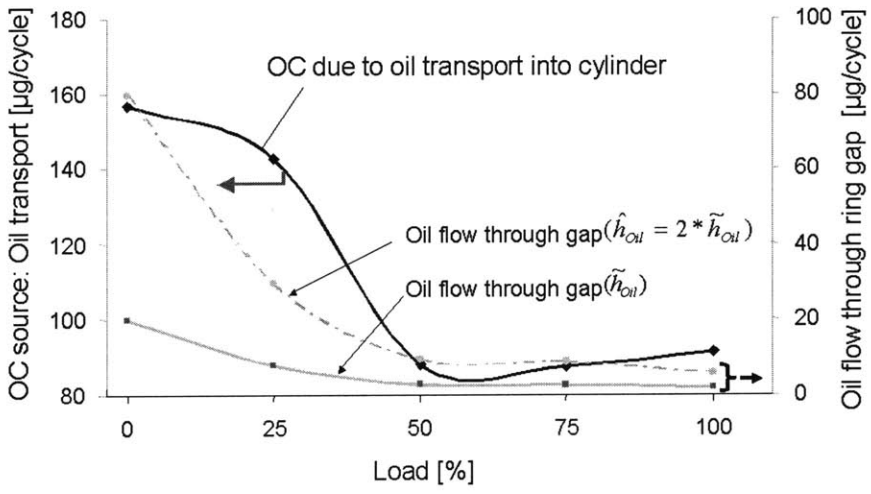

Figure 4-40 Computed oil flow with reverse gas flow through top ring gap and separated oil transport rate at different engine load

Figure 4-40 shows the results for the oil flow rate through the top ring gap for the two different average oil film thickness values that were used along with the obtained values for the oil transport into the cylinder (from Figure 4-38). The results show that the highest oil flow rates through the top ring gap occur at 0% load. This oil flow decreases as engine load is increased to 50% load. As engine load is increased further, there is little change in the oil flow through the ring gap to the cylinder, because at higher loads little oil is present on the second land to be transported. It is also for this reason that the two average oil film thicknesses used for the calculation only show a difference in the reverse oil flow through the gap at low load conditions. It is clear that the computed oil flow rate through the top ring gap (using $\hat{h}_{Oil} = 2 * \tilde{h}_{Oil}$) exhibits a similar response to increasing engine load as the total oil transport rate into the cylinder. As engine load increases, both the obtained oil transport and the calculated oil flow decrease by the same amount. Therefore, it is plausible that the main contributor to oil transport into the cylinder is the reverse oil flow through the top ring gap.

Oil evaporation and blowby contribution

Oil evaporation from the liner is the most significant contributor to total evaporation during engine operation, as discussed in Section 4.2.5. The liner oil evaporation rate into the cylinder is smallest at 0% load and increases continuously with increasing engine load to reach its maximum at 100% load. This increase of oil evaporation with engine load is attributed to the increase of the engine thermal loading and thus to increased liner temperatures.

As discussed above, the blowby oil consumption rate increased continuously with increasing engine load from negligible contributions at 0% load to considerable consumption rates at full load. This increase is due to increased oil entrainment in the piston-ring-pack due to higher oil dragging on the piston lands through the ring gaps where oil atomization and entrainment is believed to occur.

The increases of both oil evaporation and oil entrainment in the blowby flow compete with the decrease in the oil transport rate into the cylinder as engine load is increased from 0% load to 50%. Consequently, all three oil consumption sources influence the oil consumption pattern in the operating region between 0% to 50% loads. The decrease in

oil transport into the cylinder has a higher impact on oil consumption than the increase of oil evaporation and blowby contribution, as engine load is increased 0 to 50%. As load is further increased to 100%, the oil consumption rate is governed only by the oil evaporation and blowby contributions.

Figure 4-41 quantifies the relative contribution of each of the three separate oil consumption sources to total engine oil consumption for different load conditions at 3500 rpm. The values displayed are the ratio of the oil consumption rate due to one source, normalized by the total engine oil consumption at each operating condition. At 0% load, oil transport into the cylinder contributes substantially to total oil consumption conditions (~90 percent). As engine load increases, the contributions of oil evaporation and oil entrainment in the blowby rise continuously, while the contribution of oil transport decreases. At 100% load, all three sources contribute to total oil consumption. While the relative importance of oil transport decreases to 40 percent, oil evaporation was found to increase to about 45 percent, and roughly 15 percent of oil consumption is due the oil entrainment in the blowby gas flow.

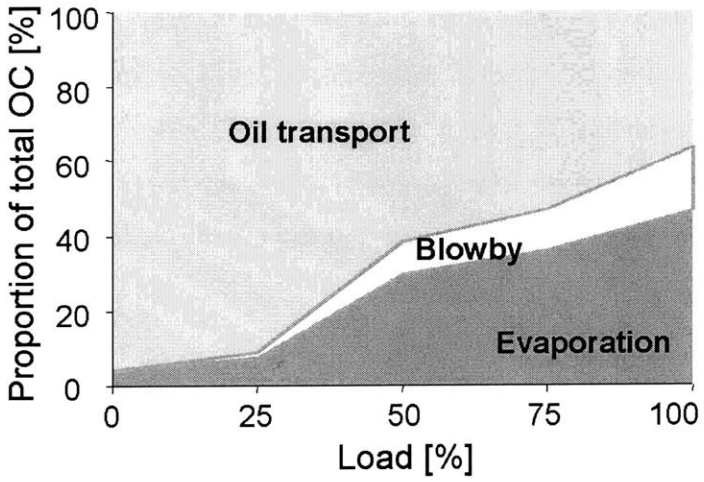

Figure 4-41 Effect of engine load on the relative importance of different oil consumption sources to total oil consumption at 3500 rpm for the baseline oil

4.3.3 Variation of the Oil Consumption Sources with Engine Speed

The influence of engine speed on the different oil consumption sources was studied at 3 different speeds and 100% load. Figure 4-42 shows the oil consumption rates of each source during one engine cycle along with total engine oil consumption. Changing engine speed affects all three oil consumption sources. Oil entrainment, oil evaporation, and oil transport all increase as engine speed is increased from 2500 to 4200 rpm. Consequently, all three oil consumption sources contribute to the increase of total oil consumption with increasing engine speed.

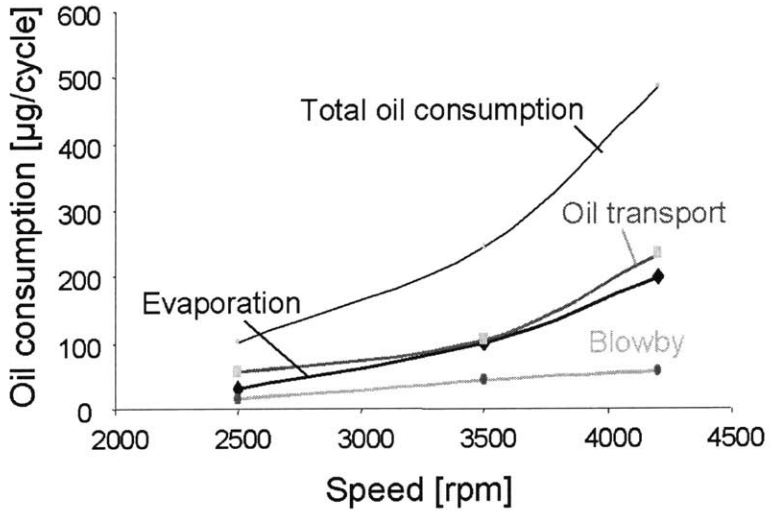

Figure 4-42 Effect of engine speed on different oil consumption sources and on total oil consumption at 100% load for the baseline oil.

The variation of engine speed affects three different mechanisms that control oil transport and distribution in the piston-ring-liner system and therefore the oil consumption sources:

- Increasing engine speed results in a decrease in the average blowby gas flow rate per cycle, and thus a decrease in interfacial shear stresses that drive the oil layer on the piston surface. Therefore, the removal of oil from the piston to the crankcase decreases with increasing speed.

- Increasing engine speed causes higher inertial forces acting on the oil volume that is accumulated on the piston due to the alternating motion of the piston. The increase of inertia is expected to increase oil flow in the axial direction to the upper piston regions. However, at high load conditions (as is the case here), inertial oil transport is believed to be important only in regions on the piston with significant oil accumulation, such as on the third land. This region is in particularly important because the oil has only a short distance to travel to reach the second ring groove.
- Increasing engine speed also increases the thermal loading on the engine. Higher piston temperatures reduce the oil viscosity, and therefore may change the oil transport along the piston. Moreover, higher liner temperatures will increase oil evaporation.

With the increase of engine speed, more oil accumulation is expected in the upper piston regions due to the decrease of blowby and the increase of inertial oil transport on the piston. Therefore, the increase of oil consumption due to oil transport with engine speed could be attributed to higher oil accumulation on the upper piston regions. It is believed that increased oil accumulation in the region between the second land and top ring groove (region (c) in Figure 1-2) may result in more oil flowing through the top ring groove and gap into the cylinder.

As speed is increased, more oil must be entrained in the blowby because the average blowby gas flow per cycle decreases, but blowby oil consumption increases. As described in Section 4.1.1, oil entrainment in the blowby could be enhanced either in the piston-ring-pack due to high velocity gas flows through the ring gaps and/or in the crankcase.

Oil evaporation is mainly governed by engine liner temperature, mass transport in the gas phase, and the available time for evaporation. Increases in engine speed increase evaporation due to the enhancement of the mass transport in the gas phase and due to the increased liner temperatures. The available time for evaporation decreases per cycle as engine speed increases, which competes with the two above effects. Since the contribution of oil evaporation increases with engine speed, the effect of higher liner

temperatures and increasing mass convection coefficients must have a higher impact than the lower time available for evaporation.

Figure 4-43 quantifies the relative contribution of each of the separate oil consumption sources to total engine oil consumption for different speeds at 100% load. The values displayed are the oil consumption rates due to each source, normalized by the total engine oil consumption at each operating condition. The importance of each oil consumption source does not change significantly as engine speed is increased from 2500 rpm to 4200 rpm. The major contribution in this range is from the oil transport, which varies between 40 to 50 percent. Oil evaporation, also a significant contributor to oil consumption at high load, exhibits a consistent trend as its relative importance increases gradually from 30 percent at 2500 rpm to 40 percent at 4200 rpm. The blowby contribution varies between 10 to 15 percent as the engine speed is increased.

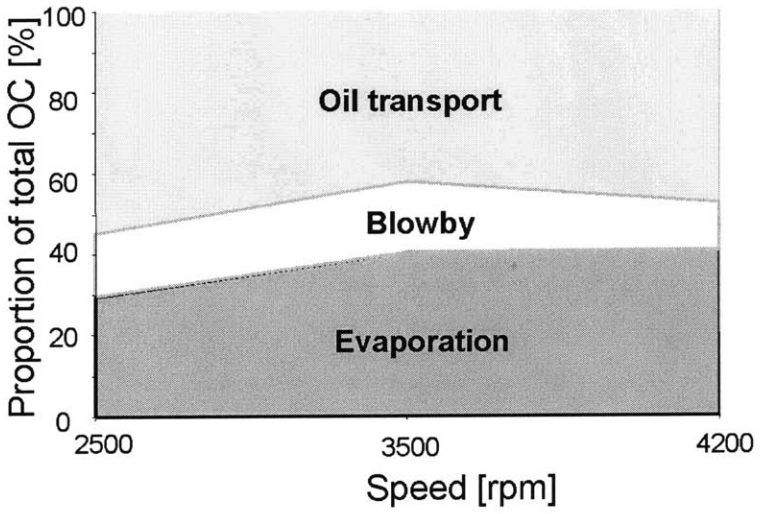

Figure 4-43 Effect of engine speed on the relative importance of different oil consumption sources to total oil consumption at 100% load for the baseline oil

4.3.4 Summary of the Contribution of Different Sources to Oil Consumption

This is the first attempt to separate and analyze the relative importance of three major oil consumption sources to the total oil consumption of a spark ignition engine at different steady state engine operating conditions. Engine test data and modeling results were combined to quantify the contribution oil evaporation, oil entrained in the blowby gas flow, and oil flow through piston and valve guide into the combustion chamber. The results show that the contribution of each oil consumption source varies with engine speed and load.

The impact of engine load on oil consumption and its sources show several important characteristics. The consumption due to the oil transport through the piston into the cylinder evinced two trends. At 0 to 50% load, oil transport was found to increase with reduction in engine load that may be related to the decrease of blowby flow and the associated increase of oil accumulation on the upper piston regions. Above 50% load, the oil consumption due to oil transport through the piston and valve guide was found to vary little with engine load. The oil evaporation rate and blowby oil consumption rate increase with increasing engine load. Also the relative importance of these oil consumption sources varied with engine load. At low load, oil transport through the piston was found to be the major consumption source (~ 90 percent), while the contribution of oil evaporation and blowby oil consumption becomes more prominent with increasing engine load.

The increase of engine speed from 2500 to 4200 rpm at 100% load increased all three oil consumption sources. The relative importance of each source varies little in this range. The major contribution is from the oil transport (40 to 50 percent) and from oil evaporation (30 to 40 percent). The importance of blowby oil consumption varies between 10 to 15 percent.

(This page was intentionally left blank)

Chapter 5 Conclusions

In this work, important oil consumption characteristics and oil consumption sources in a production spark ignition engine were analyzed and quantified for different engine operating conditions.

On a 2 liter, four-cylinder production spark ignition engine, a comprehensive diagnostic system was implemented to measure engine oil consumption and in-cylinder parameters that affect major oil transport mechanisms and oil consumption sources. A sulfur-based oil consumption method was used to measure real-time oil consumption. A blowby flow meter was used to measure the leakage gas flow past the piston-ring-liner system. Several additional measurement probes were implemented to gain information on the in-cylinder parameters. The one-point Laser Induced Fluorescence (LIF) technique was used to study the oil distribution in the piston-ring-pack. Two pressure transducers were positioned along the cylinder liner to measure inter-ring land pressures. An additional pressure transducer mounted on the cylinder head provided cylinder pressure traces. Two temperature probes along the cylinder liner provided liner temperatures.

Total engine oil consumption, blowby, and in-cylinder parameters affecting oil transport were measured at different engine operating conditions. Steady state oil consumption and blowby measurements exhibited typical trends for spark ignition engines. Oil consumption increased with increasing engine speed, and load and blowby (per cycle) increased with engine load and decreased with speed.

Engine oil consumption behavior during ramp transients in load was analyzed by combining oil consumption measurements, in-cylinder measurements, and modeling tools. Increased oil consumption was observed during transients from low load to full load. The analysis revealed that high oil accumulation in the top ring groove was the main source of the additional oil consumed during the transient. At low load, the oil transport to the upper piston regions was enhanced due to low blowby flow rates into the crankcase. As a result, more oil accumulated on the piston and in the top ring groove. After the

transient to full load, the oil in the top ring groove was transported toward the combustion chamber with the reverse gas flow through the top ring groove due to top ring flutter.

The relative importance of different oil consumption sources, and their dependence on engine operating conditions was systematically analyzed.

The contribution of oil entrained in the blowby gas flow to total oil consumption was quantified at several steady state engine load and speed conditions. Blowby contribution to total oil consumption was found to increase with engine load. An insignificant amount of oil was consumed due to blowby at low load but this contribution reached significant levels at high load conditions

Oil evaporation from the liner was subsequently characterized. Analysis of the evaporation process demonstrated that the gas side convection process limits the oil evaporation from the cylinder liner. A multi-species liner evaporation model was developed and verified by testing two oils with different volatility at varying cylinder liner temperatures and steady state engine speed and load conditions. The results show that total engine oil consumption is substantially affected by liner evaporation. Liner evaporation, however, was found to be sensitive to liner temperatures, oil composition, and oil transport to regions of high evaporation. High evaporation rates combined with insufficient oil supply (generally in the region above the top dead center position of the oil control ring) can alter the local oil composition on the liner, and thus the evaporation rate. Therefore, the temperature distribution on the liner, local oil composition, oil supply to the regions of high evaporation, and the convection of the oil vapor from the gas side of the liquid-vapor interface all govern the amount of oil that is evaporated.

Finally, the relative importance of three major oil consumption sources to the total oil consumption was analyzed. Engine test data and modeling results were combined to quantify the contribution of oil evaporation, oil entrained in the blowby gas flow, and oil flow through various pathways into the combustion chamber.

The relative importance of these oil consumption sources varied with engine load. At low load, oil transport past the piston system was found to be the major consumption source (90%), while the contribution of oil evaporation and blowby oil consumption became more significant with increasing engine load.

The variation of engine speed (2500 to 4200 rpm) at full load increased the contribution of all three oil consumption sources. However, the relative importance of each source did not vary significantly with engine speed. The major contributions were from the oil transport (40 to 50 percent) and oil evaporation (30 to 40 percent). The importance of blowby oil consumption varied between 10 to 15 percent.

This work is an important step in advancing the understanding of oil consumption in spark ignition engines. It connects oil consumption data and comprehensive in-cylinder measurements with advanced modeling. The obtained oil consumption characteristics and trends for the oil consumption sources at different operating conditions can provide important guidelines for developing analytical tools to predict oil consumption in spark ignition engines.

(This page was intentionally left blank)

References

[1] Hill, S., H., Sytsma, S., J.: "A Systems Approach to Oil Consumption", SAE paper 910743, 1991.

[2] Heywood, J. B., *Internal Combustion Engine Fundamentals*, McGraw-Hill, 1988.

[3] Mayer, W. J., Lechman, D. C., and Hilden, D. L.: "The Contribution of Engine Oil to Diesel Exhaust Particulate Emissions," SAE paper 800256, 1980.

[4] Lepperhoff, G., and Schommers, J.: "Einfluss des Schmieröls auf die PAH-Emissionen von Verbrennungsmotoren," Motorentechnische Zeitschrift (MTZ) Vol. 47, 1986.

[5] Drury, C., and Withehouse, S.: "The Effect of Lubricant Phosphorus Level on Exhaust Emissions in a Field Trial of Gasoline Engine Vehicles," SAE paper 940233, 1994.

[6] Ueda, F., Sugiyama, S., Arimura, K., Hamaguchi, S., and Akiyama, K.: "Engine additive Effects on Deactivation of Monolithic Three-Way Catalysts and Oxygen Sensors," SAE paper 940746, 1994.

[7] Froelund, K.: " Real-Time Steady-State Measurement of PCV-Contribution to Oil Consumption on Ford 4.6 L SI-Engine", SAE paper 2000-01-2876, 2000.

[8] Maassen, F., "New Approaches to Crankcase Ventilation and Oil Separation - Design of Oil Separators for Crankcase Ventilation Systems", FEV Motorentechnik, 1997.

[9] Busen, J., Klein, M., and Pietschner S.: "Kurbelgehäuseentlüftung Entwicklungspartner Hengst", enclosure to Motorentechnische Zeitschrift (MTZ).

[10] Sauter, H. L., and Trautmann, P.: "Messung und Absheidung von Ölnebelaerosolen aus der Kurbelgehäuseentlüftung von Verbrennungsmotoren. Teil 1: Messung der Tropfengrößenverteilung und der emittierten Ölmenge," Motorentechnische Zeitschrift (MTZ) Vol. 61, No. 12, pp. 874-878, 2000.

[11] Sauter, H. L., Trautmann, P., and Abendschein, M.: "Messung und Abscheidung von Ölnebelaerosolen aus der Kurbelgehäuseentlüftung von Verbrennungsmotoren. Teil 2: Konzepte zur Abscheidung von Öltröpfchen bei der Kurbelgehäuseentlüftung," Motorentechnische Zeitschrift (MTZ) Vol. 62, No. 1, pp. 80-83, 2001.

[12] Wentworth, J.: "Effect of Top Compression Ring Profile on Oil Consumption and Blowby with the Sealed Ring-Orifice Design," SAE paper 820089, 1982.

[13] Fesser, R.: "Small Engine Piston Ring Design for Reduced Oil Consumption," SAE paper 881327, 1988.

[14] Jakobs, R. J., and Westbrooke, K.: " Aspects of Influencing Oil Consumption in Diesel Engines for Low Emissions," SAE paper 900587, 1990.

[15] Yoshida, H., Kusama, K., and Kobayashi, H.: "Diesel Engine Oil Consumption Depending on Piston Ring Design," SAE paper 911699, 1991.

[16] Mihara, K, and Inoue, H.: "Effect of Piston Top Ring Design on Oil Consumption," SAE paper 950937,1995.

[17] Hill, S. H., Troy, C. K., Brown, J. R., and Hamelink, J. C.: "An Experimental Study of the Effect of Cylinder Bore Finish on Engine Oil Consumption," SAE paper 950938, 1995.

[18] Hegemeier, T., and Stewart, M.: "Some Effects of Liner Finish on Diesel Engine Operating Characteristics," SAE paper 930716, 1993.

[19] Hill, S. H.: "Cylinder Bore Finish and their Effect on Oil Consumption," SAE paper 2001-01-3550, 2001.

[20] Schneider, E.W., Blossfeld, D.H., Lechman, D.C., Hill, R., Reising, R., and Brevick, J. E.: "Effect of Cylinder Bore Out-of Roundness on Piston Ring Rotation and Engine Oil Consumption," SAE paper 930796, 1993.

[21] Hitosugi, H., Nagoshi, K., Komada, M., and Furuhama, S.: "Study on Mechanism of Lubricating Oil Consumption Caused by Cylinder bore Deformation," SAE paper 960305, 1996.

[22] Furuhama, S., Hiruma, M., and Yoshida, H.: "An Increase of Engine Oil Consumption at High Temperature of Piston and Cylinder", SAE paper 810976, 1981.

[23] Orrin, D. S., and Coles, B. W.: "Effects of Engine Oil Composition on Oil Consumption", SAE paper 710141, 1971.

[24] Stewart, R. M., and Saely, T. W.: "The Relationship between Oil Viscosity Engine Performance - A Literature Search", SAE paper 770372, 1977.

[25] Furuhama, S., Hiruma, M., and Tsuzita, M.: "Piston Ring Motion and Its Influence on Engine Tribology," SAE paper 790860, 1979.

[26] Burnett, P.: "Relationship between Oil Consumption, Deposit Formation, and Piston Ring Motion for Single-Cylinder Diesel Engines," SAE paper 920089, 1992.

[27] TSI Incorporated, Model 3934 SMPS (Scanning Mobility Particle Sizer) instruction manual, 1996.

[28] Hoult, D. P., Lux, J. P., Wong, V. W., and Billian, S. A.: "Calibration of Laser Fluorescence Measurements of Lubricant Film Thickness in Engines", SAE paper 881587, 1988.

[29] Wong, V. W., and Hoult, D. P.: "Experimental Survey of Lubricant-Film Characteristics and Oil Consumption in a Small Diesel Engine", SAE paper 910741, 1991.

[30] Hoult, D. P., and Takiguchi, M.: "Calibration of the Laser Fluorescence Technique Compared With Quantum Theory," Society of Tribology and-5ubrication Engineers Transactions, Vol. 34, No.3, 440-444, 1991.

[31] Richardson, D. E., and Borman, G. B.: "Using Fiber Optics and Laser Fluorescence for Measuring Thin Oil Films with Application to Engines", SAE Paper 912388, 1991.

[32] Tamai, G.: "Experimental Study of Engine Oil Film Thickness Dependence on Liner Location, Oil Properties and Operating Conditions", MS Thesis, Department of Mechanical Engineering, MIT, August 1995.

[33] Noordzji, B. L.: "Measurement and Analysis of Piston Inter-Ring pressure and Oil Film Thickness and their Effects on Engine Oil Consumption", MS Thesis, Department of Mechanical Engineering, MIT, June 1996.

[34] Arcoumanis, C., Duszynski, M., Pyke, E., and Preston, H.: "Cold-Start Measurements of the Lubricant Film Thickness in the Cylinder of a Firing Diesel Engine", SAE paper 982436, 1998.

[35] Casey, S.: "Analysis of lubricant Film Thickness and distribution along the Piston/Liner Interface in a Reciprocating Engine," MS Thesis, Department of Mechanical Engineering, MIT, February 1998.

[36] Nakashima, K., Ishihara, S., and Urano, K.: " Influence of Piston Ring Gaps on Lubricant Oil Flow into the Combustion Chamber", SAE paper 952546, 1995.

[37] Saito, K., Igashira, T., and Nakada, M.: " Analysis of Oil Consumption by Observing Oil Behavior around Piston Ring Using a Glass Cylinder Engine", SAE paper 892107, 1989.

[38] Inagaki, H., Saito, A., Murakami, M., and Konomi, T.: "Development of Two-Dimensional Oil Film Thickness Distribution Measuring System", SAE paper 952346, 1995.

[39] Thirouard, B., Tian, T., and Hart, D. P.: "Investigation of Oil Transport Mechanisms in the Piston Ring Pack of a Single Cylinder Diesel Engine, Using Two Dimensional Laser Induced Fluorescence", SAE paper 982658, 1998.

[40] Wahiduzzaman S., Keribar, R., Dursunkaya, Z., and Kelley, F. A.: "A Model for Evaporative Consumption of Lubricating Oil in Reciprocating Engines", SAE paper 922202, 1992.

[41] De Petris, C., Gigilio, V., and Police, G.: "A Mathematical Model of the Evaporation of the Oil Film Deposed on the Cylinder Surface of IC Engines", SAE paper 972920, 1997.

[42] Audette III, W. E., and Wong, V. W.: "A Model for Estimating Oil Vaporization from the Cylinder Liner as a Contributing Mechanism to Engine Oil Consumption", SAE paper 1999-01-1520, 1999.

[43] Tian, T.: "Modeling the performance of the Piston Ring-Pack in Internal Combustion Engines," Ph.D. Thesis, Department of Mechanical Engineering, MIT, June 1997.

[44] Tian, T.: "Dynamic behaviours of piston rings and their practical impact. Part 1:ring flutter and ring collapse and their effects on gas flow and oil transport", Proc. Instn Mech. Engrs, Vol. 216, Part J, Journal of Engineering Tribology, pp. 209-228, 2002.

[45] Tian, T., Wong, V. W., and Heywood, J. B.: "Modeling the Dynamics and Lubrication of Three Piece Oil Control Rings in Internal Combustion Engines," SAE paper 982657, 1998.

[46] Thirouard, B.: "Characterization and Modeling of the Fundamental Aspects of Oil transport in the Piston-Ring Pack of Internal Combustion Engines," Ph.D. Thesis, Department of Mechanical Engineering, MIT, May 2001.

[47] Bailey, B. K., and Ariga, S.: "On-Line Diesel Engine Oil Consumption Measurement", SAE paper 902113, 1990.

[48] Froelund, K., Menezes, L. A., Johnson, H. R., and Rein, W. O.: "Real-Time transient and Steady-State Measurement of Oil Consumption for Several Production SI-Engines", SAE paper 2001-01-1902, 2001.

[49] Inoue, T., Maeda, Y., Masashi, T., and Nakada, M.: "Study of Transient Oil Consumption of Automotive Engine", SAE paper 892110, 1989.

[50] Lizumi, S., and Koyama, T.: "Measurement of Oil Consumption of Diesel Engine by S-Trace Method", SAE paper 860545, 1986.

[51] Ariga, S.: "Observation of Transient Oil Consumption with In-Cylinder Variables", SAE paper 961910, 1996.

[52] Carrié, O., and Maerky, C.: "U-Flex as an Oil Control Ring for New Generation Engines", Motorentechnische Zeitschrift (MTZ) Vol. 60, No. 4, pp. 570-575, 1999.

[53] Yilmaz, E., Thirouard, B., Tian, T., Wong, V. W., Heywood, J. B., and Lee, N.: "Analysis of Oil Consumption Behavior during Ramp Transients in a Production Spark Ignition Engine", SAE paper 2001-01-3544, 2001.

[54] Tian, T., Wong, W. V., Heywood, J. B., and Rabute, R.: "Effects of Piston-Ring Dynamics on Ring/Groove Wear and Oil Consumption in a Diesel Engine", SAE paper 970835, 1997.

[55] Tian, T.: "Dynamic behaviours of piston rings and their practical impact. Part 2: oil transport, friction and wear of ring/liner interface and the effects of piston and ring dynamics", Proc. Instn Mech. Engrs, Vol. 216, Part J, Journal of Engineering Tribology, pp. 229-247, 2002.

[56] Thompson, M., and Saville, S. B.: " The Use of Top Ring Zone oil Sampling and Analysis to Investigate Oil Consumption Mechanisms," I. Mech. E. Conference, "Automotive Power Systems – Environmental Conservation", Paper No. C394/041, Chester 1990.

[57] Mills, A. F., *Heat and Mass Transfer*, Richard D. Irwin, 1995.

[58] Kayes, D.: "Particulate Matter Formation in Spark Ignition Engines," Ph.D. Thesis, Department of Mechanical Engineering, MIT, January 1999.

[59] Didot, F. E., Green, E., and Johnson, R. H.: "Volatility and Oil Consumption of SAE 5W-30 Engine Oil", SAE paper 872126, 1987.

[60] Carey, L. C., Roberts, D. C., and Schaub, H.: "Factors Influencing Oil Consumption in Today's Automotive Engines", SAE paper 892159, 1989.

[61] Manni, M., and Ciocco, G.: "An Experimental Study of Oil Consumption in Gasoline Engines", SAE paper 922374, 1992.

[62] Mahle, *Mini Piston Manual*, Mahle GmbH, D-70369 Stuttgart, 1995

[63] Woschni, G., and Fieger, J.: " Experimentelle Bestimmung des örtlich gemittelten Wärmeübergangskoeffizienten im Ottomotor", Motorentechnische Zeitschrift (MTZ) Vol. 42, No.6, pp. 229-234, 1981.

[64] Poulos, S. G., and Heywood, J. B.: "The Effect of Chamber Geometry on Spark Ignition Engine Combustions", SAE paper 830334, 1983.

[65] Woschni, G., and Zeilinger, K.: "Vorausberechnung des Kolbenringverhaltens", FVV Workshop, Tribosystem Kolben-Kolbenring-Zylinderlauffläche, 10. Oktober, VDMA-Haus Frankfurt, 1989.

[66] Reid, R. C., Prausnitz, J. M., and Sherwood, T. K., *The Properties of Gases and Liquids*, 3rd Ed., McGraw-Hill, 1977.

[67] Zwolinski, B. J., Wilhoit, R. C., *Handbook of Vapor Pressures and Heats of Vaporization of Hydrocarbons and Related Compounds*, College Station: Thermodynamics Research Center, Dept. of Chemistry, Texas A & M University, 1971.

[68] Tian, T., Wong, V. W., and Heywood, J. B.: "A Piston Ring-Pack Film Thickness and Friction Model for Multigrade Oils and Rough Surfaces", SAE paper 962032, 1996.

[69] Norris, G.M., and Hochgreb S.: "Novel Experiment on In-Cylinder Desorption of Fuel from the Oil Layer", SAE paper 941963, 1994.

(This page was intentionally left blank)

Appendices

Appendix A LIF window surface profiles

The surface characteristics of the liner with the windows were measured with stylus instrument (Taylor Hubson Form Talysurf profiler) at ambient conditions. The unfiltered primary surface profile measurements along the cylinder liner are shown in Figures A-1 to A-4.

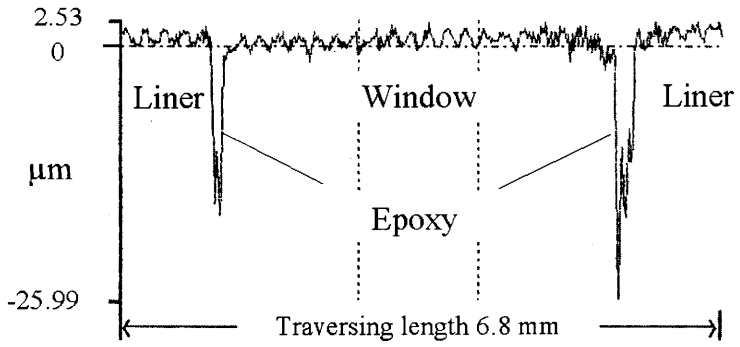

Figure A-1 LIF Window 2 and its adjacent liner

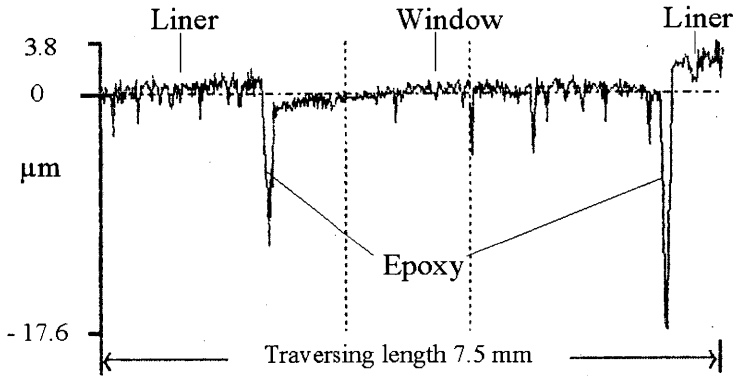

Figure A-1 LIF Window 2 and its adjacent liner

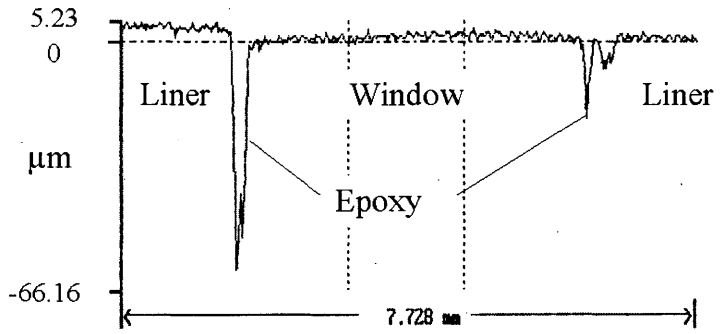

Figure A-3 LIF Window 3 and its adjacent liner

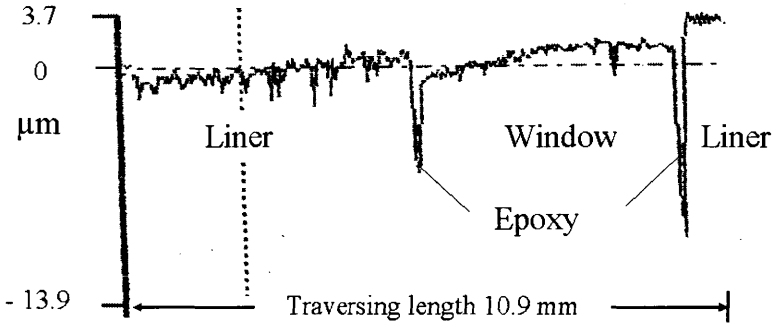

Figure A-4 LIF Window 4 and its adjacent liner

Appendix B Heat transfer correlation

The semi-empirical Woschni correlation is used to estimate the instantaneous spatially averaged heat transfer coefficient for the combustion chamber surface [63]:

$$h = 0.013 D^{-0.2} p^{0.8} T^{-.053} \left[c_1 c_m + c_2 \frac{V_h T_1}{p_1 V_1} (p - p_0) \right]^{0.8} \quad [W/m^2K];$$

where h is the instantaneous spatially averaged heat transfer coefficient, D the cylinder bore, p and T the mean cylinder pressure and temperature, c_m the average piston velocity, V_h the displaced volume, p_1, T_1, V_1 the bulk working-fluid pressure, temperature and Volume at the beginning of compression stroke, and p_0 the motored cylinder pressure at the same crank angle as p.

The constants c_1 and c_2 are expressed as follows:

$c_2 = 3.24 * 10^{-3}$, [m/sK]

During intake and exhaust strokes: $c_1 = 6.18 + 0.417\ c_u/c_m$,

During compression and expansion strokes: $c_1 = 2.28 + 0.308\ c_u/c_m$.

Here c_u is the circumferential speed of the paddle used to determine the swirl coefficient.